The impact of immunoproteasomes in murine CVB3-associated myocarditis

DISSERTATION

zur Erlangung des akademischen Grades

doctor rerum naturalium

(Dr. rer. nat.)
im Fach Biologie

eingereicht an der
Mathematisch-Naturwissenschaftlichen Fakultät I
der Humboldt-Universität zu Berlin
von
Elisa Opitz, M.Sc.

Präsident der Humboldt-Universität zu Berlin
Prof. Dr. Jan-Hendrik Olbertz

Dekan der Mathematisch-Naturwissenschaftlichen Fakultät I
Prof. Dr. Stefan Hecht

Gutachter/innen:
1. Prof. Dr. Peter-Michael Kloetzel

2. Prof. Dr. Thomas Sommer

3. Prof. Dr. Birgit Sawitzki

Tag der mündlichen Prüfung: 21. März 2013

TABLE OF CONTENT

1 ABSTRACT

The standard proteasome is the major ATP-dependent multi-catalytic protein complex that is important for the proteolytic processing of short-lived and regulatory proteins. It also degrades exogenous or improperly synthesized, misfolded, and damaged proteins. Cells of hematopoietic origin predominantly express an alternative variant - the immunoproteasome (IP), which is characterized by three specific catalytically active subunits (β1i/LMP2, β2i/MECL-1 and β5i/LMP7). In non-immune cells, these immunosubunits are also induced and incorporated into newly assembling IPs upon exposure to interferons. As compared to standard proteasomes, IPs display altered cleavage site preferences, resulting in the generation of a different spectrum of antigenic peptides for MHC class I presentation. Thus, IP-formation has long been linked to the optimization of the $CD8^+$ T cell response to viral infections. However, contrary *in vivo* studies recently reported on sufficient virus-specific $CD8^+$ T cell responses despite the lack of individual IP subunits, which suggests a more complex physiological role of IPs.

The present thesis investigates the impact of β1i/LMP2- and β5i/LMP7 within the context of viral heart disease, making use of the well-established murine model of coxsackievirus B3 (CVB3) infection. β5i/LMP7-deficient mice demonstrate a potent $CD8^+$ T cell capacity to control CVB3 infection, resulting in viral clearance after the acute stage of disease. The expression of pro-inflammatory cytokines, innate antiviral mediators, and CVB3-specific IgG antibodies argue against a specific role of IPs in the induction of an effective immune response against CVB3 infection. However, the impaired incorporation of all three immunosubunits in β5i/LMP7-deficient hearts coincides with severe inflammation and myocardial tissue damage. Exposure to IFN-γ gives rise to prolonged accumulation of oxidant-damaged, poly-ubiquitylated proteins in IP-deficient cardiomyocytes and inflammatory cells. Along with the restricted degradation of toxic protein aggregates, inflammatory cells and the adjacent myocardium are prone to increased apoptotic cell death. By contrast, the deletion of β1i/LMP2 results in the formation of intermediate proteasomes containing both, β2i/MECL-1 and β5i/LMP7 subunits, and does not affect the phenotype of CVB3 myocarditis.

Collectively, these findings point towards a pivotal role of IPs in the adaptation to oxidant protein damage. The formation of IPs preserves protein homeostasis and cell viability in the pro-inflammatory cytokine milieu of viral heart disease.

2 ZUSAMMENFASSUNG

Das Proteasom ist ein multikatalytischer, ATP-abhängiger Enzymkomplex, der kurzlebige und regulatorische Proteine in der Zelle abbaut und somit verschiedene Prozesse wie die Signalübertragung oder Zelldifferenzierung beeinflusst. Im Rahmen der Proteinqualitätskontrolle werden durch das Proteasom auch fehlerhaft synthetisierte bzw. falsch gefaltete oder chemisch geschädigte Proteine degradiert. Zellen hämatopoetischen Ursprungs exprimieren sogenannte Immunoproteasomen (IP), die durch drei alternative katalytische Untereinheiten (β1i/LMP2, β2i/MECL-1 sowie β5i/LMP7) charakterisiert sind. Unter dem Einfluss von Interferonen kommt es auch in nicht-hämatopoetischen Zellen zur *de novo* Assemblierung von IP. Sie weisen im Vergleich zu Standardproteasomen einen erhöhten Substratumsatz sowie veränderte Schnittpräferenzen auf. Dadurch können Standard- und Immunoproteasomen verschiedene MHC (major histocompatibility complex) Klasse I-restringierte antigene Peptide generieren. Vor allem in viralen Erkrankungen wurde die Expression von IP daher lange Zeit hauptsächlich mit einer effizienten Induktion der $CD8^+$ T-Zellantwort in Verbindung gebracht. Aktuelle Untersuchungen zeigen jedoch, dass die Expression von IP nicht in allen Modellen zur Optimierung der Antigenprozessierung führt. Dies lässt auf eine komplexe physiologische Funktion von IP neben der Epitopgenerierung schließen. Die vorliegende Arbeit untersucht die Relevanz der β1i/LMP2- bzw. der β5i/LMP7- Untereinheit im Rahmen der viralen Myokarditis. Hierfür stellt die murine CVB3 (Coxsackievirus B3) Infektion ein gut charakterisiertes Modell dar.

β5i/LMP7-defiziente Mäuse zeigen eine suffiziente $CD8^+$ T Zell Antwort, die zur vollständigen Viruselimination nach der akuten Entzündungsphase beiträgt. Die reguläre Expression pro-inflammatorischer Zytokine und antiviraler Signalwege sowie CVB3-spezifischer IgG-Antikörper spricht gegen eine spezielle Funktion von IP bei der Induktion einer effektiven Immunantwort in diesem Modell. Es konnte jedoch gezeigt werden, dass der verminderte Einbau aller IP-Untereinheiten in β5i/LMP7-defizienten Mäusen mit einer schweren Inflammation und Myokardschädigung einhergeht. Der verringerte Substratumsatz führt zur Akkumulation von polyubiquitinylierten, oxidativ geschädigten Proteinen sowie zur verstärkten Apoptose IP-defizienter Kardiomyozyten und inflammatorischer Zellen. Des Weiteren ist die Regulation NF-κB-abhängiger Signalwege durch die IP-Defizienz

beeinträchtigt. Die Deletion von β1i/LMP2 führt hingegen zur Expression sogenannter Mischproteasomen, in denen sowohl β2i/MECL-1 als auch β5i/LMP7 inkorporiert sind. Im Gegensatz zur IP-Defizienz in β5i/LMP7$^{-/-}$ Mäusen hat das Fehlen der β1i/LMP2 Untereinheit keinen Einfluss auf die Ausprägung der CVB3-Myokarditis. Zusammenfassend trägt diese Arbeit maßgeblich zum Verständnis der biologischen Relevanz von IP bei. Im proinflammatorischen Zytokinmilieu der akuten CVB3 Myokarditis erhalten IP die Proteinhomöostase und damit letztlich die zelluläre Funktionalität.

3 INTRODUCTION

3.1 Myocarditis and dilated cardiomyopathy

Myocarditis is defined as a cardiac disease associated with the inflammation of the myocardium and necrosis and (or) degeneration of adjacent myocytes in the absence of an ischemic event (1). Susceptibility to viral heart disease seems to be age related, as about 52% of myocarditis occur in children and young adults (2). The clinical manifestation of myocarditis is highly variable, ranging from asymptomatic courses or nonspecific signs (e.g. fever, myalgia) to acute heart failure and sudden death (1-3). Due to this vast diversity of clinical presentations, diagnosis is rather difficult. A combination of different magnetic resonance imaging methods represents the most useful noninvasive tool to diagnose myocarditis, but no information about the degree of inflammation or presence or type of causative agents can be obtained (4). Therefore, endomyocardial biopsy remains gold standard for the diagnosis of myocarditis (4;5). Following the Dallas criteria, the first endomyocardial biopsy is classified into acute (myocytolysis) and Borderline (no myocytolysis) myocarditis. Subsequent biopsies differentiate between persistent, resolving and resolved myocarditis (1;6;7). According to the WHO/ISFC Task Force, the myocardium is considered to be inflamed after immunohistochemical detection of focal or diffuse mononuclear infiltrates with >14 leukocytes per mm^2 ($CD3^+$ T lymphocytes and/or $CD68^+$ macrophages) (8). Of note, the Dallas criteria are limited by interobserver variability and lack of prognostic value (5;9).

Acute myocarditis can improve spontaneously in approximately 50% of patients, or it progresses to a chronic form, and may subsequently deteriorate to dilated cardiomyopathy (DCM) (10). DCM is characterized by ventricular dilatation with normal LV wall thickness and systolic dysfunction of the left or both ventricles (11). Arrhythmias, conduction system abnormalities, thromboembolism and sudden or progressive heart failure-related deaths are common and may occur at any stage of disease (8).

Whereas acute myocarditis with preserved left ventricular ejection fraction or its normalization during short-term follow up is linked to high rates of spontaneous improvement (4;12), clinical presentation with heart failure is a predictor for incomplete long-term recovery

(4;13). Patients of the latter cohort more likely develop DCM or need heart transplantation (12). Progress to chronic dilated cardiomyopathy is correlated to a poor 5-year survival rate of less than 50% (3).

Apart from idiopathic myocarditis where the causative agent is not known, major etiologies include viral, bacterial, protozoan or mycotic infections, gene mutations, autoimmune inflammation, and exposure to toxins (3;14).

3.2 Coxsackievirus B3

Coxsackieviruses are human-pathogenic enteroviruses within the family of *picornaviridae*. There exist two serogroups (A and B), both being primarily transmitted by the fecal-oral route or respiratory aerosols. Whereby Coxsackievirus A serotypes mainly cause enteric disorders, all known Coxsackie B viruses are associated with a broad range of severe diseases, including pancreatitis, aseptic meningitis, or type I diabetes mellitus (2;15;16). The serotype CVB3 has long been reported to be among the most frequent causes of viral myocarditis, especially in young infants (2). During the last years, the epidemiologic spectrum of most frequent viruses shifted from classic enteroviruses such as CVB3 and adenoviruses to parvovirus B19 and human herpes virus 6 (4;17;18). Nonetheless, the experimental model of murine CVB3 myocarditis is well-established. Different resistant and susceptible mouse strains mimic the diverse human disease progression and allow a mechanistic investigation of host genetic factors.

3.2.1 Structure and life cycle of CVB3

CVB3 is a non-enveloped, icosahedral virus, encompassing a 7.4 kb positive sense, single-stranded RNA genome ((+)ssRNA). After attachment of CVB3 to the decay-accelerating factor (DAF) on the apical cell surface, Rac-dependent actin rearrangement permits virus movement to tight junctions (19), where the coxsackievirus and adenovirus receptor (CAR) is located (20;21). Interaction of CVB3 with CAR promotes conformational alterations within the virus capsid, which are crucial for virus entry and RNA release (21). In the cytoplasm, the viral RNA serves as a template for the translation of a large polyprotein (**Fig. 1**). The genome of CVB3 does not contain a 7-methyl guanosine cap structure as it is found at the 5′ end of eukaryotic genomic RNAs. Instead, viral VPg protein is involved in the initiation of protein synthesis via a cap-independent mechanism that utilizes an internal ribosome entry site

(IRES) in its 5' untranslated region (UTR) (22). Subsequently, the virus-encoded proteases $2A^{Pro}$ and $3C^{pro}$ cleave the synthesized polyprotein into three precursor molecules (P1, P2, and P3) (2;22). $3CD^{Pro}$ then cleaves P1 into structural capsid proteins (VP1 – VP4), while the P2 and P3 segments will result in nonstructural viral proteases and polymerases ($2A^{pro}$, 2B, 2C, 3A, 3B/VPg, $3C^{pro}/3CD^{pro}$, $3D^{pol}$). These processes occur since proteases (2A, 3C) are capable to fold into an active conformation and to auto-cleave during translation (2;22). In addition, several cellular proteins are cleaved by viral proteases, including the translation initiation factor eIF4G, thereby inhibiting cap-dependent host cell translation (23).

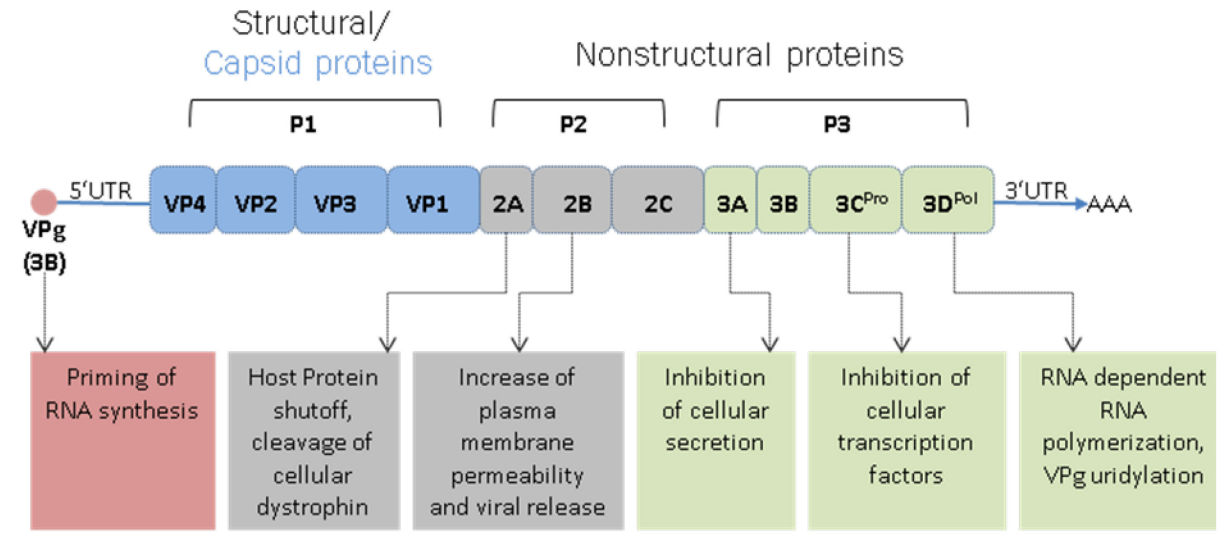

Fig. 1 The CVB3 polyprotein and proposed functions of single components (based on Esfandiarei, 2008).

Viral $3D^{pol}$, an RNA-dependent RNA-polymerase, generates the protein primer VPg-pU-pU (VPg uridylation) to initiate negative-strand RNA synthesis at the 3' poly(A) region of the viral genome (24). In turn, multiple copies of negative-sense RNA serve as templates for the production of positive-strand RNA genomes. These can either be packaged and released as progeny viruses, or they act as templates for subsequent rounds of *cap*-independent translation (2;22). From entry to the release of progeny virus, this lytic replication cycle occurs within approximately 6-8 h (25).

3.2.2 Mechanisms of virus replication and inflammation in experimental CVB3-associated myocarditis

The experimental model of murine CVB3 myocarditis allows the investigation of mechanisms that contribute to the onset and progression of human viral myocarditis. Resistant mouse strains (e.g. C57BL/6 or DBA/1J) are capable of eliminating the virus, leading to complete

recovery. By contrast, susceptible mice (e.g. A.BY/SnJ or A/J) develop chronic myocarditis, which is accompanied by virus persistence in the myocardium (2). Accordingly, the host's genetic background and the nature of the immune response influence the pathophysiology of viral myoarditis.

Following intraperitoneal injection, CVB3 replicates in the pancreas, spleen, heart, and brain (26). Concomitant with prominent virus replication, substantial necrotic and apoptotic cardiomyocyte death is observed during the viremic stage 3 to 4 days postinfection (2;27). Although no inflammatory processes take place in the myocardium at this time point, cytolytic CVB3 replication may cause a high mortality rate in certain susceptible mice (14;28). However, in most resistant as well as susceptible mice, the non-inflammatory phase is not immediately lethal, but followed by acute myocardits around day 8 postinfection (14;27). This is initialized by the injurious infection, which causes immunogenic cell debris and elevated myocardial expression of cytokines e.g. interleukin 1α and interleukin 6 (IL-1α, IL-6), tumor necrosis factor α (TNF-α), and interferon γ (IFN-γ) up to day 5 postinfection (2;27). Thereby, the migration of natural killer-like cells that express cytolytic perforin is stimulated (29). The substantial increase of proinflammatory cytokines then triggers the second wave of immune cell infiltration, primarily consisting of $CD4^+$ T helper cells and cytotoxic $CD8^+$ T cells (27;30) as well as macrophages (30). These infiltrating cell types are found in human myocarditis and, by day 11 postinfection, also in the murine model of CVB3 myocarditis (27;31;32).

Multifactorial mechanisms participate in the transition from acute myocarditis to chronic manifestation and its late sequelae, dilated cardiomyopathy and heart failure (14;27). At the acute stage, the balance between viral clearing and healing in contrast to myocardial damage and exaggerated immune activation is crucial for the outcome of infection. For example, cytotoxic $CD8^+$ T cells (CTLs) are required to limit CVB3 replication in the myocardium (33) however, the release of perforin by these CTLs causes severe myocardial fibrosis (34). Moreover, the development of chronic myocarditis can be triggered by persistent, Th-17 cell-mediated IL-17 secretion, which induces a prolonged inflammatory environment and in turn facilitates the generation of autoreactive antibodies (27). In murine myocarditis, such autoantibodies e.g. against cardiac myosin heavy chain, desmin, and actin develop as early as day 7 postinfection (2;35) and can induce injury of both, infected and uninfected cardiomyocytes (2). Also, a highly reactive inflammatory environment can result from synergistic signaling by proinflammatory cytokines such as TNF-α and viral replication (27).

Actually required for pathogen defense, activation of NF-κB (nuclear factor kappa-light-chain-enhancer of activated B cells) by the PI3K/Akt (phosphatidylinositol 3-kinase/ protein kinase B) pathway is utilized by CVB3 for successful replication in infected cells (36). TNF-α was shown to enhance cell viability via the NF-κB pathway (36), thereby promoting provirus replication signals in infected cells (27).

3.3 The Ubiquitin-Proteasome System

In the heart, the high metabolic rate and mechanical work load, but also neurohumoral regulation and exposure to various cellular stressors represent a particular challenge to the ubiquitin-proteasome system (UPS) (37). The UPS is involved in the maintenance of cellular protein homeostasis, which is a very complex and precisely regulated process encompassing RNA metabolism and processing, protein synthesis and folding, protein assembly/disassembly, translocation, and degradation. The latter function is mainly carried out by the UPS. Proteins that are involved in various cellular processes such as signal transduction, transcription, cell-cycle control, differentiation, or apoptosis, are degraded by this ATP-dependent system (38;39). Aside from removing short-lived regulatory proteins, the UPS also degrades structurally aberrant proteins (40), which is particularly important in long-lived, non-proliferating cells such as cardiomyocytes or neurons (41). Furthermore, the proteasome is involved in the efficient immunosurveillance of cellular and pathogenic translation products by the generation of specific peptides for MHC class I antigen presentation (38). The structural composition of proteasomes varies between different organs (42) and adapts to organ-specific requirements and pathophysiological conditions. In many cardiomyopathies, including diabetic cardiomyopathy (43), ischemia-reperfusion injury (44) and CVB3-associated myocarditis (45), the expression and activity of so-called immunoproteasomes (IPs) is significantly elevated. It has been reported that UPS dysfunction is a pathogenic factor for a large subset of cardiovascular disorders, such as pressure overload cardiac hypertrophy or ischemic heart disease (37). These diseases have been associated with oxidative modifications and/or downregulation of proteasome subunits, and decreased proteasome activity. Impaired proteasome function compromises protein quality control in heart muscle cells; determining the progression to chronic heart failure. However, pharmacological inhibition of proteasome activity was also shown to be a potential

therapeutic strategy, as it protects against cardiac remodeling e.g. in pressure-overload cardiac hypertrophy (37).

3.3.1 Ubiquitylation and the standard 26S proteasome

Throughout eukaryotes, ubiquitin (Ub) is a highly conserved small protein of 76-amino-acids, which regulates virtually all aspects of cellular protein metabolism. Posttranslational substrate modification by the conjugation of ubiquitin either marks a protein for degradation, or it changes its conformation, activity, stability, or location (46;47). Catalyzed by an enzymatic cascade - the ubiquitylation, ubiquitin is activated, transferred, and covalently attached to lysine residues of target proteins. The activating enzyme E1 uses ATP to adenylate ubiquitin at its C terminus, resulting in the formation of a thioester bond between the sulfhydryl group of the E1 active-site cysteine and the glycine residue of ubiquitin while expelling AMP. Second, activated ubiquitin is passed to the active-site cysteine of an E2 family member (conjugation). The Ub-E2 complex is finally recruited to an E3 ligase which specifically binds the C terminus of Ub to the ε-amino group of a lysine in the substrate by an isopeptide linkage (ligation) (47-49). Ubiqitylation is a dynamic and reversible process of protein modification. De-ubiquitylating enzymes (DUBs), that are also important for C-terminal processing of immature ubiquitin prior to ubiquitylation (47), cleave Ub from proteins and residual proteasome-associated peptides. Furthermore, DUBs recycle ubiquitin by the disassembly of multi-Ub chains (50).

Whether a protein is degraded or otherwise modified depends on the structure of the Ub chain that is transferred to the target protein. Monoubiquitylation is the attachment of a single Ub to a protein, and is involved e.g. in targeting cell-surface proteins for internalization and subsequent lysosomal degradation (51). Multiubiquitylation describes the tagging of multiple lysine residues of the target protein with single Ub molecules. Polyubiquitylation occurs, when ubiquitin itself is modified at one of its seven internal lysine residues (52;53). While chain linkage through the lysine residue at position 63 of ubiquitin (Lys-63) is reported to be involved in numerous non-proteolytic processes e.g. DNA damage tolerance, Lys-48-linked polyubiquitin chains mostly target substrates for degradation by 26S proteasomes (46;54). The 26S proteasome is a large protein complex, consisting of the catalytically active 20S core and a 19S regulatory particle that recognizes and unfolds Ub-tagged proteins (**Fig. 2**A). Axial stacking of four heteroheptameric rings - two outer α- and two inner β-rings forms the cylindrical 20S core.

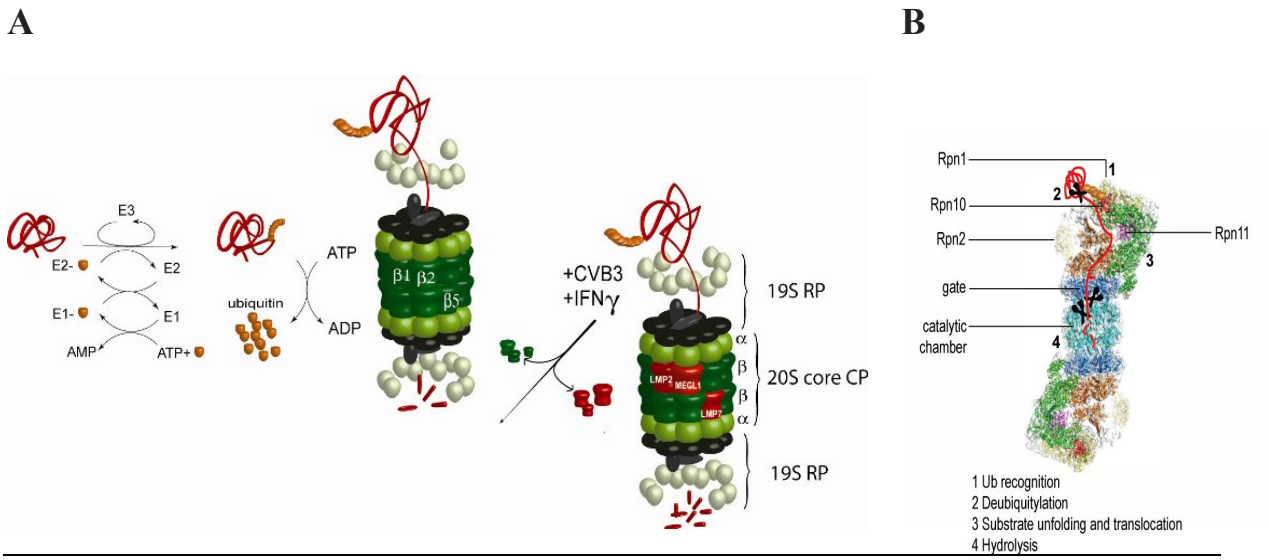

Fig. 2 Ubiquitylation, the 26S proteasome and formation of immunoproteasomes. A: ATP-dependent substrat ubiquitylation is mediated by E1 activating, E2 conjugating, and E3 ligating enzymes. For degradation, ubiquitylated proteins are directed to the 26S proteasome, which consists of the catalytic 20S core and 19S regulatory proteins. Upon CVB3 infection/cytokine induction, the immunosubunits β1i/LMP2, β2i/MECL-1 and β5i/LMP7 are incorporated into the 20S core via *de novo* synthesis. **B**: Molecular model of the 26S proteasome subunits and their function (modified from da Fonseca *et al.* (55) and Saeki *et al.* (56).

Each ring comprises seven structurally similar α- and β-subunits (α1-7; β1-7). Only the β1, β2 and β5 subunits contain catalytically active sites for the cleavage of peptide bonds at the carboxyl side of acidic, basic and hydrophobic amino-acid residues, respectively. These specific cleavage preferences are referred to as caspase-, trypsin- and chymotrypsin-like activities (57-59). The outer α-subunits form a channel through which substrates enter the catalytic 20S core protein (CP). The N-terminal tails of these α-subunits function as a gate and restrict unregulated protein degradation (60;61) (**Fig. 2**B). Gate opening is mediated e.g. by 19S regulatory proteins (RP) (62), which comprise two subcomplexes, namely the lid and the base. Both subcomplexes consist of different subunits that are classified into regulatory particle of triple-ATPases (Rpt) or regulatory particle of non-ATPases (Rpn) (59).

The base is constituted of four non-ATPase subunits (Rpn1, 2, 10 and 13) and six homologous AAA-ATPases (Rpt1-6) (59). Rpn10 and Rpn13 function as integral ubiquitin receptors and trap polyubiquitylated substrate proteins via a C-terminal ubiquitin-interacting motif (Rpn10) or a N-terminal "pleckstrin-like receptor for ubiquitin domain" (Rpn13) (55;59). The ATPase subunits promote gate opening as well as substrate unfolding before translocation of target proteins into the 20S cavity (58;59). The lid subcomplex, which is composed of at least nine non-ATPase subunits (Rpn3, Rpn 5, Rpn6, Rpn 7, Rpn 8, Rpn 9,

Rpn 11, Rpn 12 and Rpn 15), deubiquitylates captured substrates, whereby the metalloisopeptidase Rpn11 plays the major role (55;58) (**Fig. 2**B**)**. The 19S complex can dock at either one or both sides to the 20S core, thus forming 26S and 30S proteasomes, respectively. However, both isoforms are mostly described as 26S proteasomes (59).

3.3.2 IFN-γ-inducible subunits: Immunoproteasomes and PA28

Immune cells and tissues constitutively express three alternative catalytic β-subunits: β1i/LMP2, β2i/MECL-1, and β5i/LMP7 (63). Both, β1i/LMP2 and β5i/LMP7 are encoded within the major histocompatibility complex class II region (MHCII) on chromosome 6 (64), whereas β2i/MECL-1 is localized in a cluster of unrelated genes on chromosome 16 (65). Similar to the majority of proteins that are related to the MHC antigen presentation pathway, expression of these proteasomal "immunosubunits" can be induced in non-lymphoid cells upon cytokine stimulation, particularly by IFN-γ (**Fig. 2**) (66;67). β1i/LMP2, β2i/MECL-1, and β5i/LMP7 substitute their homologous standard counterparts (β1, β2 and β5, respectively) by cooperative assembly into nascent 20S cores (38;66). Whether standard or immunosubunits are incorporated into *de novo* synthesized proteasomes depends on specific interactions between the subunits and the post-transcriptional downregulation of standard β-subunits (68-70). The proteasome maturation protein (POMP), which is also induced by IFN-γ, determines the recruitment of β5i/LMP7. The accelerated degradation of POMP is directly linked to the fast maturation of β5i/LMP7 upon IFN-γ stimulation (70). Consequently, β5i/LMP7 is incorporated preferentially over β5 into pre-proteasomes containing β1i/LMP2 and β2i/MECL-1, whereby β2i/MECL-1 requires β1i/LMP2 for efficient incorporation into these pre-proteasomes (69-71). Mature immunoproteasomes (IPs) are characterized by an altered catalytic profile compared to their standard counterparts. *In vitro,* β5i/LMP7 increases the capacity to cleave after basic and hydrophobic amino acid residues (referred to as trypsin- and chymotrypsin-like activity), whereas the incorporation of β1i/LMP2 reduces the cleavage after acidic residues (=decreased caspase-like activity) (72;73). These differential proteolytic activities contribute to the diversification of the antigenic peptide repertoire for MHC class I presentation (74).

IFN-γ also induces the expression of the proteasome activator PA28/11S, which belongs to the family of 20S proteasome regulators. PA28 is composed of two homologous subunits, PA28α and PA28β, that assemble into a heteroheptamer ($\alpha_3\beta_4$) (75-77). PA28 binds to the 20S proteasome in an ATP-independent way, thus facilitating α-ring opening. It can attach to

both sides of the 20S core [PA28-20S-PA28] or it is found in complexes that also contain a 19S regulator, thus forming so called hybrid proteasomes [19S-20S-PA28] (78). Formation of PA28-20S-PA28 complexes activates cleavage of peptides but not of intact native or ubiquitinylated proteins (75;79). Kinetic studies demonstrated, that binding of PA28 to 20S cores does not affect the maximal activity of the enzyme complex, but that it increases substrate affinity and enhances either the uptake or release of products (80;81).

3.3.3 Antigen processing by standard and immunoproteasomes

Antigen presentation constitutively occurs in almost all nucleated cell types of vertebrates as a side product of normal protein turnover. The main source for major histocompatibility complex (MHC) class I presentation are endogenous, pathogenic or tumor-associated proteins that are primarily degraded by the proteasome (82). Oligopeptides that are generated by proteasomes are either of the correct size or subsequently trimmed on their N-termini by aminopeptidases in the cytosol and the endoplasmatic reticulum (ER) (83). Translocation into the endoplasmatic reticulum (ER) is mediated by transporters associated with antigen processing (TAPs) (84). In the ER, peptides of 8-9 amino acid residues are loaded onto MHC class I dimers. MHC class I molecules are heterodimers, consisting of a heavy chain folding into three domains (α1, α2 and α3) and β_2-microglobulin. The α1 and α2 domains form the peptide-binding groove on the upper surface of the MHC class I molecule (85). Antigenic peptides stabilize the MHC complex; otherwise its stability is mediated by ER-associated chaperone proteins such as calreticulin, ERp57, and tapasin. Tapasin, which is directly linked to TAPs, couples peptide transportation into the ER and peptide binding to nascent MHC class I molecules (82). Peptide-loaded MHC class I molecules are released from the chaperones and transported to the cell surface via the Golgi complex, finally resulting in the presentation of high-affinity complexes to $CD8^+$ CTLs (82;85) (see **Fig. 3**). MHC class I molecules, which are unable to assemble correctly, are translocated to the cytosol by the ER-associated protein degradation (ERAD) system and ultimately degraded by proteasomes (86).

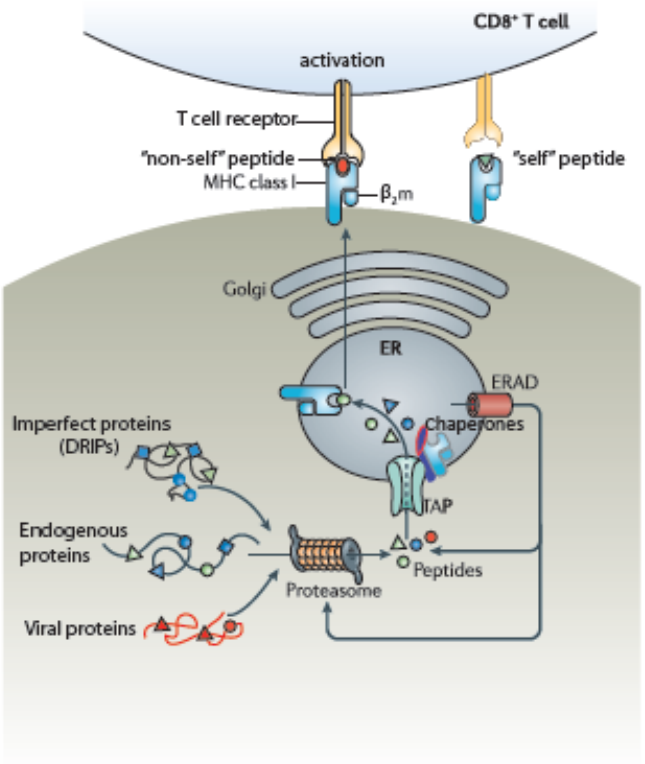

Fig. 3 Generation and presentation of MHC class I antigens. The proteasome degrades timely regulated cytosolic and nuclear proteins, but also structurally aberrant or pathogenic proteins. Generated peptides are actively transported into the lumen of the endoplasmatic reticulum (ER) by transporters for antigen processing (TAPs). Several chaperones like tapasin, calreticulin, calnexin, and ERp57 facilitate peptide binding to MHC class I molecules. Loaded MHC class I complexes are released into the Golgi, transported to the cell surface, and presented to $CD8^+$ cytotoxic T cells. Due to T cell maturation, T cell receptors (TCRs) can discriminate between "self" and "non-self" antigens (87) (modified from Neefjes *et al*., 2011 (82)).

A large fraction of peptide ligands for MHC class I complexes arises from nascent proteins that are degraded and presented shortly after synthesis (88) (see **Fig. 3**). These so called defective ribosomal products (DRiP hypothesis) consist of prematurely terminated and misfolded polypeptides that can result from defective transcription or translation, ribosomal frame shifting, oxidative stress or virus associated alterations of the cellular translation machinery (82;88-91). Thus, the DRiPs hypothesis explains the prompt MHC class I presentation of viral antigens within 1.5 hours post-infection despite the relatively long half-life of most viral proteins, as demonstrated for Influenza A neuraminidase (92).

In contrast to standard proteasomes, which are located throughout the cytoplasm and nucleus, IPs are enriched at the ER (93). In fact, IPs and PA28 are directly associated with MHC class I-TAP complexes on the ER by physical interaction (94). The enrichment of IPs at the ER may mediate the efficient transport of IP-generated peptides into the lumen of the ER as

compared SPs (93). Many studies show that IPs favor the generation of peptides with C-terminal hydrophobic or basic residues while suppressing cleavages after acidic residues *in vitro* (66;95;96). Peptides with C-terminal hydrophobic and basic residues preferentially bind to TAP transporters and MHC class I molecules (83). However, processing of larger polypeptides and protein substrates demonstrated that different catalytic subunits are able to cleave after the same residues (97).

In an experimental infection model, HeLa cells were infected with vaccinia virus expressing the hepatitis B virus core antigen. Stimulation of HeLa cells with IFN-γ and thus expression of IPs was required for the efficient liberation and presentation of the hepatitis B epitope ($HBVcAg_{141-151}$) (98;99). *Sijts et al*. found that the incorporation of a functional β5i/LMP7 subunit and of an inactive β5i/LMP7 T1A mutant both led to the generation of the CTL epitope (98). Thus, an altered cleavage profile must not necessarily be caused by the cleavage specificity, but rather by structural changes on the proteasome complex due to the presence of immunosubunits (98). However, mass spectrometrical analysis revealed that not only IPs, but also SPs were able to generate low levels of $HBVcAg_{141-151}$. *Strehl et al*. discuss, that IPs more likely influence the available amount and therefore the quantity of a given epitope, and that an immunological effects only becomes detectable once a quantitative threshold is reached (99). The specific effect of IP-expression on the $CD8^+$ T cell repertoire seems to depend on the underlying model: while β1i/LMP2- and β5i/LMP7-deficient mice mount strong lymphocytic choriomeningitis virus-specific $CD8^+$ T cell responses (100), the immunodominance hierarchy of $CD8^+$ T cell responses is altered in response to influenza virus infection in β1i/LMP2-deficient mice (101).

3.4 Proteostasis

In eukaryotes, protein folding is a highly complex mechanism and misfolded proteins need to be distinguished from those that obtain their native conformation. The balance between protein translation, folding and degradation by the proteasome is sensitive to regular development and aging. Cellular stressors such as viruses additionally challenge proteostasis, as they require enhanced protein folding and trafficking capacity for viral replication and assembly (102).

To maintain the protein equilibrium, there exists the inducible heat shock response (HSR) pathway that regulates the adaptation of the cytoplasmatic proteostasis (102). The HSR is

orchestrated by heat shock factor 1 (Hsf1) (103;104). Upon protein-damaging stress conditions, activated heat shock transcription factors bind to promoter elements upstream of heat shock inducible genes via a N-terminal DNA binding domain, thereby initiating their enhanced transcription (103). Heat shock proteins promote refolding of misfolded proteins and prevent protein aggregation (103).

Furthermore, two types of protein quality control - the endoplasmic-reticulum-associated degradation (ERAD) and the unfolded protein response (UPR) - are responsible for the recognition and degradation of conformationally aberrant and toxic proteins of the exocytic pathway (105). The UPR is controlled by three ER-bound proteins: the activating transcription factor 6 (ATF6), the type I transmembrane protein kinase and endoribonuclease (IRE1), and the RNA-activated protein kinase-like ER kinase (PERK) (106;107). Upon activation, ATF6 is relocalized from the ER to the Golgi apparatus where it is cleaved to a nuclear transcriptation factor that activates stress-responsive genes. Turnover of ATF6 is regulated by the ubiquitin-proteasome system (108). PERK, like IRE1, contains a luminal domain that detects misfolded proteins. Activation of PERK results in the generalized inhibition of protein synthesis (104). IRE1 kinase activation leads to splicing of the transcription factor XBP1 (X-box binding protein 1), which removes a translational inhibitory region. The protein product then activates the transcription of genes that are required for protein folding, ER growth, ER-to-Golgi trafficking, and the ER-associated degradation system ERAD (104;106) (see **Fig. 4**).

If the correct protein conformation cannot be achieved, proteins are eventually degraded by the ERAD. There are at least two distinct ERAD mechanims – ERAD-L for misfolded lumenal (soluble or membrane-tethered) domains and ERAD-C, which detects cytosolic domains of transmembrane proteins (104). Aberrant proteins of both pathways are ubiquitylated, retrotranslocated to the cytosol and degraded by proteasomes (106). The central player of all ERAD pathways are multi-protein transmembrane complexes formed around E3 ubiquitin ligases. One of the best characterized class of eukaryotic E3s are the HRD (3-hydroxy 3-methylgutaryl coenzyme A reductase degradation protein) ligases (109). Adaptor proteins such as the mammalian SEL1L (protein sel-1 homolog 1) are peripheral components of the E3 complex, that contain a transmembrane domain and a large luminal domain composed of multiple tetratricopeptide repeats that facilitate protein-protein interactions (109;110). SEL1L recognizes ERAD substrates and recruits them to the side of dislocation, as it binds to HRD1 (111). Translocation across the ER membrane is driven by the cytosolic AAA ATPase p97/VCP (valosine-containing protein) (109;112).

In contrast to the UPR, which regulates the secretory pathway, the HSR is predominantly a mechanism to cope with cytosolic stress conditions. However, the HSR is also activated by ER-stress and enhances the ER export of misfolded proteins if the UPR is unable to cope with the accumulation of abberent proteins (105).

3.4.1 Aggresome-like induced structures

Upon various stress conditions including infection, inflammation and oxidative stress, polyubiquitylated proteins can also be transiently stored in cytosolic aggresome-like induced structures (ALIS) (113). ALIS formation and maintenance is dependent on protein synthesis, indicating that most of the proteins are newly synthesized proteins respectively DRiPs (113;114). A recent study by Liu *et al*. demonstrated that ALIS formation requires the polyubiquitin-binding protein p62 (nucleoporin 62; also called sequestosome-1), NF-κB, and the activation of the mTOR (mammalian target of rapamycin) pathway. ALIS are storage compartments that efficiently sequester aggregating proteins from the remaining cellular protein pool, representing a cytosolic unfolded protein response. Notably, p62-mediated ALIS formation is sensitive to ER stress. Cells that lack the IRE1-XBP1 branch of the classic UPR show exaggerated up-regulation of p62 levels, suggesting cross talk between the UPR in the ER and cytosolic ALIS formation (**Fig. 4**).

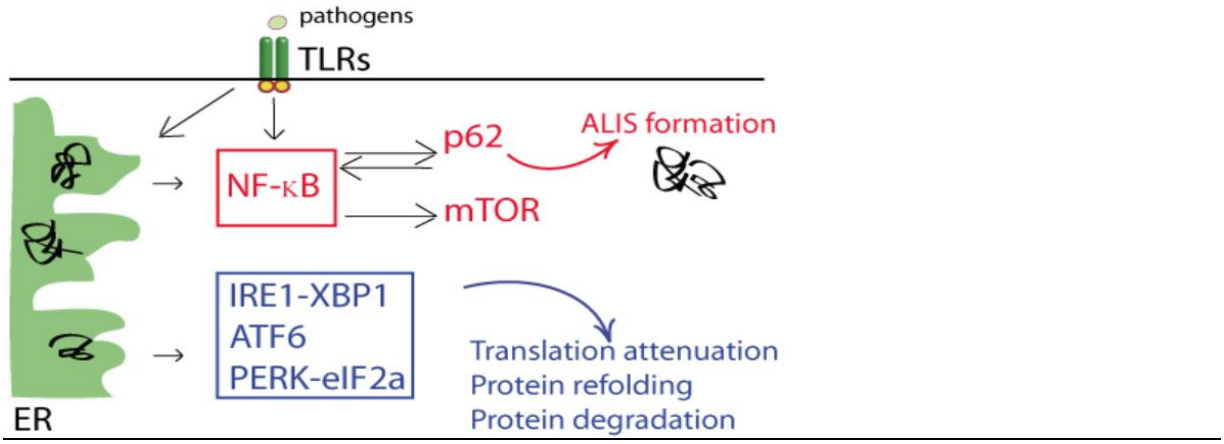

Fig. 4 ALIS formation in response to inflammation and ER stress. mTOR signaling is induced by pathogen-associated TLR activation and/or inflammation. Activation of mTOR is involved in protein synthesis and is unavoidably linked to an increased level of unfolded proteins in the cytosol. The UPR in the ER is also activated upon inflammation in order to reduce protein translation, and to increase protein refolding and degradation. As an adaptive physiologic mechanism, p62 recruits unfolded proteins in the cytosol to form ALIS. NF-κB is required for p62 mRNA transcription, whereby p62 is important for sustained NF-κB activation (adapted from Liu *et al.* (115)).

Clearance of ALIS is independent from autophagy and might be a combination of protein refolding and translocation as well as degradation by the proteasome (115). ALIS were also described in dendritic cells during lipopolysaccharide (LPS)-induced maturation, thus specified as dendritic cell aggresome-like induced structures (DALIS) (116). Lelouard *et al*. demonstrated, that selection and inclusion of DRiPs into DALIS is a well-organized process and that DRiPs are initially protected from proteasome degradation. The capacity to extend the half-life of aberrant proteins is likely to influence the MHC class I presentation in maturing DCs. Ubiquitylated DRiPs are stored in DALIS until the proteasome-mediated degradation is initiated, whereby proteasome inhibition increases the accumulation of DRiPs/DALIS at a later stage of DC maturation (114).

3.5 Aims of this study

The substantial impact of the UPS on cell physiology is predictive for consequences of UPS dysfunction. There is a growing body of evidence that several cardiovascular diseases are associated with defects in this degradation system (117). However, no conclusive studies about the implication of the UPS in viral heart disease have been performed to date.

As an essential component of immune surveillance, the proteasome generates peptides from intracellular or pathogenic proteins, which are presented at the cell surface by MHC class I molecules. IPs have long been linked to the optimization of antigen presentation upon inflammation and viral infections. In mice being susceptible to coxsackievirus B3 myocarditis, the formation of IPs as well as the liberation of virus-specific epitopes is delayed (118). These findings suggest disease-modifying effects of IP-formation in viral heart disease, qualifying this model for further investigation. Therefore, this thesis aims to examine the impact of β1i/LMP2- as well as β5i/LMP7-deficiency on cellular function and the induction of an effective $CD8^+$ T cell response in murine CVB3-induced myocarditis.

4 MATERIALS AND METHODS

4.1 Mouse experiments

4.1.1 Mice

strain	source of supply
C57BL/6 (J) wildtype	initially from Jackson Laboratory, FEM Unit 3
B6.SJL-Ptprca Pepcb/BoyJ (CD45.1)	Jackson Laboratory
C57BL/6 β5i/LMP7$^{-/-}$ (background: C57BL/6 (J) N6)	Ulrich Steinhoff (MPI for Infection Biology, Berlin)/ Hans Jörg Fehling
C57BL/6 β1i/LMP2$^{-/-}$ (for background information see 5.3.2)	Hansjoerg Schild (Institute for Immunology, Mainz)/ Luc van Kaer

Mice were kept at the animal facilities of the Charité University Medical Center according to the European and Berlin State guidelines for animal welfare. The protocol was approved by the Committee on the Ethics of Animal Experiments of Berlin State authorities (Permit Numbers: G0311/06, H0204/08, H0076/08). Unless otherwise specified, all analyzed groups contained similar numbers of both, female and male animals. Background analysis was performed by a mouse 384 SNP panel at the Charles River Laboratories.

4.1.2 Virus infection and organ preparation

Four to six week-old mice were infected i.p. with 1x10^5 PFU Coxsackievirus B3 (Nancy strain, from Prof. Karin Klingel, Tuebingen (119), diluted in 100 µl sterile PBS. Control mice were sham treated with 100 µl PBS. Mice were sacrificed at indicated time points using Isofluran. Hearts were perfused with PBS and weighted; all organs were quickly frozen in liquid nitrogen before storage at -80°C. Parts of organs were fixed in 4% Roti® Histofix for paraffin embedding or were cryo-conserved with Tissue-Tek. Serum clotted for at least 30 min at room temperature and was then centrifuged at 1100 rpm for 10 min. Supernatant was stored at -80°C.

4.1.3 CD8$^+$ T cell transfer

C57BL/6, β1i/LMP2$^{-/-}$, β5i/LMP7$^{-/-}$ mice (CD45.2) and B6.SJL-Ptprca Pepcb/BoyJ (CD45.1) mice were infected with 1x10^5 PFU CVB3 as described above. At day 8 post infectionem, mice were sacrificed and a single cell suspension of splenocytes was prepared as described in section 4.3.4. Following lysis of erythrocytes, cells were counted and CD8$^+$ cells were selected using magnetic activated cell sort (MACS) as described in section 4.3.5. An aliquot of each sample was taken before and after CD8$^+$ selection and analyzed by flow cytometry to verify the purity of isolated CD8$^+$ cells. The isolated cells were diluted in 150 µl sterile PBS and injected i.v. into the tail vein. 1-2x10^6 cells yielded from one donor mouse were injected into one recipient mouse. Immediately after the transfer, recipient mice were infected with CVB3 as described above and sacrificed 8 days later. Again, splenocytes were isolated and analyzed by flow cytometry to determine the percentage of donor T cells by CD45.1- respectively CD45.2-specific antibody stainings. Myocarditis scores of recipient mice were determined as described above.

4.1.4 Hemodynamic measurements

Microconductance catheter measurments were realized by Dr. Konstantinos Savvatis (Berlin) as previously described (120). On account of different numbers of male animals between the investigated strains, only female animals were analyzed.

4.2 Histological stainings

4.2.1 *In situ* hybridization and HE-staining

In situ hybridization of genomic CVB3 RNA and histological staining with hematoxylin-eosin (HE) and were carried out by Prof. Karin Klingel (Tübingen) (30). To quantify myocardial damage comprising cardiac cell necrosis, inflammation, and scarring, a myocarditis score from 0 to 4 was applied (0: no inflammatory infiltrates, 1: small foci of inflammatory cells between myocytes, 2: larger foci of >100 inflammatory cells, 3: ≤ 10% of cross-section involved, 4: 10 to 30% of a cross-section involved) (121). Immunohistochemistry for detection of CD3$^+$ T lymphocytes and Mac-3$^+$ macrophages were carried out by Prof. Karin Klingel and analyzed as described (122). Staining for B cells was carried out by Dr. Stefan Prokop/Prof. Frank Heppner (Berlin) on a Ventana Benchmark

stainer using the Vectostain Elite ABC Kits (Vector Laboratories) using CD45R/B220 1:100 (BD Pharmingen) and a biotin-labeled secondary antibody 1:100 (Dianova).

4.2.2 Ubiquitin-staining

Immunofluorescence: 6 µm cryosections were fixed in 4% paraformaldehyde for 3 min, washed in washing buffer for 5 min, permeabilized in 1% Triton X-100 for 10 min and blocked in blocking buffer for 1h. These steps were performed at room temperature while gently shaking. Monoclonal antibody FK1 (BIOMOL/Enzo Life Science) was added to each section 1:100 in staining buffer and incubated at 4°C overnight while gently shaking. After washing three times for 10 min, 200 rpm, secondary antibody was incubated 1:1000 at room temperature. Secondary antibody (anti-mouse IgG Alexa 488, Invitrogen) was co-stained with 1:3000 DAPI. Subsequently, sections were washed three times for 10 min and rinsed once with distilled water. All buffers were filter-sterilized. Finally, sections were mounted with immumount and confocal images were acquired on a Leica TCS SP2 microscope (Leica Microsystems) with the help of Dr. Annett Koch. ALIS were quantified by counting poly-ub conjugates (focused staining over background defined as ub-rich inclusions) in defined areas (1088 μm^2) at 200-fold magnification.

washing buffer
0.1% Triton X-100 in sterile PBS
blocking buffer
500 µl goat serum 50 µl BSA 40 µl 20% Triton X-100 ad 10 ml sterile PBS
staining buffer
500 µl goat serum 40 µl 20% Triton X-100 ad 10 ml sterile PBS
permeabilization buffer
1% Triton X-100 in sterile PBS

Immuohistochemistry: Paraffin embedded tissues were deparaffinized according to the protocol specified below. Ub-staining was performed by Dr. Stefan Prokop on a Ventana

Benchmark stainer using the Vectostain Elite ABC Kits (Vector Laboratories; Burlingame). Anti-ubiquitin antibody 1:1000 (DAKO Cytomation) and biotin-labeled secondary antibodies (Dianova) at a dilution of 1:100 were used. All slides were counterstained with hematoxylin and mounted with Eukitt after passing the sections through a series of increasing alcohol concentrations.

deparaffinization		**mounting**	
xylene I	5 min	ethanol 80% I	rinse
xylene II	15 min	ethanol 80% II	rinse
ethanol absolut I	3 min	ethanol absolut I	2 min
ethanol absolut II	3 min	xylene	5 min
ethanol 95% I	3 min	Eukitt	
ethanol 95% II	3 min		
ethanol 70% I	3 min		
ethanol 70% II	3 min		
distilled H_20	3 min		
distilled H_20	rinse		

4.2.3 TUNEL-assay

DNA strand breaks (TUNEL assay) were determined by *in situ* cell death detection kit, TMR red (Roche) or *in situ* cell death detection kit, POD (Roche) according to the manufacturer's instructions. In brief, paraffin embedded heart sections were deparaffinized and permeabilized for 8 min at room temperature. After rinsing sections with PBS twice, one section representing the positive control was pretreated with 1000 U/ml DNAse at room temperature for 10 min and rinsed with PBS three times. During this time, all other sections were covered with PBS. Then, 50 µl TUNEL reaction mix was added to each section and incubated for 60 min at 37°C in a humified atmosphere in the dark. After washing with PBS for 10 min twice, sections were incubated with DAPI diluted 1:1000 in PBS for 10 min at room temperature. Sections were rinsed with PBS three times and mounted with Eukitt after passing through a series of increasing alcohol concentrations (see 4.2.2). For TUNEL-POD staining, 50 µl converter solution were added to the sections after the TUNEL reaction. After rinsing three times, converter was incubated at 37°C for 30 min. Sections were rinsed in PBS three times and 50 µl DAB substrate was applied for 10 min at room temperature. Endogenous

POD was blocked by immersing sections for 10 min in 3% H_2O_2 in methanol prior to cell permeabilization.

By contrast, cryosections were fixed in 4% PFA/PBS, washed with PBS for 3 min twice, and permeabilization buffer was incubated for 2 min on ice. The positive control was pretreated with 3 U/ml DNAse. TUNEL assay was performed as described above. After final washing, sections were directly mounted with Immumount.

permeabilization buffer
0.1% Triton X-100
0.1% sodium citrate
in PBS

4.3 Cell culture experiments

4.3.1 Cells

All cell culture experiments were performed under sterile conditions. Cells were incubated at 37°C, 5% CO_2.

cell line	**characteristics**	**source of supply**
HeLa	human epithelial carcinoma cell line	lab stock
MEF	murine embryonal fibroblast	primarily isolated, E13/E14
cardiomyocytes	murine embryonal cells	primarily isolated, E13/E14
Vero C1008	kidney epithelial cells from African green monkey	ATCC
splenocytes	murine splenoctes, B cell depleted	primarily isolated

4.3.2 Cell culture media

medium for	**medium and supplements**	**source of supply**
primary cardiomyocytes	DMEM F0435, 4.5g glucose	Biochrom
	10 U/ml penicillin/streptomycin	Biochrom
	10% fetal calf serum	Biochrom

medium for	medium and supplements	source of supply
Vero	MEM Eagle	Lonza
	10% fetal calf serum	Biochrom
	2 mM L-Glutamin	Biochrom
	0.5 mg/ml Gentamycin	PAA Laboratories
MEF	DMEM, 1g glucose	
	10 U/ml penicillin/streptomycin	Biochrom
	10% fetal calf serum	Biochrom
	2 mM L-Glutamin	Biochrom
B cell depleted splenocytes	RPMI + L-Glutamin	
	10 U/ml penicillin/streptomycin	Biochrom
	10% fetal calf serum	Biochrom

4.3.3 Isolation and infection of primary cardiomyocytes

Pre-cooled solutions and organs were hold on ice during preparation. Embryos were separated at embryonic day 13 (E13). Uterus horns were placed in PBS; embryos were separated from the embryonic envelopes. The thorax was opened with fine forceps; the heart was isolated and incubated in 50 µl Trypsin/EDTA (PAA Laboratories) at 4°C over night. Following incubation at 37°C, 400 rpm for 15 min, cardiomyocytes were carefully resuspended in 1 ml pre-warmed medium and seeded in uncoated 12 well plates. Cells were cultured up to 7 days prior to experiments; the medium was changed every 3rd day. For immunoproteasome induction, cells were stimulated with IFN-γ (100 U/ml, PBL Biomedical Laboratories) 16h prior to infection.

Cardiomyocytes were infected with CVB3 at MOI 0.1, 0.5 or 1.0 (Nancy strain, stock: 2x10^8, MOI= $\frac{PFU}{cell\ number}$) in complete medium for 1h. The supernatant was removed, complete medium was added and cells were cultured up to 24 h.

4.3.4 Isolation of splenocytes

Spleens were isolated from non-infected or CVB3-infected mice. During the following steps, cells were kept on ice. A single cell suspension was prepared by gently pressing the cells through a 70 µm nylon filter. Cells were washed with PBS and centrifuged for 5 min at 1200 rpm, 4°C. The pellet was resuspended in 1 ml erythrocyte lysis buffer, incubated at

room temperature for 3 min and washed with 10 ml PBS twice. After centrifugation, the pellet was prepared for FACS analysis or MACS separation.

erythrocyte lysis buffer
10 mM $KHCO_3$
155 mM NH_4Cl
0.1 mM EDTA
in dist. H_20
FACS buffer
1% bovine serum albumin
0.01% NaN_3
in PBS

4.3.5 MACS separation

A single cell suspension of splenocytes was prepared (see 4.3.4). Total splenocytes were counted and $CD8^+$ T cells respectively B cell were separated using magnetic activated cell sort (MACS) according to the manufacturer's protocol (Miltenyi Biotec). In brief, cells were resuspended in 90 µl of MACS buffer per 10^7 cells and incubated with 10 µl of CD8a (Ly-2) or CD45R (B220) microbeads (Miltenyi Biotec) for 15 min at 4°C. Cells were washed twice with MACS buffer, resuspended in 500 µl per 10^8 cells and separated on MS (CD8a) repectively LD (CD45R) columns (Miltenyi Biotec). An aliquot of each sample was taken before and after cell selection and analyzed by flow cytometry to determine the purity of isolated cells.

B cell depletion kit	**source of supply**
CD45R (B220) mouse	Miltenyi Biotec
$CD8^+$ T cell selection kit	
CD8a (Ly-2) mouse	Miltenyi Biotec
MACS buffer	
0.5% BSA	
2 mM EDTA	
in PBS	

4.3.6 Pentamer staining

Spleens and lymph nodes were isolated from single CVB3-infected animals at d8 p.i. and single cell suspensions were prepared (see section 4.3.4). Pentamer staining was performed as previously reported (118). In brief, $CD8^+$ T cells were separated by MACS (see 2.3.5). MACS columns were washed with pentamer buffer to obtain the $CD8^+$ positive cell fraction. $1.5x10^6$ cells were labeled with 10 µl H-2^b-phycoerythrin (PE) pentamers for virus capsid protein 2 (VP2) [285-293] (ProImmune) and incubated at room temperature for 15 min, shielded from light. Cells were washed and stained with anti-CD8-FITC and anti-CD19-PE/Cy5 antibodies at a dilution of 1:100 for 20 min. After washing, cells were fixed and fluorescence-activated cell sorting-analysis was performed on a FACSCalibur (BD, Germany). CD19-positive B cells were excluded from the analysis.

pentamer washing buffer
0.1% sodium azide
0.1% BSA
in PBS
fix solution
1% fetal calf serum
2.5% formaldehyde
in PBS

4.3.7 FACS analysis

Splenocytes were resuspended in 1 ml FACS buffer (1% BSA in PBS) and aliquoted for staining. Antibodies (see below) were diluted 1:100 in FACS buffer and cells were incubated with appropriate antibodies for 45 min on ice in the dark. Cells were washed twice with FACS buffer and were then resuspended in FACS buffer containing 2% paraformaldehyde for fixation (at least 15 min). For intracellular staining, cells were prepared in saponin buffer (0.5% saponin, 1% BSA, 0.01% sodium azide in PBS). The fluorescence intensity was measured on a Beckman Coulter Cyan ADP or BD FACSCalibur (Becton Dickinson) using the Summit v4.3 software.

surface marker	**fluorescent dye**	**source of supply**
CD3	PE	BD Pharmingen
CD4	PerCP-Cy5.5	BD Pharmingen

surface marker	fluorescent dye	source of supply
CD8	PB	BD Pharmingen
CD19	FITC	BD Pharmingen
B220/CD45R	PE	Miltenyi Biotech
CD45.1	PerCp-Cy5.5	BD Pharmingen
CD45.2	FITC	BD Pharmingen
Troponin I	uncoupled	Abcam

4.3.8 Plaque assay

Organ pieces frozen at -80°C were weighed and pestled in DMEM with Penicillin/Streptomycin. Three freeze-thaw cycles were followed by centrifugation at 13000 rpm. A serial dilution of the supernatant was produced and 0.5 ml were added to Vero C1008 cells (seeded one day before at a density of $4x10^5$ cells per well (6 well). Each sample was tested in 3 dilutions: 10^{-1} to 10^{-3}. Another 0.5 ml media were added and the cells were incubated for 1h. The supernatant was removed and 5 ml Plaque assay medium were added. After incubation for 48h, cells were fixed with 1 ml 5% trichloracetic acid for 2h at room temperature, the overlay was removed and cells were stained with crystal violet to detect the plaques as light spots in the stained cell layer.

medium for	medium and supplements	source of supply
2x DMEM	26.76g DMEM	Gibco
	7.4g $NaHCO_3$	
	ad 1l H_2O dest., pH 7.2-7.4	
plaque assay medium	1:1 mixture of	
	2x DMEM, 10% fetal calf serum and	
	2% seaplaque agarose	Biozym
	30 mM $MgCl_2$ in H2O dest.	
crystal violet solution	0.25% crystal violet	Merck
	1.85% formalin	
	10% ethanol	
	35mM Tris Base	
	0.5% $CaCl_2$	

4.4 Molecular biology

4.4.1 RNA isolation

Organs were pestled in 1 ml Trizol (Invitrogen). 200 µl chloroform were added, and the solutions were mixed by thorough shaking and incubated at room temperature for 3 min. After centrifugation for 20 min at 4°C, 13000 rpm, the upper liquid phase containing the RNA was transferred into a new tube and 500 µl isopropanol were added. The RNA was precipitated at room temperature for 20 min, centrifuged for 20 min at 4°C, 13000 rpm and the supernatant was removed. The RNA was washed with 1 ml ethanol, centrifuged for 10 min at 4°C, 13000 rpm, and diluted in 50-100 µl DEPC-H_2O with 0.1 mM EDTA (Ambion) (depending on the pellet size). RNA isolation from cultured cells was performed with half the volume of solutions, centrifugation time was increased to 30 min, the RNA was precipitated at least 4h at 4°C or overnight at -20°C and diluted in 10-30 µl DEPC-H2O with 0.1 mM EDTA. RNA concentration was measured using a NanoDrop 1000 (PeqLab).

4.4.2 cDNA synthesis

500 ng RNA were diluted in 9 µl H2O (Aqua ad iniectabilia, Braun). Contaminating DNA was digested with 0.5 µl DNAse I (Ambion) for 15 min at 37°C, followed by enzyme deactivation for 5 min at 75°C. 2 µl random hexameres (0.5 µg/µl; TIB Molbiol) were added and the mixture was annealed 10 min at 70°C. Reverse transcription was performed at 37°C for 60 min with the following master mix: 4 µl 5x PCR buffer (Invitrogen), 2 µl DTT (0.1M, Invitrogen), 1 µl dNTPs (10mM each, Roche), 0.5 µl RNase Inhibitor (Roche), 1 µl MMLV Reverse Transcriptase (Invitrogen). All incubation steps were performed in a PCR cycler (Eppendorf Thermocycler Gradient).

4.4.3 Quantitative real-time PCR/TaqMan®

cDNA was diluted 1:1 in aqua ad iniectabilia (Braun) to a final concentration of 12.5 ng/µl. Reaction mix was prepared as indicated below. TaqMan® PCR was performed using the Applied Biosystems 7300 cycler and analyzed using SDS v1.3.1 software (Applied Biosystems). mRNA expression was normalized to the housekeeping gene HPRT by means of the ΔCt method.

Reaction mix using Gene Expression Assays (Applied Biosytems), FAM-none (non-fluorescent)		
final concentration or volume	**reagent**	**source of supply**
0.5 µl	5 µM TaqMan® primers and probes	Applied Biosystems
6.5 µl	TaqMan Universal PCR Gene Expression Master Mix	Applied Biosystems
1 µl	cDNA (12.5 ng/µl)	
ad 13 µl	aqua ad iniectabilia	Braun

Reaction mix using mHPRT, CVB3, IFN-γ, FAM-TAMRA		
final concentration or volume	**reagent**	**source of supply**
0.5 µl	probe (5 µM)	Applied Biosystems
6.5 µl	TaqMan Universal PCR Gene Expression Master Mix	Applied Biosystems
1 µl	cDNA (12.5 ng/µl)	
3 µl	forward and reverse primers 300 nM	
ad 13 µl	aqua ad iniectabilia	Braun

TaqMan® PCR conditions		
temperature	**duration**	**cycles**
50°C	2 min	
95°C	10 min	
95°C, 60°C	15 sec, 1 min	40x

Primer and probe sequences mHPRT, CVB3, IFN-γ	
mHPRT	forward: 5´-ATCATTATGCCGAGGATTTGGAA-3´
	reverse: 5´-TTGAGCACACAGAGGGCCA-3
	probe: 5'FAM-TGGACAGGACTGAAAGACTTGCTCGAGATG-TAMRA-3'
CVB3	forward: 5'-TCCTCCGGCCCCTGA-3'
	reverse: 5'-GATTGTCACCATAAGCAGCCA-3'
	probe: 5'-FAM-CGGAACCGACTACTTTGGGTGTCCGT-TAMRA-3'
IFN-γ	forward: 5'-AGCAACAGCAAGGCGAAAAA-3'
	reverse: 5'-AGCTCATTGAATGCTTGGCG-3'
	probe: 5'-FAM-ATTGCCAAGTTTGAGGTCAAACAACCCACA-TAMRA-3'

4.4.4 Microarray

For microarray analysis, RNA (2 µg per time point/group, n=4) was sent to Signature Diagnostics AG (Postdam, Germany) for labelling, fragmentation and hybridisation to Affymetrix gene chips. The cDNA synthesis and *in vitro* transcription was performed using the Ambion MessageAmp™ Premier RNA Amplification Kit. Biotinylated cRNA was hybridized on Affymetrix U133 2.0 plus arrays. The hybridised chips were washed and stained on FS 450 fluidic stations and subsequently scanned on a GeneChip® Scanner 3000 according to Affymetrix standard protocols.

The scanner operating software converted the signal on the chip into a DAT file, which was used for generating subsequent CEL and CHP files for analysis. A quality check (QC) preliminary analysis was undertaken whereby the samples were required to conform to several parameters and quality checks before further analysis was performed. Further analysis was based on expression filter 20-100%, fold change≥2, GO analysis p-value <0.05; pairs of conditons.

4.5 Protein biochemistry

4.5.1 Isolation of 20S proteasomes and quantification of immunosubunits

Five hearts were pooled and homogenized with Ultra Turrax® in 5 ml homogenization buffer. After 10 to 20 min on ice, homogenates were centrifuged for 30 min at 17,000 rpm (JA25.5 rotor). Supernatant was decanted and ammonium sulfate was added to 35% saturation. After 20 min centrifugation at 14,000 rpm; 4°C, supernatant was concentrated by ammonium sulfate addition to 70% saturation. After 20 min centrifugation at 14,000 rpm; 4°C, pellets were dissolved in up to 2 ml TEAD buffer. Protein fractions were separated by ultra centrifugation on sucrose gradients (10 to 40%) and ultracentrifuged at 40,000 rpm for 16 hrs in a Beckman Coulter SW40 rotor. Fractions containing proteasomes were pooled and applied to a MonoQ® HR5/5 column (FPLC Amersham) and eluted with a linear gradient of 100 mM to 400 mM NaCl in TEAD. The proteolytic active fractions were collected. Immunoblot analysis of IP subunits was performed by separating 500 ng of purified proteasomes by SDS-PAGE. Silver staining was performed to confirm equal load.

homogenization buffer
10 mM Tris, pH 7.2
0.1 mM EDTA
10 mM NaCl
25 mM KCl
1.1 mM $MgCl_2$
10% glycerol
1x complete
10x TEAD
20 mM Tris, pH 7.2
1 mM EDTA
1 mM azide
add 1 mM DTT to 1x TEAD

The relative quantification of proteasome subunits was carried out by Dr. Frank Schmidt/ Prof. Uwe Völker (Greifswald) (123).

4.5.2 Silver staining

Silver staining of proteins was performed according to a protocol by Heukeshoven and Dernick (modified) (124).

procedure	**buffer**
fixing solution ≥ 1h	20 ml ethanol 5 ml acetic acid ad 50 ml dist. H_20
sensitizing solution 30 min	15 ml ethanol 250 µl glutaraldehyd (25%) 2 ml sodium thiosulfate (5%) 3.4g sodium acetate (MW 82.03g)
wash 3x 5 min	dist. H_20
silver staining solution 20 min	125 mg silver nitrate 20 µl formalin (37% formaldehyde) ad 50 ml dist. H_20

wash 2x 1 min	dist. H_20 dist. H_20
developing solution approx. 20 min	1.25g sodium carbonate 10 µl formalin (37% formaldehyde)
stop solution 10 min	750 mg sodium EDTA ad 50 ml dist. H_20
wash 3x 5 min	dist. H_20
dry	

4.5.3 20S Proteasome activity

100 ng purified 20S proteasomes were diluted in 11 µl of 1x TEAD buffer (see 4.5.1) and pipetted into a black 96 well microtiter plate. 50, 100, or 150 µM of fluorogenic substrates (Z-LLE-AMC, Bz-VGR-AMC, and Suc-LLVY-AMC) were added in 100 µl 1x TEAD buffer. Free AMC was measured fluorometrically at ex.: 355 nm em.: 460 nm cut off: 455 nm for S-LLVY and at ex.: 370 nm em.: 445 nm cut off: 435 nm for Z-LLE and Bz-VGR.

4.5.4 Protein isolation and quantification

For protein isolation, organs were pestled in 200 µl lysis buffer followed by 3 freeze-thaw cycles in liquid nitrogen and at 37°C, respectively. After centrifugation for 30 min at 4°C, 13000 rpm, the supernatant was stored at -80°C. Adherent cells were washed with PBS, covered with 40 µl lysis buffer (12 well) and hold on ice for 10 min. Cells were then scraped off and centrifuged for 10 min at 4°C, 13000 rpm. For protein quantification, 5 µl protein solution was diluted with 20 µl distilled H_2O. Lysis buffer diluted 1:5 in H_2O was used as blank and a dilution series (1, 0.5, 0.25, 0.125, 0.025 µg/µl bovine serum albumin) was used as standard. 10 µl of each were pipetted in duplicates into a flat-bottom 96 well plate. 200 µl of BCA Protein Assay Reagent (Thermo Scientific) A:B = 50:1 were added and the plate was incubated for 30 min at 37°C and 10 min at room temperature before measuring the optical density at 570 nm in a plate reader (Anthos ht III).

Lysis buffer (general)	**inhibitors**
TrisHCl pH 7.5	10 µM MG132
10 mM EDTA	5 mM NEM
100 mM NaCl	1x complete
1% NP40	

Lysis buffer (for Oxy/Ub-staining)	inhibitors
50 mM Tris HCl pH8	for Oxy-Blot: only 1x complete
150 mM NaCl	for Ub-Blot: 1x complete, 10 µM MG132,
1% NP40	5 mM NEM
0.5% sodium deoxycholate (fresh)	
0.1% SDS	
1 mM EDTA	

4.5.5 SDS-PAGE and Western Blotting

The protein lysate was diluted in distilled H_2O to a volume of 20 µl and 6x loading buffer were added. Samples were denatured for 5 min at 95°C and then quickly cooled on ice. Samples and a molecular weight marker (Prestained Protein Ladder, Fermentas) were loaded on a polyacrylamid gel. The proteins were separated according to size by SDS-PAGE for approximately 1.5h at 150V, 50 mA, 100W (maximum).

substance	stacking gel	10% PAA separating gel	15% PAA separating gel
1M Tris pH 8.8	-	3.75 ml	3.75 ml
1M Tris pH 6.8	3.75 ml	-	-
acrylamide Rotiphoresegel 30	1.95 ml	5 ml	7.5 ml
distilled H_20	9.15 ml	6.25 ml	3.75 ml
TEMED	15 µl	10 µl	10 µl
APS	75 µl	50 µl	50 µl

loading buffer 6x Laemmli	SDS running buffer 1x
6 ml glycerol	30.25g Tris
7 ml 1M Tris pH 6.8	142.5g glycine
2g SDS	10g SDS
1.86g DTT	ad 1l distilled H_20
0.001g bromphenole blue	
ad 20 ml distilled H_20	

Proteins were then transferred to a PVDF membrane (Immobilon-P, Milllipore) using a discontinuous semi-dry blotting method. The blotting chamber was assembled in the following order from anode to cathode: 4 layers of chromatographic paper (Whatman) in

anode buffer I, 3 layers of paper in anode buffer II, the membrane (activated in methanol and in anode buffer II), the gel (in anode buffer I) and 4 layers of paper in cathode buffer. The blotting occurred at 35 V, 400 mA, 5 W (maximum) for 1h 5 min and success of the transfer was controlled by reversible Ponceau S staining (0.5% solution). Membranes were incubated in Ponceau S for 3 min and destained by washing in distilled H_2O.

anode buffer I	anode buffer II	cathode buffer
0.3 M Tris	25 mmol/l Tris	-
10% (v/v) methanol	10% (v/v) methanol	20% (v/v) methanol
-	-	40 mM 6-aminohexanoic acid
-	-	0.01% SDS
distilled H_20 ad 1l	dist. H_20 ad 1l	dist. H_20 ad 1l

4.5.6 Immunoblot - protein detection

To block unspecific binding of antibodies, membranes were incubated in PBS containing 10% RotiBlock (10x) for 1h at room temperature. Next, membranes were incubated with the primary antibody at 4°C over night while gently shaking. After washing 4 times for 5 min in washing buffer, the membranes were incubated with the secondary antibody for 1h at room temperature, followed by further 3 washing steps. The antibodies were diluted in PBS containing 10% RotiBlock. Proteins were detected by a chemoluminescent reaction with ECL Plus (GE Healthcare) according to manufacturer's protocol. The membranes were posed on an x-ray film (CL-X Posure Film, Thermo Scientific), and the films were developed automatically (Colenta RDM8-1/S1, developing solution: X-OMAT EXII, fixing solution: RP X-OMAT LO, both Kodak). To remove bound primary antibodies, membranes were incubated in stripping buffer in a rotator for 30 min at 50°C. After washing twice in washing buffer for 10 min, blocking and protein detection were carried out as described above.

stripping buffer	washing buffer
10 mM 2-mercaptoethanol	PBS
2% (v/v) SDS	0.05% Tween 20
62.5 mM Tris pH 6.7	
dist. H_20 (boiled) ad 25 ml	

Antibodies:

target protein (clone)	species	clonality	source of supply	dilution
GAPDH (FL-335)	rabbit	polyclonal	Santa Cruz	1:1000
β5i/LMP7 (K63)	rabbit	polyclonal	lab stock	1:20000
α6 (K379)	rabbit	polyclonal	lab stock	1:20000
β2i/MECL-1 (K65)	rabbit	polyclonal	lab stock	1:5000
target protein (clone)	**species**	**clonality**	**source of supply**	**dilution**
β1i/LMP2 (ab3328)	rabbit	polyclonal	Abcam	1:1000
β1i/LMP2 (K620/21)	rabbit	polyclonal	lab stock, cross-reaction with β1	1:1000
GBP1 (M18)	goat	polyclonal	Santa Cruz	1:1000
ubiquitin (Z0458)	rabbit	polyclonal	DAKO	1:1000
CAR (H300)	rabbit	polyclonal	Santa Cruz	200 µg/ml

secondary antibody	species	conjugat	source of supply	dilution
anti-rabbit IgG	goat	HRP	Santa Cruz	1:5000
anti-mouse IgG	goat	HRP	Santa Cruz	1:5000
anti-goat IgG	donkey	HRP	Santa Cruz	1:5000

4.5.7 Immunoblot- detection of oxidative stress

Oxidized proteins were visualized with the OxyBlot protein oxidation detection kit (Chemicon International) via immunodetection of carbonyl groups. Carbonyl groups are derivatized to 2,4-dinitrophenylhydrazone (DNP) by reaction with 2,4-dinitrophenylhydrazine (DNPH). This derivatization captures the oxidative state immediately during or after homogenization of the tissue. DNP-derivatized protein samples are separated by polyacrylamide gel electrophoresis followed by Western blotting. Specific DNP antibody and HRP-coupled secondary antibody are used to visualize carbonyl-groups. OxyBlots were carried out by Daniela Ludwig/Prof. Elke Krüger (Berlin).

4.5.8 Detection of CVB3- specific antibodies by ELISA

Several dilutions of the serum in dilution buffer (Enterovirus ELISA Testkit, Genzyme Diagnostics) and dilution buffer used as blank were pipetted in duplicates into an antigen coated 96 well plate (Enterovirus ELISA Testkit, Genzyme Diagnostics). After incubation for

30 min at 37°C, the samples were removed and the plate was washed 4 times with washing buffer (PBS, 0.05% Tween20, pH 7.2-7.4). 100 µl of the secondary antibody (POX anti-mouse IgG, Dianova) were added and incubated for 30 min at 37°C. After another washing step, 100 µl of a 1:1 mixture of the substrate solutions (TMB Substrate Reagent Set BD OptEIA, BD) A and B were added and incubated for 20 min at room temperature. The reaction was stopped with 50 µl 2M H_2SO_4, the plate was shaken and measured at 450 nm in a plate reader (Anthos ht III). CVB3-specific antibody titers are presented at the highest dilution of serum showing an optical density greater than the mean optical density of sera obtained from naive mice plus threefold the SD.

4.5.9 NFκB ELISA

After induction of IPs with 100 U/ml IFN-γ, primary cardiomyocytes and B-cell depleted splenocytes were stimulated with 30 ng/ml TNF-α for 30 min. p50 NFκB was determined in whole cell homogenates by ELISA according to the manufacturer's instructions (ActiveMotif).

4.5.10 Luminex assay

Serum samples from control and CVB3-treated mice were analyzed using the MILLIPLEX^{TM} mouse cytokine/chemokine kit (Millipore) system according to the manufacturer's instructions (n=5/group). Samples were measured using Luminex 200 xPONENT System [LX200 IS v.1.7, serial number LX10008099406] and xPONENT software 3.0.380.0.

4.6 Statistical analysis

Results of continuous variables are expressed as mean+standard error of mean (SEM) if not indicated otherwise. Data were analyzed using GraphPad Prism v5 software and IBM SPSS Statistics 19. Two group comparisons of non-parametric data were performed using the Mann-Whitney test. Statistical significance between multiple groups was determined using two-way ANOVA and post hoc analysis with a Bonferroni test. Significance was assessed at the $p<0.05$ level (* indicates significant differences).

4.7 Programs and websites

programs	websites
SDS v1.3.1	NCBI www.pubmed.gov
GraphPad Prism v5	ExPASy www.expasy.org
Summit v4.3	EMBL-EBU www.ebi.ac.uk
Image J v1.41o	UniProt www.uniprot.org
UNICORN™	
IBM SPSS Statistics 19	

4.8 Appliances

	source of supply
agarose gel imager	Intas
agarose electrophoresis chamber	Easy Cast B2
gel blotting chamber	PeqLab
centrifuges	Millifuge Millipore
	Heraeus Instruments Megafuge 1.0
	Heraeus Thermo Electron Corporation Fresco 17
cryostat microtome	Leica
confocal microscope	Leica TCS SP2
developing machine	Colenta RDM8-1/S1
electrophoresis chamber (PAA gels)	Hoefer
electric pipettes	Eppendorf
fluorospectrometer	PeqLab NanoDrop 1000
fluorescence microscop	Zeiss Axiovert 200M
flow cytometer	Beckman Coulter Cyan ADP
	BD FACSCalibur
FPLC	Amersham
heating block	Eppendorf Thermocycler Comfort
hybridization oven	HB-500, Minidizer, UVP
incubator for cell culture, CO_2 gased	Biosafe Integra Bioscience

	source of supply
light microscop	Leica Leitz DM IL
magnetic stirrer	Heidolph
MACS magnet/rack	Miltenyi Biotec
micro scale	Sartorius
pH-meter	WTW
power supply	Biometra Standard Power Pack P25
	PeqLab EV202
PCR cycler	Eppendorf Thermocycler Gradient
plate reader	Antosh ht III
real time PCR cycler	Applied Biosystems 7300
sterile work banch	LaminAir® HS9 Hereais Instruments
shaker platform	Rocky® LTF LAbortechnik
shaker	Heidolph Promax 1020
ultra centrifuge	Beckman Coulter SW40
vortex mixer	Heidolph Reax 2000
vaccum pump	KNF Lab
water bath	Memmert

4.9 Consumables

	source of supply
BCA 96 well plate	Greiner
black 96 well plate	Greiner
centrifuge tubes 15,50 ml	BD Falcon
cryogenic tubes	Sarstedt
chromatographic paper	Whatman®
cell culture flasks	BD Falcon
cell culture plates 6,12,24 well	BD Falcon
cell strainer 40,70 µm	BD Falcon
canula 26G $^{1/4}$	BD Falcon
CL-X Posure Film	Thermo Scientific
disposable pipettes 1,2,5,10,25 ml	BD Falcon

	source of supply
ELISA 96 well plate	Nunc
FPLC	GE Healthcare, Amersham
FACS tubes	Micronic, Falcon
MACS columns	Miltenyi Biotec
Neubauer chamber, hemocytometer	Digital Bio
PVDF membrane	Immobilon-P, Millipore
pipette tips 10,20,100,200,1000 µl	Sarstedt
parafilm	American National Can
reaction vessels 0.5,1,2 ml	Sarstedt
RTQ opical 96 well reaction plate	Applied Biosystems
sterile filter	Whatman®
sterile syringes 2,5,10 ml	BD Falcon
sterile syringe 1 ml	BD Falcon
super frost object slides	R Langenbrinck

4.10 Chemicals

	source of supply
2-mercaptoethanol	Western blot: Sigma Aldrich cell culture: GIBCO
6-aminohexanoic acid	Merck
Ammonium sulfate	Serva
APS	Serva
Acrylamide (Rotiphoresegel 30)	Carl Roth GmbH&Co
Azetic acid	Merck
Ammonium chloride	Fluka
Aqua iniectabilia	Braun
BSA	AppliChem
BCA protein assay reagent	Thermo Scientific
Bromphenol blue	Biomol
Calcium chloride	Sigma
Chloroform	Merck

	source of supply
Complete protease inhibitor	Roche
Crystal violett	Merck
DEPC-H_20 (0.1 mM EDTA)	Ambion
DAPI	AppliChem
DTT	Sigma Aldrich
ECL Plus	Amersham
Ethanol	J.T. Baker
EDTA TitriplexIII	Merck
FCS	Biochrom AG
Formaldehyde	Merck
Glycerol	Merck
Glutaraldehyde	Serva
Glycine	Roth
H_2O_2	Merck
Isopropanol	J.T. Baker
Isofluran (Forene®)	Abbott
IFN-γ	Roche
Immumount	Thermo Scientific
Methanol	Carl Roth GmbH&Co
Magnesium chloride	Fluka
MG132	Calbiochem
NEM	Fluka
PBS	PAA Laboratories
Ponceau S	Sigma
Penicillin/Streptomycin (10000 U/ml)	Biochrom AG
Potassium hydrogen carbonate	Merck
Potassium chloride	Merck
Roti®-Block 10x	Carl Roth GmbH&Co
Roti® Histofix (4%PFA)	Roth
SDS	Roth
Seaplaque agarose	Biozym
Sodium hydrogen carbonate	Sigma

	source of supply
Sodium carbonate	Sigma
Sodium azide	Fluka
Sodium citrate	Sigma
Sodium chloride	Carl Roth GmbH&Co
Sodium thiosulfate	Merck
Sodium acetate	Roth
Silver nitrate	Roth
Sodium EDTA	Serva
Tris Base	Carl Roth GmbH&Co
Tissue-Tek	Sakura
TNF-α	Roche
Trizol	Ambion
Trypan blue	ICN BIochemicals
Tween® 20	Serva
TEMED	Sigma Aldrich
Triton® X-100	Ferak
Xylene	J.T.Baker

5 RESULTS

5.1 Phenotypic characterization of β1i/LMP2$^{-/-}$ and β5i/LMP7$^{-/-}$ mice

To obtain insights concerning the function of IPs in CVB3-associated myocarditis, detailed characterization of IP-competent C57BL/6 as well as β5i/LMP7$^{-/-}$ and β1i/LMP2$^{-/-}$ mice was performed at an early (d4 p.i.), acute (d8 p.i.), and chronic (d28) stage of disease.

5.1.1 Determination of myocardial damage by hematoxylin-eosine staining

First, myocardial infection was histologically correlated to the extent of lymphocyte infiltration and myocyte necrosis by hematoxylin-eosine staining. Apart from a few scattered macrophages, no focal inflammatory infiltrates were detectable in the hearts of C57BL/6, β5i/LMP7$^{-/-}$ and β1i/LMP2$^{-/-}$ mice at d4 p.i. (**Fig. 5**A). At the same time point, the pancreas as the primary organ of CVB3 replication was massively inflamed in all three strains. At d8 p.i, pancreatic acinar cell destruction with fibrous and fatty tissue replacement was observed in β5i/LMP7$^{-/-}$ mice. By comparison, some pancreatic cells were still present in C57BL/6 and particularly in β1i/LMP2$^{-/-}$ mice at this time point. This referred to accelerated pancreas destruction in β5i/LMP7-deficient mice early upon CVB3 infection (**Fig. 5**B).

Moreover, massive myocyte necrosis was detected in β5i/LMP7$^{-/-}$ mice at d8 p.i. as representatively illustrated in **Fig. 5**A. Inflammatory lesions were considerably larger than in C57BL/6 mice. By contrast, myocardial damage was found to be less pronounced in β1i/LMP2$^{-/-}$ mice as compared to C57BL/6. Quantification of heart muscle injury resulted in a significantly higher myocarditis score of 2.8±0.2 in β5i/LMP7$^{-/-}$ mice vs. 2.0±0.14 in C57BL/6 mice (*$p<0.05$). Small inflammatory foci and marginal myocyte necrosis revealed a significantly lower myocarditis score in β1i/LMP2$^{-/-}$ mice (0.6±0.08; *$p<0.01$) as compared to C57BL/6 mice. In C57BL/6 and β1i/LMP2$^{-/-}$ mice, no relevant signs of ongoing chronic myocardial inflammation were observed at d28 p.i. (**Fig. 5**A). Also, only marginal inflammatory lesions were observed in β5i/LMP7$^{-/-}$ mice at this time point.

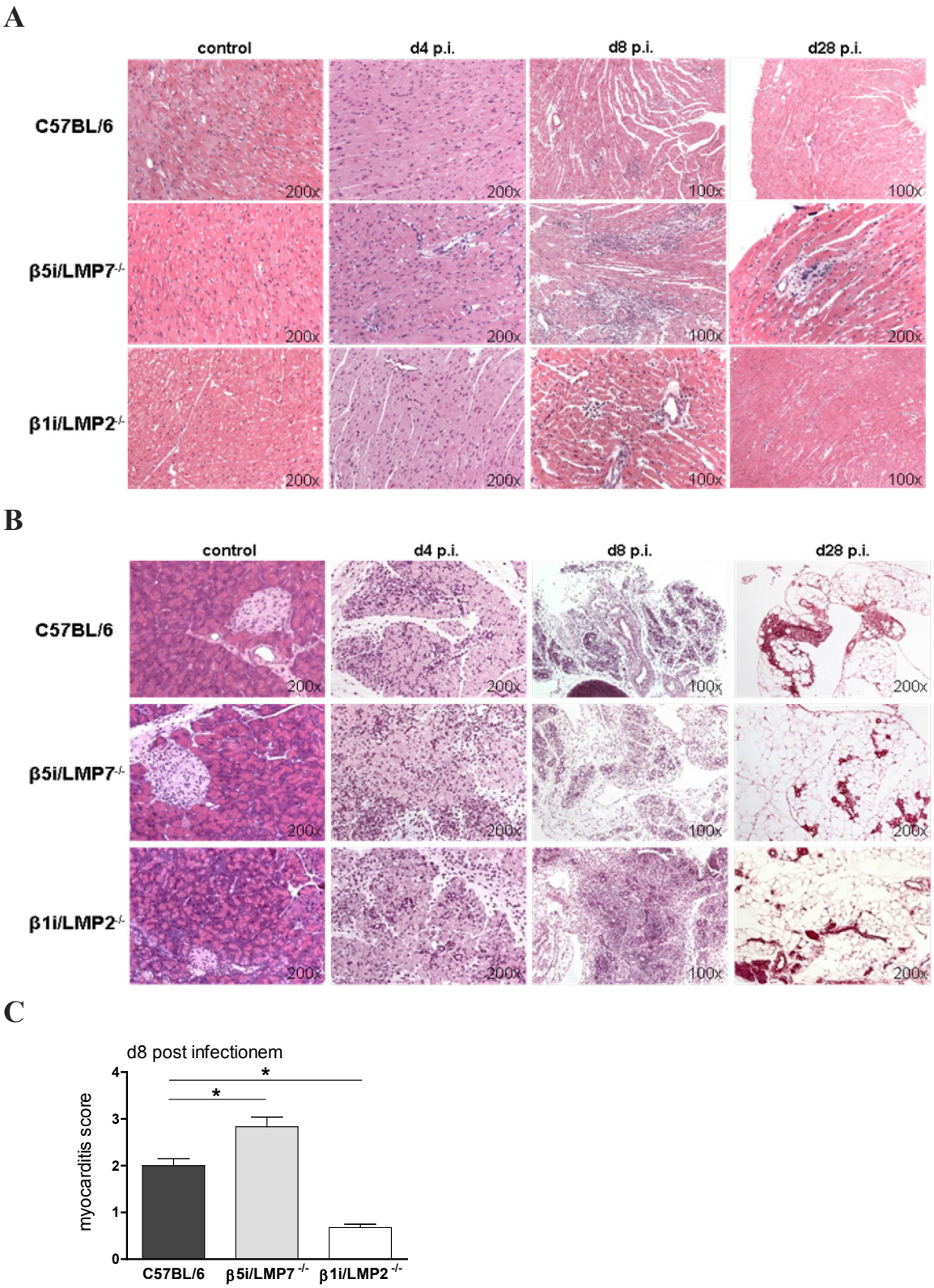

Fig. 5 Quantification of myocardial inflammation. Hematoxylin-eosine (HE-) stainings of heart **(A)** and pancreas **(B)** sections of different time points post infectionem are shown (representative for n≥10 mice/group). **C:** Myocardial damage was quantified by applying a myocarditis score from 0 to 4 (0: no inflammatory infiltrates, 1: small foci of inflammatory cells between myocytes, 2: larger foci of >100 inflammatory cells, 3: ≤10 % of cross-section involved, 4: 10 to 30 % of a cross-section involved) (*p<0.001, one-way ANOVA; n≥9 mice+SEM).

To further characterize the composition of inflammatory lesions, immunohistological stainings of C57B/6 and β5i/LMP7$^{-/-}$ heart sections were evaluated. The major fraction of invading inflammatory cells was comprised of Mac-3^{+} macrophages and CD3^{+} T lymphocytes in both strains (**Fig. 6**A). Quantification of positive cell signals per visual field at a 20-fold magnification resulted in significantly enhanced absolute numbers of T lymphocytes in β5i/LMP7$^{-/-}$ mice as compared to C57BL/6 mice (**Fig. 6**B).

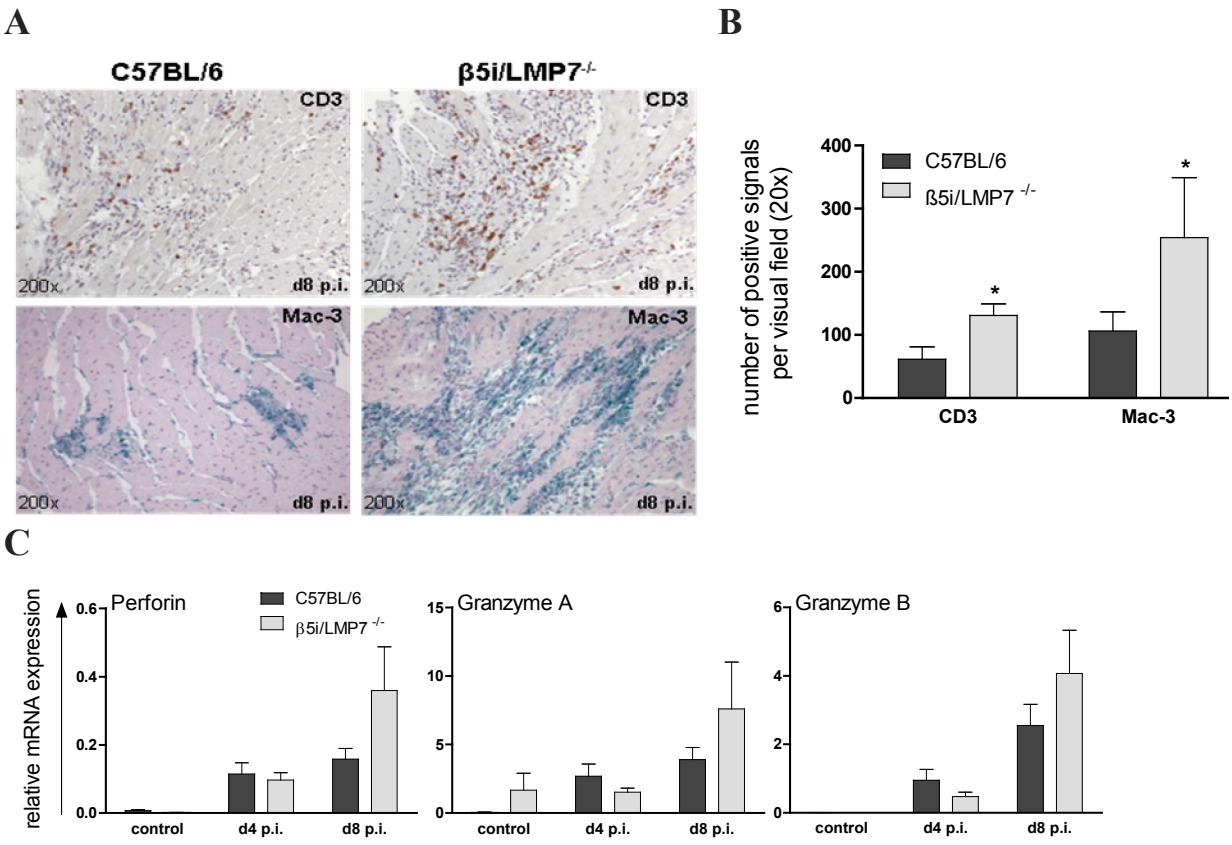

Fig. 6 Characterization of myocardial lesions. A: Immunostaining for CD3^{+} T lymphocytes and Mac-3^{+} macrophages was performed. Representative d8 p.i. cardiac tissue sections are shown (n≥6 mice/group). No specific signals were detected in non-infected control mice. **B:** Quantification of immunohistochemically positive cells in C57BL/6 and β5i/LMP7$^{-/-}$ heart sections was achieved by counting all positive cells per visual field at a magnification of x20 (n≥5 mice/group+SEM). **C:** The mRNA expression of T cell-induced cytotoxic mediators was determined by quantitative real-time PCR in the hearts of C57BL/6 and β5i/LMP7$^{-/-}$ mice at d0, d4, and d8 p.i. (n≥6 mice+SEM).

Significantly more Mac-3^{+} macrophages were found in β5i/LMP7$^{-/-}$ mice, whereby the differentiation of single signals was limited due to massive infiltration and staining, thus quantitative data do not reflect absolute macrophage numbers here. In non-infected control mice, no specific CD3^{+} T cell or Mac-3^{+} cell signals were detected.

Despite significant differences in T cell numbers, mRNA levels of perforin, granzyme A and granzyme B, which are released by cytotoxic T cells to eliminate virus-infected cells (125),

were detected to be within the same range in CVB3-infected C57BL/6 and β5i/LMP7-deficient hearts as determined by quantitative real-time PCR (**Fig. 6**C).

5.1.2 Investigation of cardiac function by microconductance pressure catheter measurement

Myocarditis-associated inflammation and cardiac cell necrosis can cause acute heart failure. With respect to the myocarditis scores of β5i/LMP7$^{-/-}$ and β1i/LMP2$^{-/-}$ mice, it was important to assess the left ventricular (LV) function at the acute stage of disease. Heart rate (HR), systolic and diastolic LV function were determined by microconductance pressure-volume catheter measurements in sham-treated and CVB3-infected mice at d8 p.i.

As shown in **Table 1**, HR was constant over the course of infection in all three strains. Also, no baseline differences for parameters of the systolic or diastolic performance were detected in non-infected β5i/LMP7$^{-/-}$ and β1i/LMP2$^{-/-}$ mice as compared to C57BL/6 mice.

Upon CVB3 infection, acute heart muscle injury in C57BL/6 and β5i/LMP7$^{-/-}$ mice was accompanied by an impaired systolic function at d8 p.i. as compared to their respective sham-treated controls (C57BL/6/β5i/LMP7$^{-/-}$: dP/dt_{max} -22.9/-28.9 %, LV P_{max} -18.2$^{\#}$/-21.1$^{\#}$ %, SV -23.5/-23.1 %). The EF, defined as the fraction of blood that is ejected out of the left ventricle relative to its end-diastolic volume, is reduced in β5i/LMP7$^{-/-}$ (-12 %), but not in C57BL/6 and β1i/LMP2$^{-/-}$ mice.

	control			CVB3 d8 p.i.		
	C57BL/6	β5i/LMP7 $^{-/-}$	β1i/LMP2 $^{-/-}$	C57BL/6	β5i/LMP7 $^{-/-}$	β1i/LMP2 $^{-/-}$
HR [bpm]	555.3 ± 12.5	521.1 ± 16.1	595.7 ± 10.8	549.2 ± 13.82	569.6 ± 21.1	567.7 ± 12.2
EF [%]	65.63 ± 1.3	66.18 ± 2.64	68.62 ± 1.2	66.4 ± 2.3	58.7 ± 8.1	72.18 ± 2.8
LV P_{max} [mmHg]	84.41 ± 2.7	81.38 ± 4.9	93.29 ± 1.2	69.03 ± 2.2 #	64.19 ± 2.7 #	81.91 ± 3.5
dP/dt_{max} [mmHg/s]	8597 ± 452.6	8116 ± 860.7	10324 ± 448.9	6620 ± 356.5	5771 ± 455.3	8252 ± 477.2
dP/dt_{min} [mmHg/s]	-4581 ± 173.5	-4160 ± 401.2	-5347 ± 145.2	-3562 ± 166.3	-3269 ± 256.4	-4311 ± 251
SV [µl]	20.9 ± 0.9	21.67 ± 0.9	20.35 ± 1.2	15.99 ± 1.4	16.66 ± 2.7	21.43 ± 1.9

HR	heart rate
LV P_{max}	maximum left ventricular pressure
dP/dt_{max}	maximum rate of left ventricular pressure rise
dP/dt_{min}	maximum rate of left ventricular pressure decrease
EF	ejection fraction
SV	stroke volume

Table 1 Investigation of left ventricular function by microconductance catheter measurement. Systolic and diastolic LV function was determined in sham-treated and CVB3-infected animals at d8 p.i. (n≥5 female mice/group±SEM, Two-Way ANOVA (SPSS): #statistical significance indicates strain-specific differences between d8 p.i. vs. respective controls d0 p.i., $p<0.05$).

Furthermore, diastolic LV function limitations were monitored in CVB3-infected C57BL/6 and β5i/LMP7$^{-/-}$ mice as demonstrated for the minimum rate of pressure change dP/dt_{min}. This parameter of left ventricular relaxation was reduced in both, C57BL/6 and β5i/LMP7$^{-/-}$ mice at d8 p.i. (C57BL/6/β5i/LMP7$^{-/-}$: dP/dt_{min} -22.2/-21.4 %). In agreement with the limited myocardial damage in β1i/LMP2$^{-/-}$ mice (**Fig. 5**A), cardiac function was preserved in these mice. Systolic and diastolic LV function parameters of CVB3-infected β1i/LMP2$^{-/-}$ mice were found to be in the same range as sham-treated C57BL/6 control mice.

5.1.3 Determination of viral load by *in situ* hybridization, qRT-PCR and plaque assay

The question whether the divergent phenotype of β5i/LMP7$^{-/-}$ respectively β1i/LMP2$^{-/-}$ mice was attributed to different CVB3 replication was analyzed by the determination of the viral load. As demonstrated by CVB3 *in situ* hybridization (ISH), virus positive cardiomyocytes were detected within inflammatory lesions (**Fig. 7**A), a fact that is pathognomonic in viral myocarditis. Scoring of CVB3-positive cardiomyocytes suggested equal viral replication in both, C57BL/6 and β5i/LMP7$^{-/-}$ mice, whereas the ISH score of β1i/LMP2$^{-/-}$ mice was significantly lower (**Fig. 7**B). Furthermore, titers of infectious CVB3 particles were found to be within the same range in heart homogenates of C57BL/6 and β5i/LMP7$^{-/-}$ mice as determined by plaque assay (**Fig. 7**C). In agreement with the lower ISH score, the viral load was found to be considerably reduced in heart homogenates of β1i/LMP2$^{-/-}$ mice (**Fig. 7**C). Observations from *in situ* hybridization and plaque assay were confirmed by quantitative real-time PCR, which demonstrated equal CVB3 replication in C57BL/6 and β5i/LMP7$^{-/-}$ hearts at an early and acute stage of disease. By contrast, viral replication was significantly reduced in β1i/LMP2$^{-/-}$ hearts. At a late stage of myocarditis, CVB3 replication was below the detection level in all three mice strains (**Fig. 7**D).

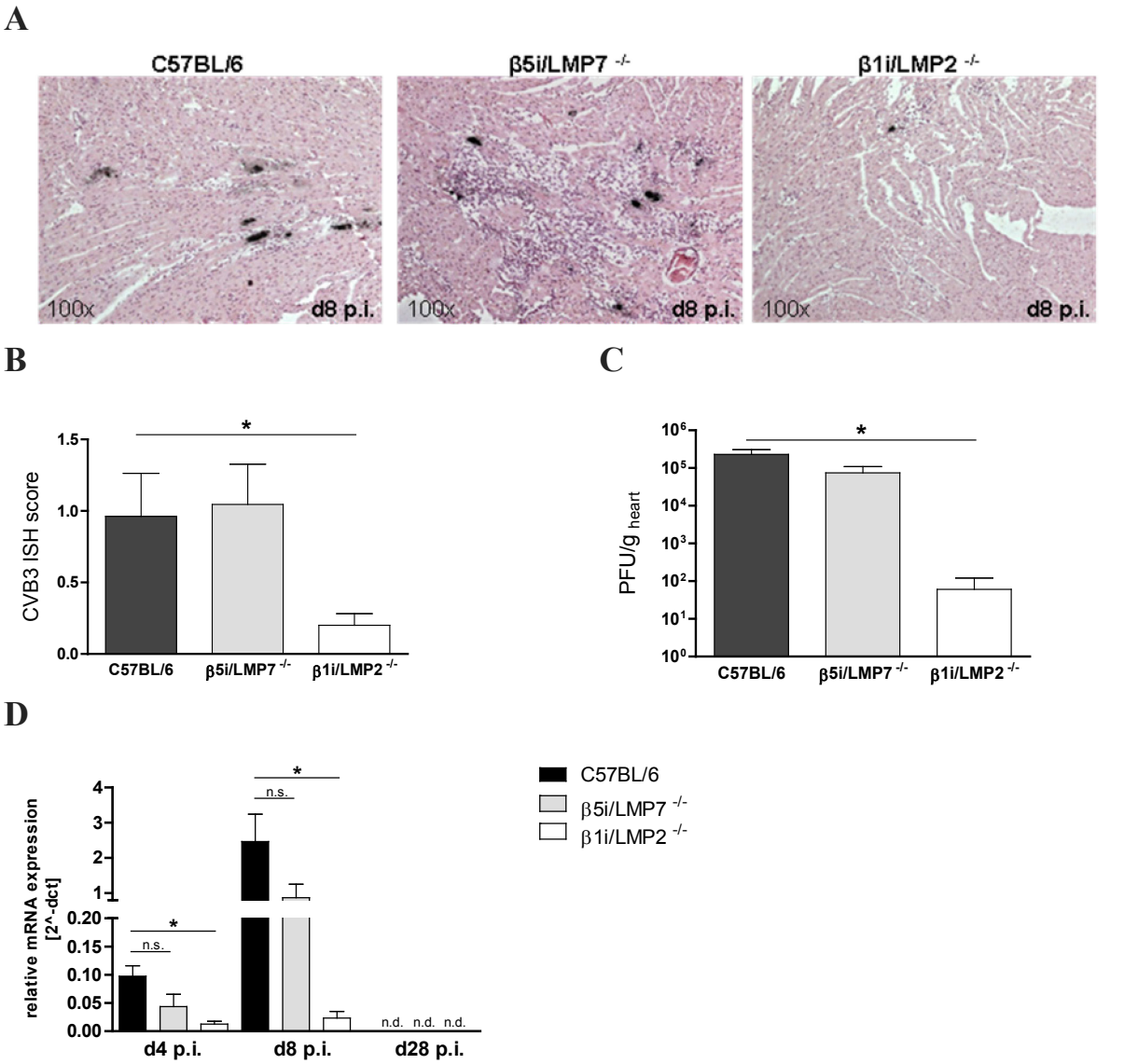

Fig. 7 Investigation of viral load. A: Representative strand-specific in situ hybridizations for genomic CVB3 RNA (black dots) in d8 p.i. hearts of C57BL/6, β5i/LMP7$^{-/-}$ and β1i/LMP2$^{-/-}$ mice are illustrated. **B:** The amount of CVB3 RNA detected by *in situ* hybridization of cardiac tissue sections was scored within a range from 0 to 4 (n≥5 mice/group). **C:** The amount of infectious viral particles in d8 p.i. hearts of CVB3-challenged mice was determined by plaque assay. **D:** Viral replication in CVB3-infected hearts was analyzed by real-time PCR at indicated time points (n≥7+SEM, *p<0.05).

To exclude potential *in vivo* factors that might have contributed to the restricted viral load in β1i/LMP2$^{-/-}$ mice, viral replication was examined in isolated primary cardiomyocytes. The purity of these *in vitro* cultures was determined by FACS analysis of troponin I expression, which is a heart muscle-specific protein. On average, more than 93 % of isolated cells expressed troponin I as exemplarily shown in **Fig. 8**B. Primary cardiomyocytes were infected

at MOI 0.5 and viral replication was determined by quantitative real-time PCR. No differences in CVB3 replication were detected in β5i/LMP7-deficient cells compared to C57BL/6 wildtype cells (**Fig. 8** left panel). On the contrary, viral replication was found to be restricted in β1i/LMP2$^{-/-}$ cardiomyocytes (**Fig. 8** right panel), which confirmed the *in vivo* findings. The use of different virus stocks and TaqMan master mixes for experiments with β5i/LMP7$^{-/-}$ and β1i/LMP2$^{-/-}$ cardiomyocytes may account for divergent relative expression values.

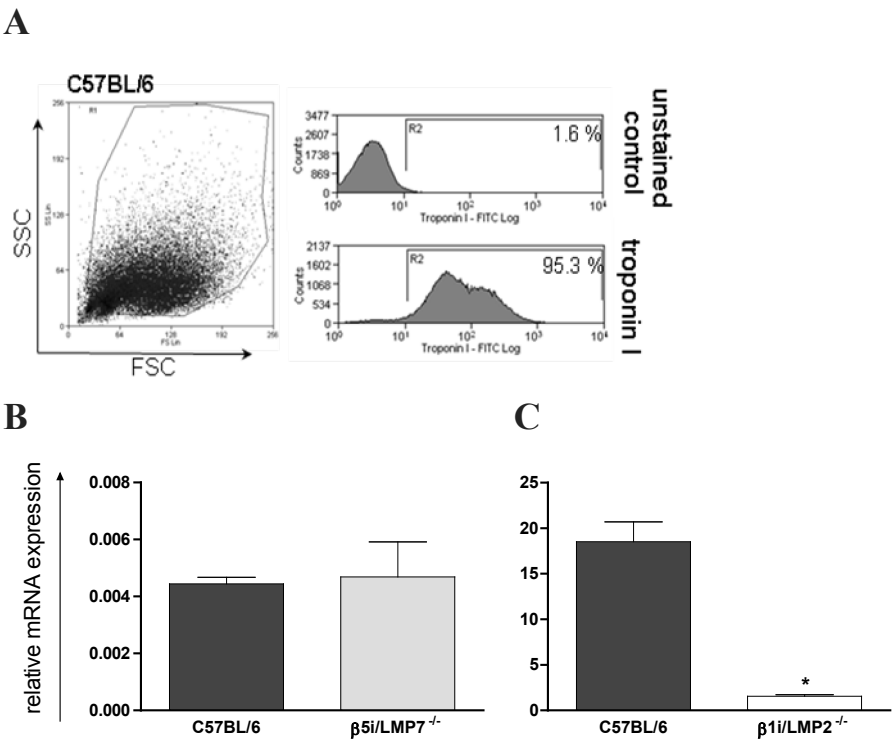

Fig. 8 Viral replication in primary cardiomyocytes. **A**: Purity of primary cardiomyocytes was determined by flow cytometry using a cardiomyocyte-specific troponin I antibody. Representative histograms are shown. **B:** CVB3 replication in primary C57BL/6 and β5i/LMP7$^{-/-}$ respectively C57BL/6 and β1i/LMP2$^{-/-}$ **(C)** cardiomyocytes was analyzed by quantitative real-time PCR. Cells were prestimulated with IFN for 24 h to induce IP-formation and infected at MOI 0.5 for 8 h. Data are representative for 3 independent experiments (*$p<0.01$).

5.1.4 Characterization of cardiac IP formation by qRT-PCR, Western blot analysis and mass spectrometry

To explain the function of IPs in the context of CVB3 myocarditis, information about the subunit composition of β5i/LMP7$^{-/-}$ and β1i/LMP2$^{-/-}$ proteasomes was required. Therefore, cardiac mRNA was isolated and 20S proteasomes were purified from sham-treated and CVB3-infected heart homogenates.

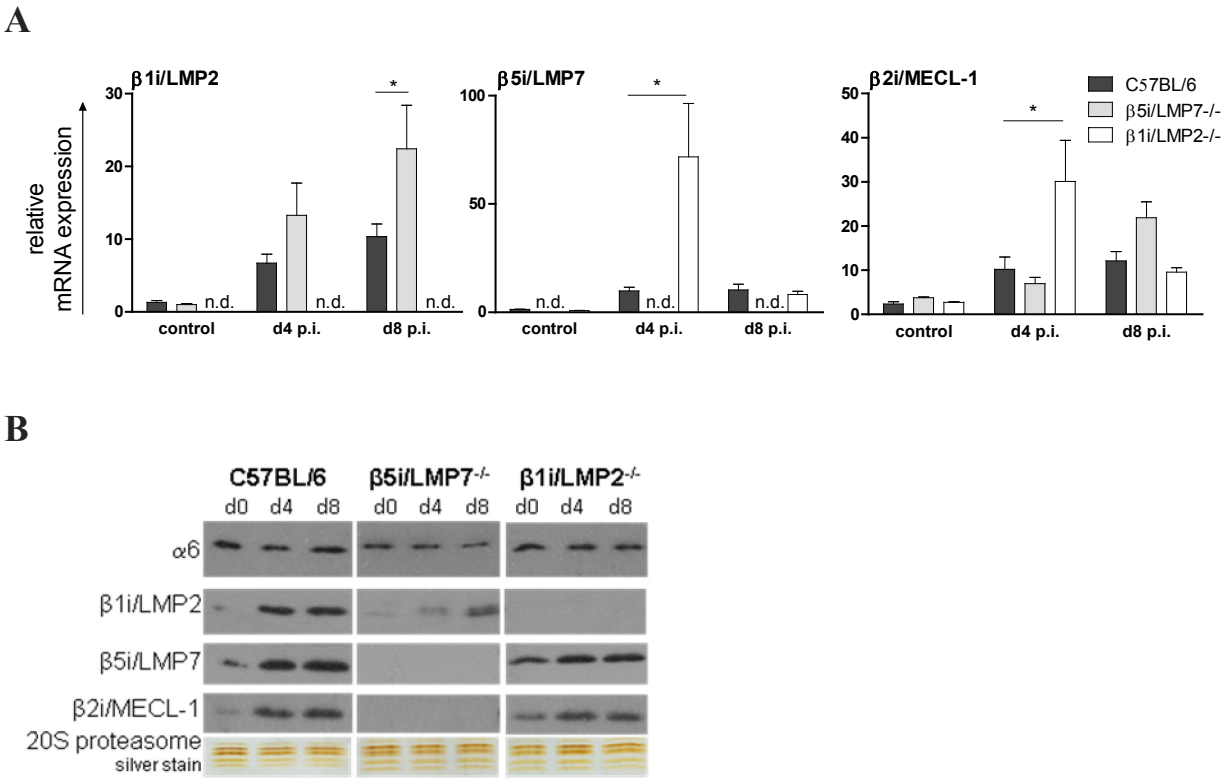

Fig. 9 Characterization of 20S proteasomes of CVB3 challengend mice. A: Cardiac mRNA expression of β1i/LMP2, β2i/MECL1, and β5i/LMP7 was quantified by real-time PCR in sham-treated control mice and at d4 and d8 p.i. (n≥5 mice/group+SEM). **B:** Subunit incorporation was investigated by immunoblotting of purified cardiac 20S proteasomes (α6 and silverstaining as loading controls). Data are representative for two individual 20S proteasome purifications (pool of n=5 mice per group and experiment).

As determined by quantitative real-time PCR, mRNA expression of β1i/LMP2 was induced in C57BL/6 and β5i/LMP7-deficient hearts upon CVB3 infection. Expression of β5i/LMP7 mRNA was enhanced in C57BL/6 and β1i/LMP2-deficient hearts; and MECL-1 mRNA expression was increased in all three strains at d4 p.i. (**Fig. 9**A). Immunoblot analysis of purified 20S proteasomes demonstrated similar levels of β5i/LMP7 and β2i/MECL-1 subunits in C57BL/6 and β1i/LMP2-deficient hearts at d4 and d8 p.i. By contrast, 20S proteasomes isolated from CVB3 infected β5i/LMP7$^{-/-}$ hearts showed no β2i/MECL-1 and only impaired β1i/LMP2 incorporation (**Fig. 9**B).

Quantification of each proteasome subunit within the 20S core was performed by high resolution LTQ-Orbitrap mass spectrometry (MS) analysis after separation of cardiac tryptic peptides by reverse phase nano HPLC. In C57BL/6 hearts, all three inducible subunits β1i/LMP2 (3.5-fold induction; $p<0.05$), β2i/MECL-1 (2.6-fold induction; $p<0.05$), and β5i/LMP7 (2.0-fold induction; $p=0.10$) were enhanced at d4 p.i. By contrast, neither

β1i/LMP2 (1.3-fold; p=0.67) nor β2i/MECL-1 (1.5-fold; p=0.38) were found to be increased in cardiac 20S proteasomes of β5i/LMP7$^{-/-}$ mice at this stage of disease.

A

C57BL/6 / β5i/LMP7$^{-/-}$	**control**		**d4 p.i.**		**d8 p.i.**	
	Ratio	**p-value**	**Ratio**	**p-value**	**Ratio**	**p-value**
α2	1.18	0.51	1.01	0.99	1.03	0.93
β4	1.17	0.51	1.06	0.84	1.12	0.68
β1	1.19	0.48	1.18	0.63	1.1	0.72
β2	1.37	0.29	1.27	0.5	1.08	0.77
β5	1.12	0.71	0.96	0.91	0.76	0.41
β5i/LMP7	**n.d.**	**-**	**n.d.**	**-**	**n.d.**	**-**
β1i/LMP2	**1.32**	**0.48**	**3.7**	**0.04**	**1.82**	**0.18**
β2i/MECL1	**5.25**	**0.01**	**9.18**	**< 0.001**	**2.64**	**< 0.001**

B

C57BL/6 / β1i/LMP2$^{-/-}$	**control**		**d4 p.i.**		**d8 p.i.**	
	Ratio	**p-value**	**Ratio**	**p-value**	**Ratio**	**p-value**
α2	1.26	0.46	1.05	0.87	0.94	0.86
β4	1.21	0.46	1	0.99	0.94	0.8
β1	1.26	0.41	1.15	0.65	1.08	0.79
β2	1.54	0.19	0.97	0.91	0.95	0.88
β5	1.39	0.38	1.11	0.76	0.96	0.92
β5i/LMP7	**1.14**	**0.64**	**0.97**	**0.93**	**1.12**	**0.65**
β1i/LMP2	**n.d.**	**-**	**n.d.**	**-**	**n.d.**	**-**
β2i/MECL1	**3.59**	**0.025**	**4.38**	**0.0031**	**3.83**	**< 0.001**

Table 2 Quantification of cardiac 20S proteasome subunits by mass spectroscopy. 20S proteasomes were isolated from heart homogenates of sham-treated or CVB3-infected mice. The total 20S fraction was separated into subtypes by reverse phase nano HPLC prior to mass spectroscopy (Orbitrap-MS). MS ion intensities are shown for each proteasome subunit as a ratio between C57BL/6 and β5i/LMP7$^{-/-}$ mice **(A)** respectively C57BL/6 and β1i/LMP2$^{-/-}$ mice **(B)**. Data represent mean±SD from two technical replicates, each perfomed with two biological replicates (*p<0.05, n.d.: ratio not determined in β5i/LMP7$^{-/-}$ respectively in β1i/LMP2$^{-/-}$ mice, statistical significance is based on C57BL/6 wildtype controls).

In accordance with mRNA expression data and immunoblot analysis of β1i/LMP2-deficient heart homogenates, β5i/LMP7 (2.9-fold; p=0.001) and β2i/MECL-1 (2.8-fold, p=0.003) subunits were incorporated into β1i/LMP2$^{-/-}$ 20S complexes at d4 p.i. despite the lack of β1i/LMP2. As expected, no significant differences in the presence of constitutive catalytic and non-catalytic subunits were detected (as exemplarily shown for β1, β2, β5 respectively α2 and β4). Notably, β5i/LMP7$^{-/-}$ (5.25-fold, p=0.01) and β1i/LMP2$^{-/-}$ (3.59, p=0.025) mice show baseline deficits to incorporate β2i/MECL-1 as compared to C57BL/6 mice (**Table 2**A/B).

This failure was exacerbated over the course of CVB3 infection. Incorporation of β5i/LMP7 was not affected by β1i/LMP2-deficiency, neither in naive nor in CVB3-challenged hearts (**Table 2**B). These data point towards a substantial impairment of IP assembly in β5i/LMP7$^{-/-}$ mice and the expression of intermediate proteasomes in β1i/LMP2$^{-/-}$ mice during acute myocarditis.

5.2 Characterization of the adaptive immune response in β1i/LMP2$^{-/-}$ and β5i/LMP7$^{-/-}$ mice

During the effector phase of a virus-specific adaptive immune response, CD8$^+$ T cells migrate to the target organ of infection. The cytotoxic T cell (CTL) response to pathogens is directed against antigenic epitopes, that are processed by proteasomes and presented by MHC class I molecules. Immunoproteasomes have been shown to optimize the quantity and quality of peptide ligands in several infection models. Due to the finding that a potent CD8$^+$ T cell response is important to mediate CVB3 virus elimination (33;126), it was of great interest to investigate the effect of β1i/LMP2- and β5i/LMP7-deficiency on CD8$^+$ T cell immunity in CVB3 myocarditis. Previous *in vitro* processing studies demonstrated, that cardiac IP formation is linked to the preferential generation of CVB3-specific epitopes as compared to standard proteasomes (118).

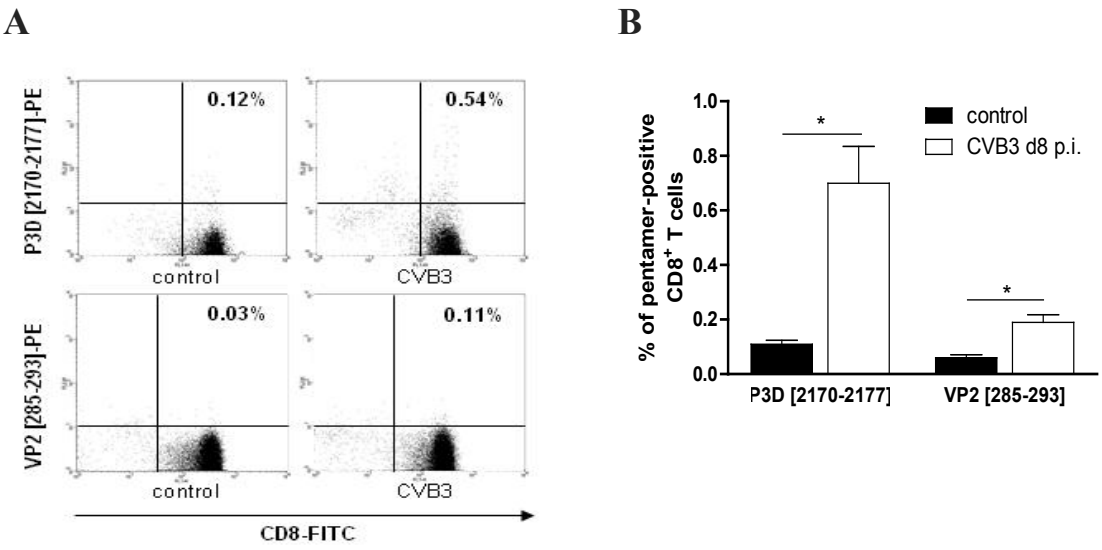

Fig. 10 Frequencies of CVB3 epitope-specific T cells in acute myocarditis. CD8$^+$ T cells isolated from naive and CVB3-infected C57BL/6 mice (d8 p.i.) were stained with H-2D^b VP2 [285-293]-PE and H-2K^b P3D [2170-2177]-PE pentamers vs. CD8-FITC. **A:** Representative dot plots for each pentamer are shown. Cells in the upper right quadrant indicate CVB3-specific CD8$^+$ T cells. **B:** The average percentage of pentamer-positive CD8$^+$ T cells is illustrated (n=4+SEM *p< 0.05).

To test the potential of these epitopes to elicit an antigen specific $CD8^+$ T cell response *in vivo*, $CD8^+$ T cell were isolated from sham-treated and CVB3-infected C57BL/6 mice and stained with epitope-specific P3D [2170-2177] and VP2 [285-293] phycoerythrin (PE)-coupled pentamers.

FACS analysis revealed a CVB3-specific response in infected C57BL/6 mice, that was predominantly directed against P3D [2170-2177] and to a lesser extend against VP2 [285-293] (**Fig. 10**B).

5.2.1 $CD8^+$ T cell function

Overall P3D- and VP2-specific $CD8^+$ T cell frequencies were rather low (<1 %, see **Fig. 10**) and the existence of other, so far unknown epitopes could not be excluded. To study whether IP-deficiency has an impact on the function of $CD8^+$ T cells despite these limitations, adoptive transfer of cytotoxic $CD8^+$ T cells was performed. For this purpose, $CD8^+$ T cells were isolated from total splenocytes of CVB3-infected C57BL/6 wildtype, β1i/$LMP2^{-/-}$ and β5i/$LMP7^{-/-}$ donor mice, respectively. MACS separation resulted in at least 89 % purity of $CD8^+$ T cells as representatively shown in **Fig. 11**.

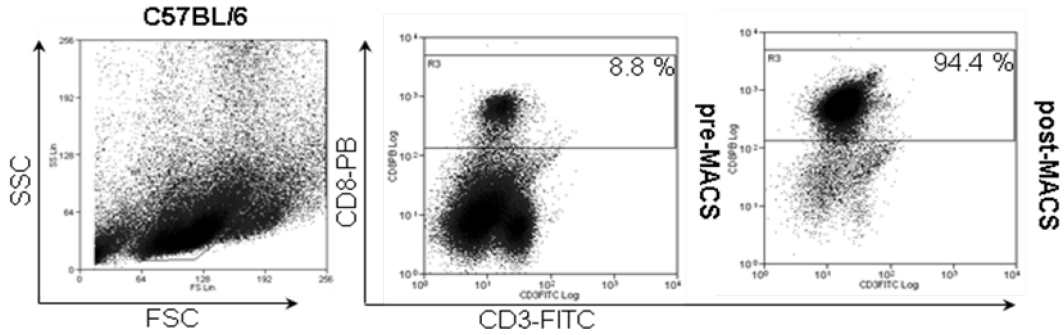

Fig. 11 Purity of $CD8^+$ T cells. $CD8^+$ T cells were isolated from total splenocytes of CVB3-infected animals by MACS separation. After fluorescent labeling of cells with anti-CD3-FITC and anti-CD8-PB antibodies, purity was determined by flow cytometry. Representative dot blots indicate the percentage of $CD3^+/CD8^+$ T cells prior and after MACS separation.

To preclude effects of IP-deficiency on T cell survival, $CD8^+$ T cells from CVB3-challenged β5i/$LMP7^{-/-}$ and β1i/$LMP2^{-/-}$ mice (both CD45.2) were transferred into B6.SJL-Ptprca Pepcb/BoyJ mice (CD45.1) and vice versa. After transfer, recipient mice were immediately infected, and the amount of donor $CD8^+$ T cells was determined at d8 p.i. Therefore, total splenocytes were stained with anti-CD8-PB and anti-CD45.1-PerCPCy5 respectively anti-CD45.2-FITC antibodies and analyzed by flow cytometry.

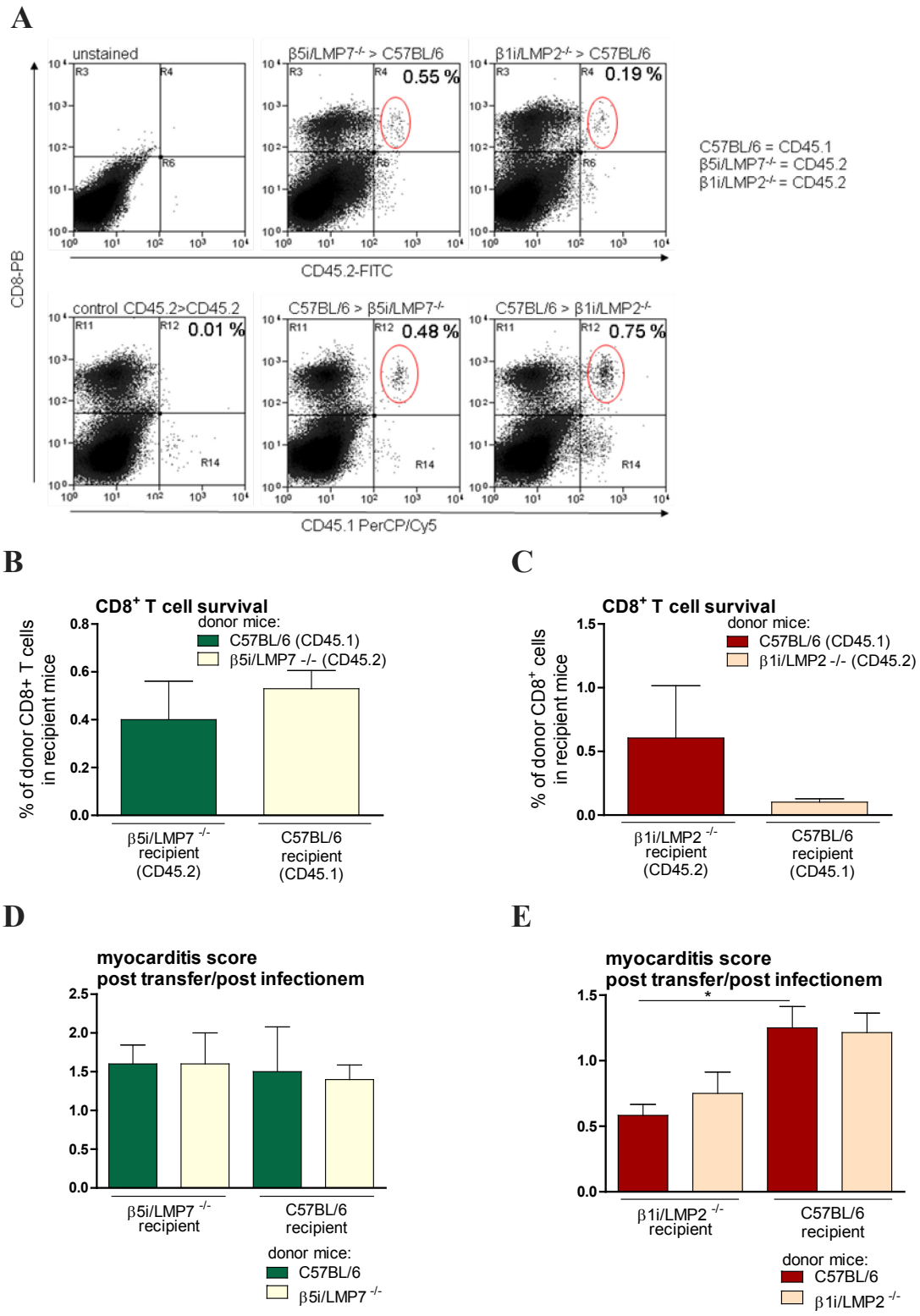

Fig. 12 Adoptive CD8$^+$ T cell transfer. 1–2×10^6 CD8$^+$ T cells were transferred from one CVB3 infected C57BL/6 (CD45.1) into one β5i/LMP7$^{-/-}$ respectively β1i/LMP2$^{-/-}$ (CD45.2) mouse and vice versa. Recipient mice were infected with CVB3 and the survival of donor CD45.1 and CD45.2 T cells was determined by FACS analysis at d8 p.i. **A:** The gating strategy is exemplarily shown for the transfer of CD8$^+$ T cells from C57BL/6 (CD45.1) respectively β5i/LMP7$^{-/-}$ (CD45.2) mice and vice versa. **B/C:** The average percentage of donor CD8$^+$ T cells is illustrated (n=5 mice/group). **D/E:** After transfer of donor CD8$^+$ T cells and CVB3 infection, the myocardial damage of the recipient mice was evaluated by hematoxylin-eosine staining at d8 p.i. (n=5 mice/group, representative for two independent experiments, *p<0.05).

CD8 positive T cells were gated as illustrated in **Fig. 12**A and the fraction of donor $CD8^+/CD45^+$ T cells was determined.

Deficiency of β5i/LMP7 had no effect on T cell survival in the respective recipients (**Fig. 12**B). By contrast, donor $CD8^+$ T cells from β1i/LMP2-deficient mice showed decreased survival rates as compared to IP-competent lymphocytes (**Fig. 12**C).

To get more functional insights concerning $CD8^+$ T cell responses with respect to the target organ of CVB3 infection, heart tissue injury was assessed after adoptive transfer of $CD8^+$ T cells by hematoxylin-eosine staining. Myocarditis scores of β5i/LMP7-competent and β5i/LMP7-deficient recipient mice were found to be within the same range, independent from the origin of donor $CD8^+$ T cells (**Fig. 12**D). By contrast, myocarditis scores of β1i/$LMP2^{-/-}$ recipient mice were significantly lower compared to C57BL/6 recipients (**Fig. 12**E). However, no protective or deleterious effects on the extent of acute myocardial injury were observed in these recipients upon transfer of β1i/LMP2-competent or β1i/LMP2-deficient $CD8^+$ T cells.

5.2.2 Determination of CVB3-specific IgG titers by ELISA

B cells isolated from C57BL/6 mice preferentially express IPs (127), and a CVB3-specific IgG antibody response contributes to an efficient virus elimination in CVB3 myocarditis (128). Therefore, it was important to characterize the function of IPs for the induction of a systemic B cell response in CVB3 myocarditis. CVB3-specific antibodies IgG titers were determined in sera of C57BL/6, β5i/$LMP7^{-/-}$ and β1i/$LMP2^{-/-}$ mice at d8 and d28 p.i.

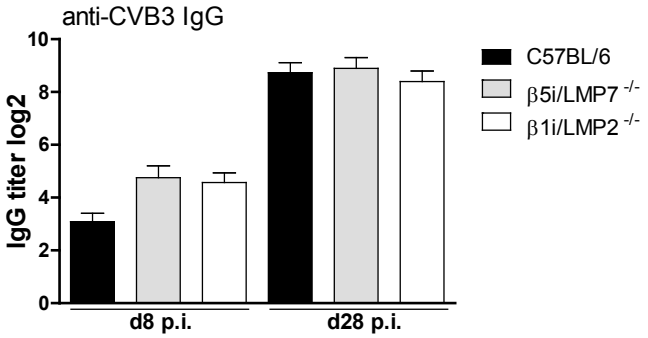

Fig. 13 Determination of CVB3-specific antibody titers. Titers of virus-specific IgG antibodies were assessed in sera of C57BL/6, β5i/$LMP7^{-/-}$ and β1i/$LMP2^{-/-}$ mice at indicated time points by a CVB3-specific ELISA (n≥8+SEM).

Serum levels of anti-CVB3 IgG antibodies were within the same range in all three investigated strains at d8 p.i. (**Fig. 13**). By day 28 p.i., an increase of IgG titers was observed,

whereby no strain-specific differences were detected, which demonstrated that β5i/LMP7- and β1i/LMP2-deficient mice were capable of generating an efficient high affinity antibody response.

5.2.3 Characterization of splenic cell subpopulations by FACS analysis

As mentioned before, immune cells, including T and B cells as well as professional APCs such as dendritic cells, constitutively express IPs (129;130). To investigate whether IP expression is important for the maintenance of homeostatic T and B cell levels, the percentage of splenic $CD3^+/CD4^+$, $CD3^+/CD8^+$ T cells, and $CD19^+/B220^+$ B cells was determined by FACS analysis over the course of CVB3 infection. The relative amount of $CD4^+$ T, $CD8^+$ T and B cells was not affected in sham-treated or CVB3-infected β5i/$LMP7^{-/-}$ mice as compared to C57BL/6 mice.

A

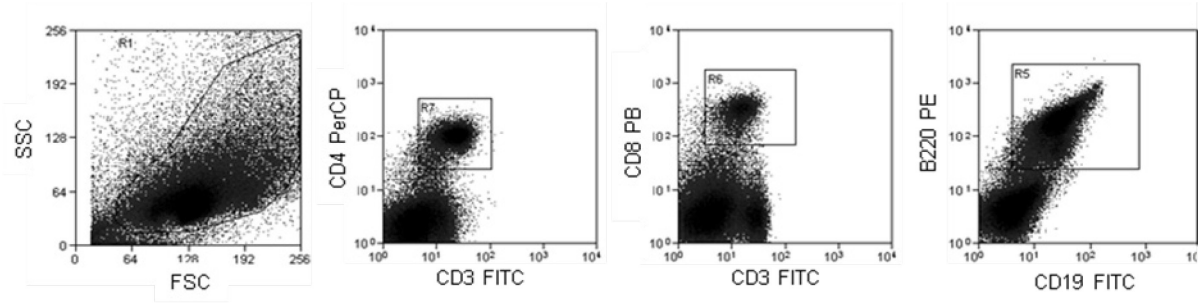

B

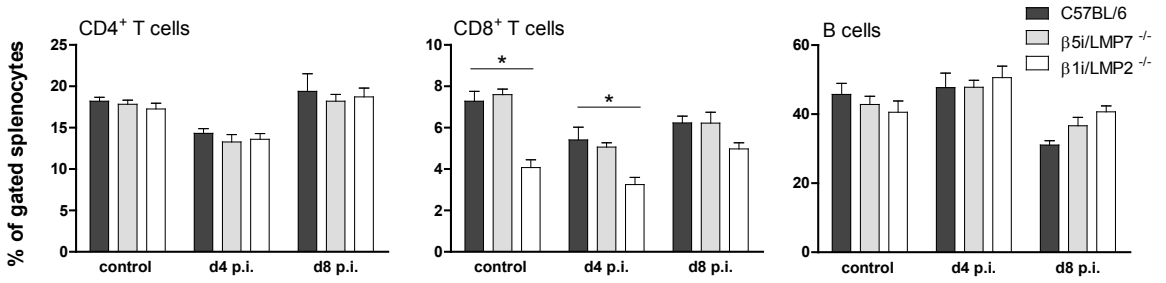

Fig. 14 FACS analysis of total splenocytes. Single splenocyte suspensions of C57BL/6, β5i/$LMP7^{-/-}$ and β1i/$LMP2^{-/-}$ mice were prepared and the percentage of splenic subpopulations was determined by flow cytometry at d0, d4 and d8 p.i. **A:** $CD3^+/CD4^+$, $CD3^+/CD8^+$ T cells, and $CD19^+/B220^+$ B cells were gated as demonstrated and **B:** the the relative amount of these subpopulations was determined ($n \geq 8$ mice/group,*$p<0.05$).

By contrast, the relative amount of $CD8^+$ T cells was significantly reduced in sham-treated β1i/$LMP2^{-/-}$ mice and in CVB3-infected β1i/$LMP2^{-/-}$ mice at d4 p.i., whereas no differences in

the relative number of $CD4^+$ T cells as well as B cells were observed as compared to C57BL/6 wildtype mice (**Fig. 14**B).

Interestingly, quantification of total splenocytes resulted in significantly lower absolute numbers in naive β1i/$LMP2^{-/-}$ control mice as compared with C57BL/6 and β5i/$LMP7^{-/-}$ control mice (**Fig. 15**A). Upon CVB3 infection, a 3-fold increase in total splenocytes was observed in β1i/$LMP2^{-/-}$ mice in contrast to C57BL/6 and β5i/$LMP7^{-/-}$ mice at d8 p.i. Absolute numbers of splenic subpopulations were determined in naive mice by multiplying splenic frequencies by the total cell number (per spleen). As illustrated in **Fig. 15**B, naive β1i/$LMP2^{-/-}$ mice had significantly reduced baseline numbers of splenic $CD4^+$, $CD8^+$ and B cells. Splenic hyperplasia as observed upon CVB3 infection in β1i/$LMP2^{-/-}$ mice explains equal relative amounts of $CD8^+$ T cells in β1i/$LMP2^{-/-}$ mice compared to C57BL/6 mice at d8 p.i. (**Fig. 7** middle panel).

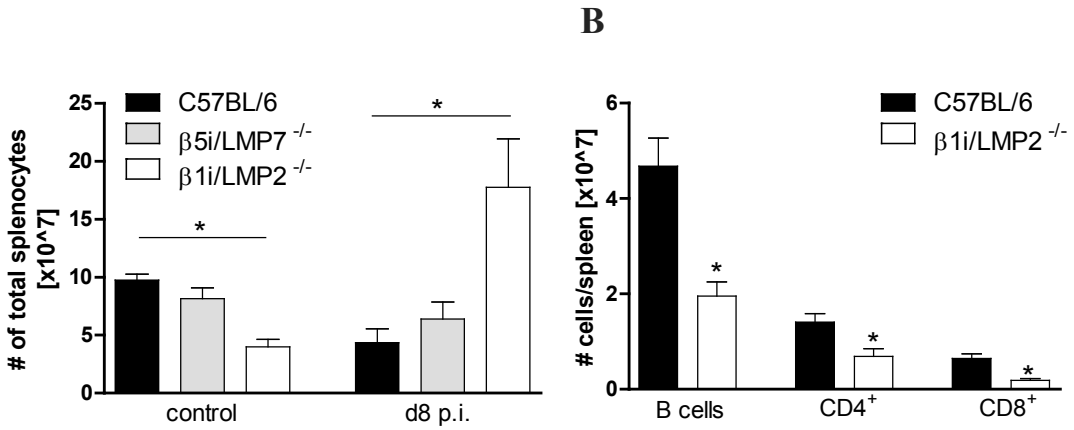

Fig. 15 Quantification of absolute splenocyte numbers in naive mice. A: The absolute number of splenocytes was determined by counting total splenocytes. **B:** Subsequent calculation of $CD3^+/CD4^+$, $CD3^+/CD8^+$ T cell and $CD19^+/B220^+$ B cell numbers based on ratios from FACS analysis by multiplying splenic frequencies by the total number of cells from each spleen ($n \geq 4$, $*p<0.05$).

5.3 The function of β1i/$LMP2^{-/-}$ in CVB3 myocarditis

The protective phenotype of β1i/$LMP2^{-/-}$ mice in CVB3 myocarditis was not expected, as β1i/LMP2- deficiency was previously linked to detrimental effects on the antiviral immune response as shown for influenza A infection models (127;131). To exclude the possibility that differences in the expression of the coxsackie- and adenovirus receptor (CAR) caused diminished viral replication in β1i/$LMP2^{-/-}$ mice, immunoblot analysis of heart homogenates

was performed. CAR expression was shown to be within the same range in β1i/LMP2$^{-/-}$ and IP-competent C57BL/6 mice (**Fig. 16**).

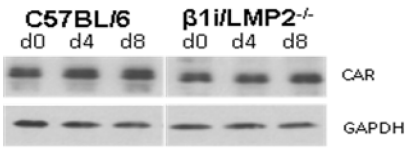

Fig. 16 Investigation of CAR expression. CAR expression was determined in heart homogenates of C57BL/6 and β1i/LMP2$^{-/-}$ mice by Western blot analysis. GAPDH is shown as loading control (pool of n=5 mice).

5.3.1 Gene expression analysis by Affymetrix microarray

A whole genome gene expression profile was generated in order to identify possible pathways or signaling regulators that may contribute to restricted viral replication in β1i/LMP2$^{-/-}$ mice. Affymetrix GeneChip microarray analysis revealed the transcriptional regulation of various genes that were differently expressed in CVB3-challenged β1i/LMP2$^{-/-}$ hearts as shown for intensity profiles in **Fig. 17**A (n=4). In sham-treated β1i/LMP2$^{-/-}$ mice, mRNA expression of interferon inducible genes Ifi202b, histocompatibility antigen HA-28 and guanylate binding protein GBP-1 was detected. Notably, mRNA levels of these genes significantly increased during the early phase of CVB3 infection, whereas no expression was detected in C57BL/6 mice, neither in sham-treated control mice nor upon CVB3 infection. These data pointed towards a more general effect of β1i/LMP2-deficiency on the modulation of interferon-induced pathways.

Several cytokine effector pathways mediate the antiviral response by the degradation of viral RNA, blocking of viral transcription, or inhibition of translation. Four major pathways are involved: the ISG15 ubiquitin-like pathway (IFN-stimulated gene 15), the Mx-GTPase pathway (Myxovirus resistance protein), the protein kinase K pathway (PKR), and the 2′-5′oligoadenylate-synthetase-directed ribonuclease L pathway (OASL-2) (132). Interestingly, ISG15, Mx1, and PKR were differentially regulated in β1i/LMP2$^{-/-}$ mice over the course of CVB3 infection. To verify these findings, mRNA expression was confirmed by quantitative real-time PCR (n=6, $p<0.05$, **Fig. 17**B).

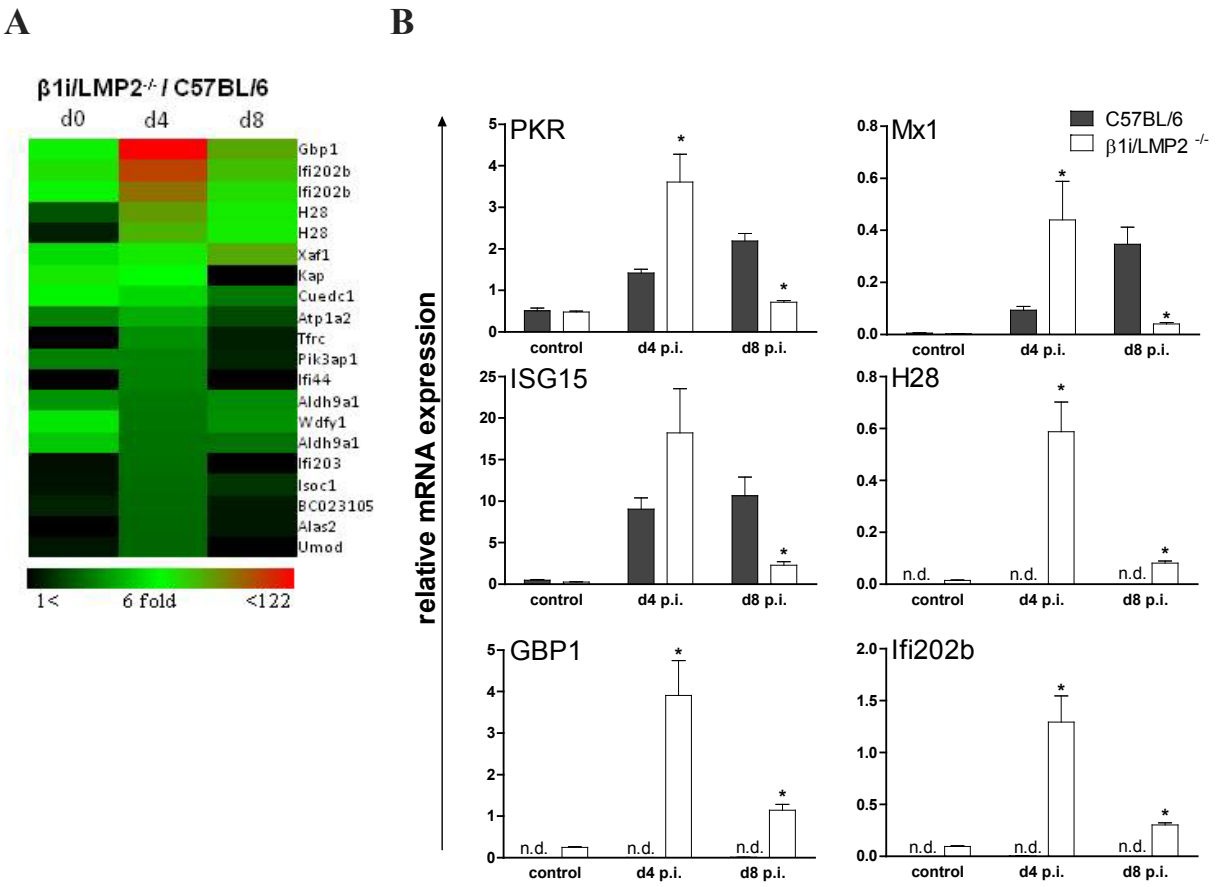

Fig. 17 Affymetrix microarray expression profiles and mRNA expression of potentially antiviral molecules. A: The affymetrix microarray heatmap depicts the regulation of genes over the course of CVB3 infection (fold change β1i/LMP2$^{-/-}$ to C57BL/6; color as illustrated, n=4 mice/group). **B:** Cardiac expression of indicated molecules at d4 and d8 p.i. was determined in the hearts of C57BL/6 and β1i/LMP2$^{-/-}$ mice by quantitative real-time PCR (n=6+SEM, *p<0.05).

5.3.2 Determination of the host genetic background by SNP analysis

At this stage, the completely different mRNA expression pattern in CVB3-infected β1i/LMP2$^{-/-}$ vs. IP-competent C57BL/6 hearts raised serious doubts, whether β1i/LMP2-deficient mice were of the required genetic background (C57BL/6). To address this question, a PCR-based single nucleotide polymorphism (SNP) panel was applied. The examined markers are spread across the genome at about 7 Mbp intervals, and allow the differentiation between the commonly used inbred mice strains C57BL/6(J), C57BL/6(N), SvJ/129, and C57BL/6 (JOlaHsd).

As illustrated in **Fig. 18**, a knockout animal is normally backcrossed against the required genetic background (here C57BL/6(J)), and with each filial generation, the average

percentage of the constant background increases. After sufficient reiterations, an animal of the desired knockout is of the required genetic background (N10, >99.9 % C57BL/6). Unfortunately, the analyzed samples only ranged from 82.68 % to 83.72 % C57BL/6(J) background, indicating that the animals had not been backcrossed to C57BL/6 for 10 generations. Instead, they looked like SvJ/129-C57BL/6 F1 offsprings that had been intercrossed for 10 generations (F10 instead of N10). SvJ/129 mice are frequently used to isolate embryonic stem cells, which can be modified by homologous recombination by gene targeting vectors (133). Importantly, these mice show a mild inflammatory response and diminished viral replication after CVB3 infection (134-136). Thus, the beneficial outcome of the β1i/LMP2$^{-/-}$ mice in comparison to C57BL/6 mice was rather caused by the genetic background than by the deletion of β1i/LMP2. Due to this finding, all obtained data regarding myocardial inflammation and viral replication cannot be interpreted appropriately. Hereinafter, the mixed background of β1i/LMP2$^{-/-}$ mice will be indicated as β1i/LMP2$^{-/-}$ (C57BL/6xSvJ129).

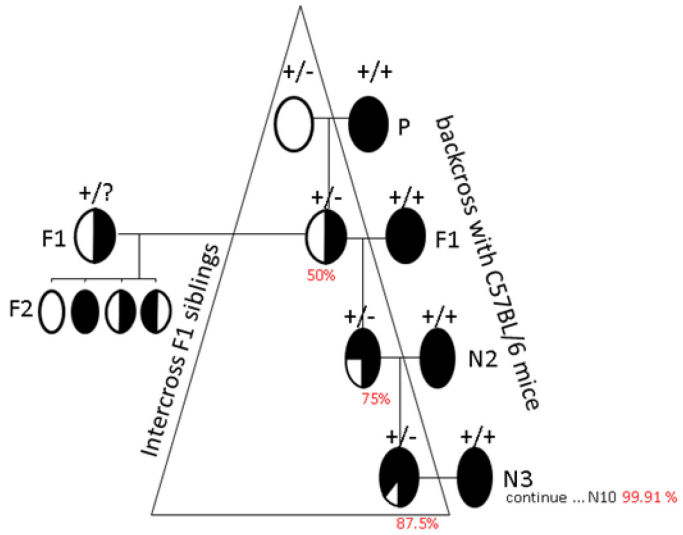

Fig. 18 Backcrossing scheme. 10 β1i/LMP2$^{-/-}$ mice were tested for their genetic background by a SNP panel directed against C57BL/6(J), C57BL/6(N) and SvJ/129 markers. Instead of correct backcrossing with C57BL/6 mice in order to obtain a constant genetic background of >99.9 % (right hand side), β1i/LMP2$^{-/-}$ offsprings of the F1 generation had been intercrossed (left hand side).

5.3.3 Characterization of myocardial damage and virus replication in C57BL/6xSvJ129 mice

To prove the idea that background artifacts caused the protective phenotype in β1i/LMP2-deficient mice and to re-examine the function of β1i/LMP2 in CVB3 myocarditis, myocardial damage was determined in β1i/LMP2-competent and β1i/LMP2-deficient mice, both having a mixed C57BL/6xSvJ129 background. For this purpose, β1i/LMP2$^{-/-\ (C57BL/6xSvJ129)}$ mice were crossed with C57BL/6(J) mice and CVB3 infection experiments were performed in β1i/LMP2$^{+/+\ (C57BL/6xSvJ129)}$ and β1i/LMP2$^{-/-\ (C57BL/6xSvJ129)}$ offsprings of the third filial generation (F3) (see **Fig. 19**A). Myocardial damage of CVB3-infected β1i/LMP2-competent and β1i/LMP2-deficient C57BL/6xSvJ129 mice was analyzed by hematoxylin-eosine staining at d8 p.i.

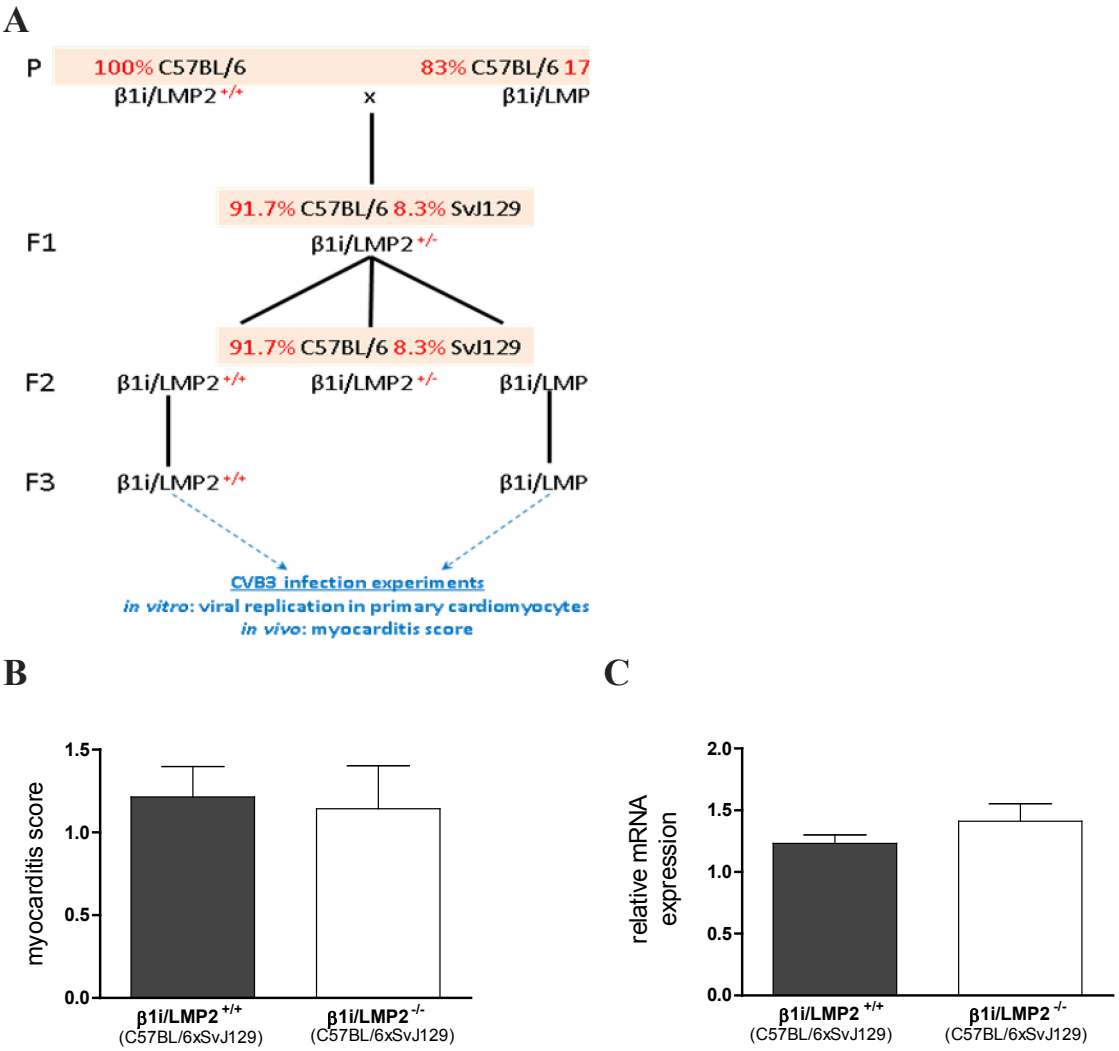

Fig. 19 Myocardial inflammation and CVB3 replication in C57BL/6xSvJ129 mice. A: β1i/LMP2$^{-/-\ (C57BL/6xSvJ129)}$ mice were crossed with C57BL/6(J) animals as depicted and CVB3 infection experiments were repeated in offsprings of the F2 generation. **B:** The myocarditis score was determined in cognate β1i/LMP2$^{+/+}$

$^{(C57BL/6xSvJ129)}$ and β1i/LMP2$^{-/-\ (C57BL/6xSvJ129)}$ mice at d8 p.i. (F2 generation; n=10 mice/group) by HE-staining. **C:** Primary cardiomyocytes were isolated from cognate β1i/LMP2$^{+/+\ (C57BL/6xSvJ129)}$ and β1i/LMP2$^{-/-\ (C57BL/6/SvJ129)}$ mice, infected at MOI 0.5 and harvested 8 h p.i. CVB3 replication was investigated by quantitative real-time PCR. Data are representative for 3 individual experiments.

By contrast to previous experiments in C57BL/6(J) and β1i/LMP2$^{-/-\ (C57BL/6xSvJ129)}$ mice, heart tissue injury was found to be within the same range in both, β1i/LMP2$^{+/+\ (C57BL/6xSvJ129)}$ and β1i/LMP2$^{-/-\ (C57BL/6xSvJ129)}$ mice (1.2±0.2 vs. 1.1±0.3; *$p<0.05$, **Fig. 19**B).

This finding indicates that β1i/LMP2-deficiency has no effect on the outcome of murine CVB3 myocarditis. Nevertheless, one has to keep in mind that the genetic background close to the target gene always reflects the original embryonal stem cell strain (133;137). Therefore, it is possible that the true effect of β1i/LMP2-deficiency in C57BL/6xSvJ129 mice was concealed by artifical transcriptional regulation.

Albeit detrimental impacts of β1i/LMP2-deficiency cannot be conclusively excluded *in vivo, in vitro* infection experiments of β1i/LMP2$^{+/+(C57BL/6xSvJ129)}$ and β1i/LMP2$^{-/-(C57BL/6xSvJ129)}$ cardiomyocytes strongly supported the notion that β1i/LMP2-deficiency has no influence on murine CVB3 myocarditis. Primary cardiomyocytes from β1i/LMP2$^{+/+\ (C57BL/6/SvJ129)}$ and β1i/LMP2$^{-/-\ (C57BL/6/SvJ129)}$ mice (see **Fig. 19**A) were pre-stimulated with IFN-γ to induce the expression of immunosubunits, infected at a MOI 0.5 and harvested after 8 h. CVB3 replication was then investigated by quantitative real-time PCR. By striking contrast to significantly reduced CVB3 replication in β1i/LMP2$^{-/-\ (C57BL/6/SvJ129)}$ cardiomyocytes in comparison to C57BL/6 wildtype cells (see **Fig. 8**A, right panel), no differences in viral replication were observed here (**Fig. 19**C). It is worth mentioning, that primary cells were isolated from up to 25 embryos per experiment. For that reason, genetic variability owing to the mixed C57BL/6xSvJ129 background was statistically better compensated *in vitro* than *in vivo*, where only ten animals per group were analyzed.

As the analysis of mixed background animals is experimentally unfavored, no further experiments concerning proteasome constitution or regulation of IFN-γ pathways were performed in β1i/LMP2-competent and -deficient C57BL/6xSvJ129 mice.

5.4 The function of β5i/LMP7$^{-/-}$ in CVB3 myocarditis

The background of the β5i/LMP7-deficient mice contained approximately 98.4 % C57BL/6-specific gene loci, which corresponds to the sixth backcross generation (N6). Consequently,

exacerbated CVB3-associated myocardial inflammation in β5i/LMP7-deficient mice was not caused by genetic background artifacts, but rather by the lack of intact IP-formation. The fact that both, C57BL/6 and β5i/LMP7$^{-/-}$ mice showed identical viral load, similar levels of CTL effectors, and viral clearance by d28 p.i. argued in favor of an effective CD8^{+} T cell response in β5i/LMP7$^{-/-}$ mice. These findings point towards other functions of β5i/LMP7 in the present model.

5.4.1 Determination of cytokine expression by qRT-PCR and Luminex® assay

Cytokines such as TNF-α, IFN-γ, and IL-6 are expressed in the myocardium upon CVB3 infection, which triggers immune cell infiltration (2;27). To study whether the *in vivo* cytokine response potentiated the inflammatory damage in β5i/LMP7$^{-/-}$ mice, TNF-α, IFN-γ, IFN-β, and IL-6 mRNA expression levels of CVB3-challenged hearts were determined by quantitative real-time PCR. The cardiac expression of the pro-inflammatory cytokines was induced in both, C57BL/6 and β5i/LMP7$^{-/-}$ mice upon CVB3 infection, but no strain-specific differences were observed for TNF-α, IFN-β, and IL-6 (**Fig. 20**). Only the mRNA level of IFN-γ was significantly increased in β5i/LMP7$^{-/-}$ hearts at d8 p.i.

Among others, IFN-γ induces the expression of IP-10 (IFN-γ-induced protein 10), which is an chemoattractive signal for macrophages and T cells. Also RANTES (**r**egulated upon **a**ctivation, **n**ormal **T**-cell **e**xpressed, and **s**ecreted), which is induced by TNF-α, recruits leucocytes to inflammatory lesions. To study whether differences in the expression of these regulatory proteins caused exacerbated inflammation, circulating levels of selected cytokines were measured in serum samples using a fluorescent bead-based assay system (Luminex®). However, serum levels of TNF-α, RANTES, IP-10, and MCP-1 (monocyte chemotactic protein-1) were found to be within the same range in both hosts during early inflammation (**Fig. 21**).

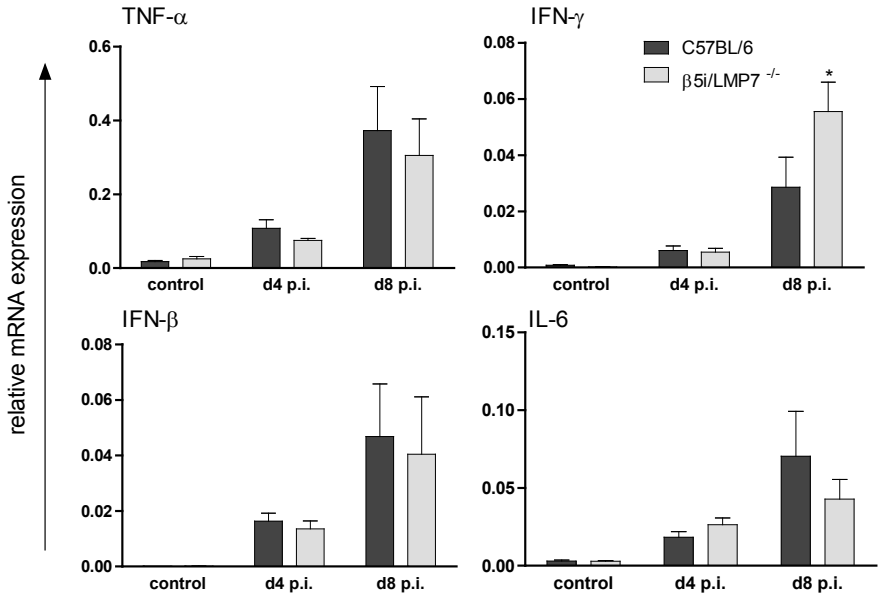

Fig. 20 mRNA expression of inflammatory cytokines. Expression of the indicated cytokines was assessed by quantitative real-time PCR in the hearts of C57BL/6 and β5i/LMP7$^{-/-}$ mice at d4 and d8 p.i. (n≥5 mice+SEM, *p<0.05).

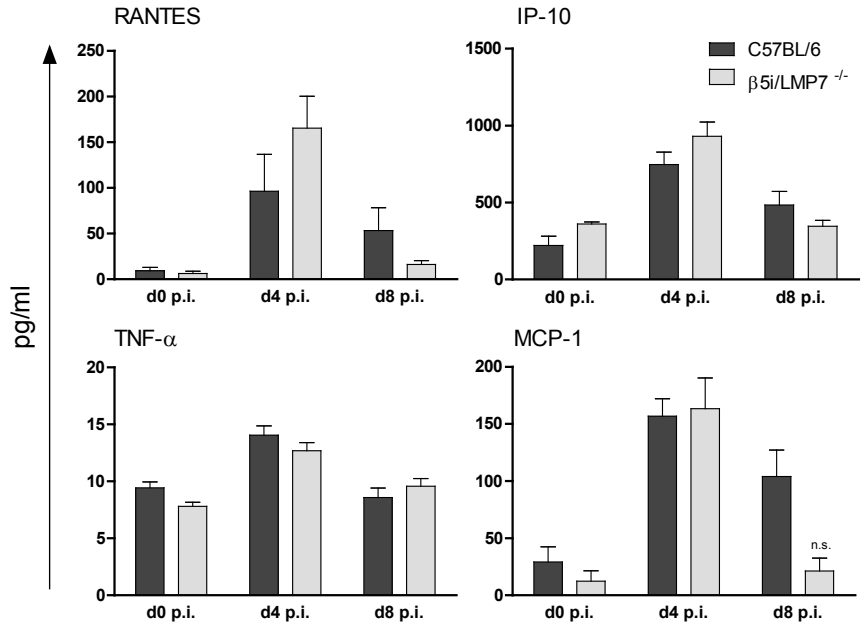

Fig. 21 Serum levels of cytokines. Serum levels of selected cytokines were analyzed by multiplex Luminex® assay at d4 and d8 p.i. (n≥5 mice+SEM).

5.4.2 Investigation of antiviral defense mediators by qRT-PCR

The expression of cytokines and antiviral genes is regulated early upon infection by a highly complex signaling system. For example, PKR mediates the activation of the central regulator

NF-κB, which in turn induces the expression of interferons. To analyze whether a differential expression of the antiviral pathway mediators ISG15, Mx1, PKR and OASL-2 played a role in the aggravation of inflammation in β5i/LMP7$^{-/-}$ mice, cardiac mRNA expression of these genes was determined in C57BL/6 and β5i/LMP7-deficient mice by quantitative real-time PCR. Upon CVB3 infection, mRNA expression levels increased in both, C57BL/6 and β5i/LMP7$^{-/-}$ mice (**Fig. 22**), but no strain-specific differences were detected.

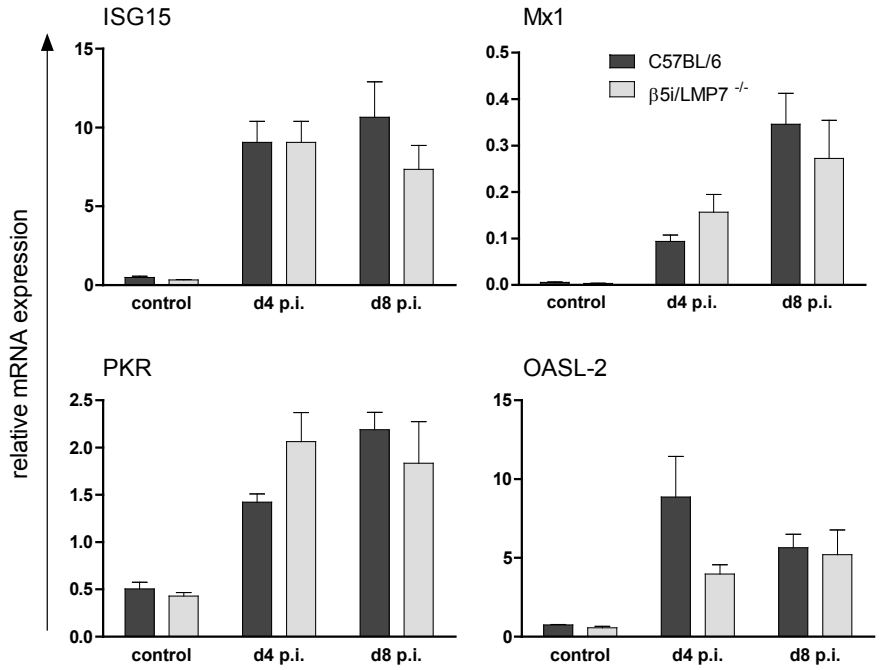

Fig. 22 mRNA expression of innate antiviral molecules. The cardiac expression of indicated antiviral molecules at d4 and d8 p.i. was determined in the hearts of C57BL/6 and β5i/LMP7$^{-/-}$ mice by quantitative real-time PCR (n≥5 mice+SEM).

5.4.3 Quantification of poly-Ub conjugates and oxidative protein damage by immunoblot analysis and immunofluorescence

As described above, exacerbated myocardial damage was detected in β5i/LMP7-deficient mice despite the induction of an effective antiviral response. Also, expression of pro-inflammatory cytokines was not enhanced in β5i/LMP7$^{-/-}$ mice, neither in the target organ of CVB3 infection nor systemically. Considering the importance of proteasomes for the maintenance of the cellular protein homeostasis, it was therefore necessary to study whether intact IP formation plays a critical role for proteostasis in response to cytokine-induced stress. As demonstrated, macrophages and T lymphocytes, that generally express IPs, represent the major fraction of the cellular infiltrate in CVB3-infected hearts (see **Fig. 6**), whereby B cells

are negligible. Upon virus infection, macrophages are activated and release pro-inflammatory cytokines such as TNF-α, but also reactive oxygen species (ROS) (138;139). Notably, exposure to cytokines (e.g. TNF-α) can induce ROS generation in non-infected target cells as well (140). This pro-inflammatory milieu represents a highly reactive environment for cardiomyocytes but also for the inflammatory cell itself. As a consequence of oxidative modification by oxygen free radicals or other reactive species, carbonyl groups are introduced into protein side chains in a site-specific manner. Here, it was investigated whether IPs are required to adapt to cytokine-induced protein accumulation and oxidation in cardiomyocytes and inflammatory cells.

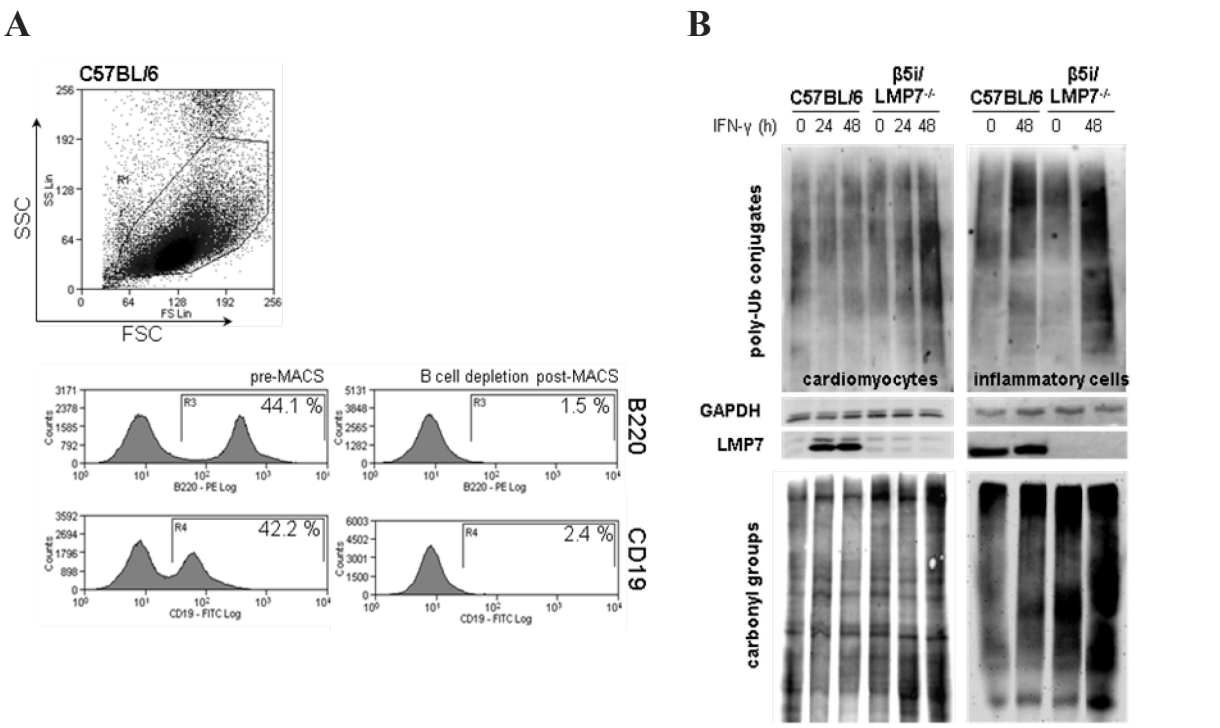

Fig. 23 Poly-ubiquitylation and oxidation of proteins in inflammatory cells and primary cardiomyocytes. **A:** Purity of B cell depleted splenocytes was determined after MACS separation by flow-cytometry, using $B220^{+}/CD19^{+}$ specific antibodies. Representative histograms are shown. **B:** Immunoblots of poly-ubiquitylated proteins and proteins that are modified by carbonyl groups are shown for IFN-γ treated primary cardiomyocytes and B-cell depleted splenocytes from C57BL/6 and β5i/$LMP7^{-/-}$ mice. GAPDH illustrates equal protein loading. Images are representative for two independent experiments.

Isolated primary cardiomyocytes and B cell depleted splenocytes from C57BL/6 and β5i/$LMP7^{-/-}$ mice were stimulated with 100 U/ml IFN-γ. Purity of B cell depleted splenocytes was controlled by flow cytometry yielding > 97 % as exemplarily shown in **Fig. 23**A. Cell lysates were either directly immunoblotted and stained for poly-Ub conjugates or carbonyl-

groups were first derivatized with 2,4-dinitrophenylhydrazine. 2,4-dinitrophenylhydrazone (DNP)-derivatized protein samples were then immunoblotted and stained for DNP.

Following IFN-γ stimulation, poly-ubiquitylated proteins accumulated in β5i/LMP7-deficient but not in C57BL/6-derived cardiomyocytes (**Fig. 23**B). Also, the accumulation of poly-Ub conjugates was stronger in IP-deficient than in IP-competent inflammatory cells. Detection of carbonyl groups by OxyBlot™ kit demonstrated, that the impairment of IP-formation in β5i/LMP7$^{-/-}$ cardiomyocytes and inflammatory cells was associated with increased accumulation of oxidatively modified proteins (**Fig. 23**B).

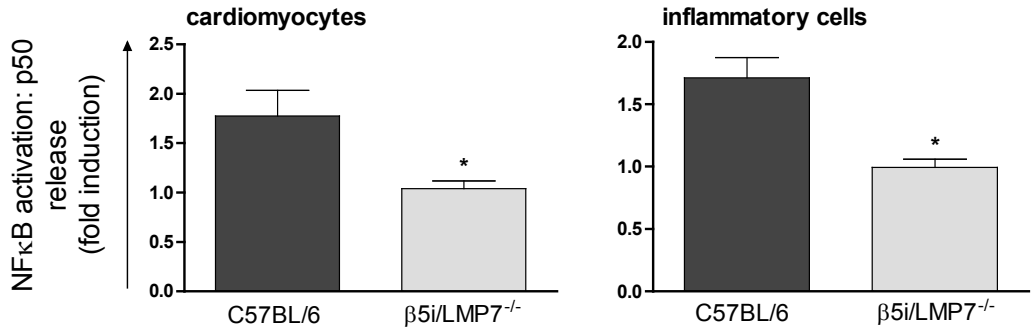

Fig. 24 NF-κB p50 expression levels. Whole cell homogenates from IFN-γ pre-treated primary cardiomyocytes and B cell-depleted splenocytes were prepared after 30 min TNF-α stimulation. NF-κB p50 expression levels were determined by ELISA (ActiveMotif). Data are shown as fold increase of p50 levels in TNF-α-treated cell lysates compared to untreated control samples (*$p<0.05$, representative means from triplicates from at least two independent experiments).

To test whether the enhanced protein accumulation in cytokine-exposed IP-deficient cells affected cell signaling, the level of activated NF-κB was determined. NF-κB is a central regulator of diverse signaling pathways. The treatment of primary cardiomyocytes and inflammatory cells with 30 ng/ml TNF-α resulted in the impaired activation of NF-κB in IP-deficient cells (**Fig. 24**). This finding reflected the reduced proteasomal degradation of NF-κB p105 precursor proteins, which was in line with the decreased capacity of IP-deficient cells to remove protein aggregates (**Fig. 23**).

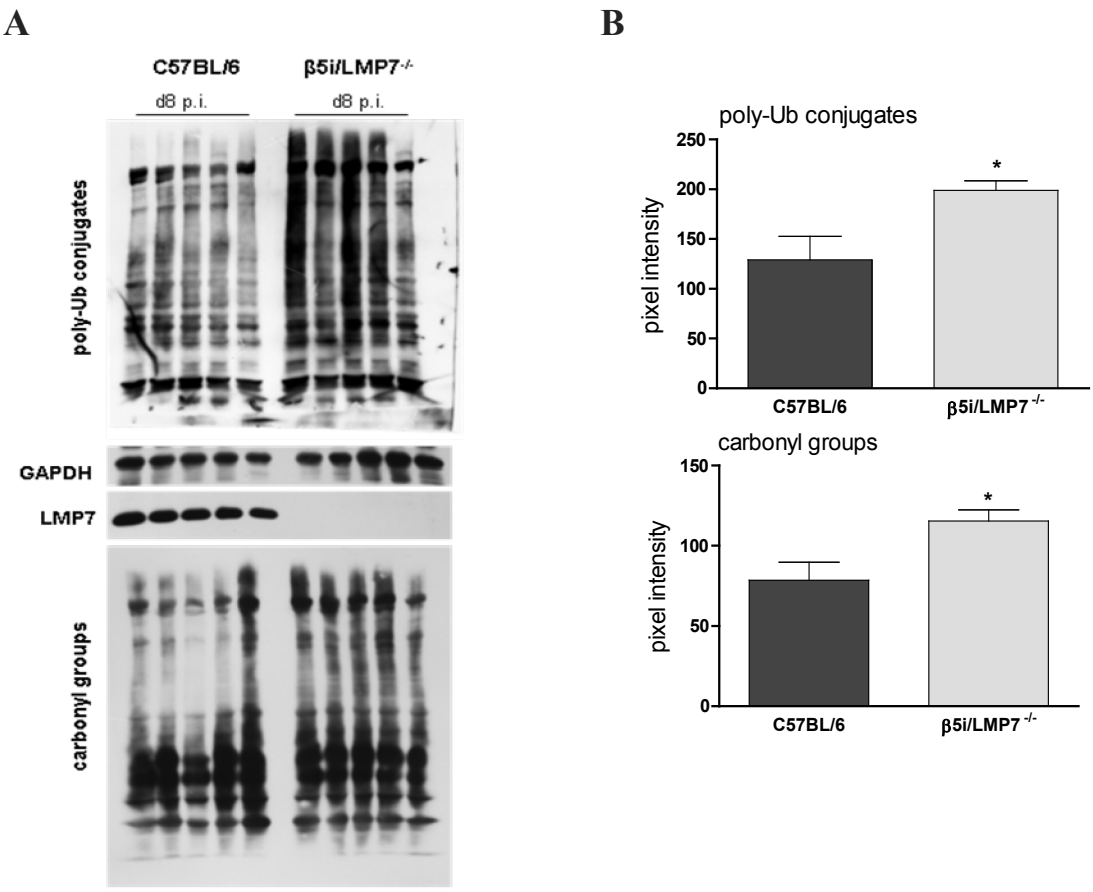

Fig. 25 Poly-ubiquitylation and oxidation of proteins in heart homogenates. A: Immunoblot of heart homogenates from CVB3 infected C57BL/6 and β5i/LMP7$^{-/-}$ mice, stained for poly-Ub proteins and carbonyl groups (d8 p.i., n=5, representative for n=10 mice). **B:** Densitometry was performed for individual lanes (n=5+SEM, * $p<0.05$).

The examination of CVB3-infected hearts confirmed that β5i/LMP7-deficiency also results in prolonged protein aggregation *in vivo*. As shown by immunoblot analysis of heart homogenates, poly-ubiquitylated, oxidant-damaged proteins accumulated in acutely inflamed β5i/LMP7$^{-/-}$ hearts at d8 p.i. (**Fig. 25**A). Densitometric quantification of individual lanes resulted in significantly increased poly-Ub and DNP signal intensity (**Fig. 25**B).

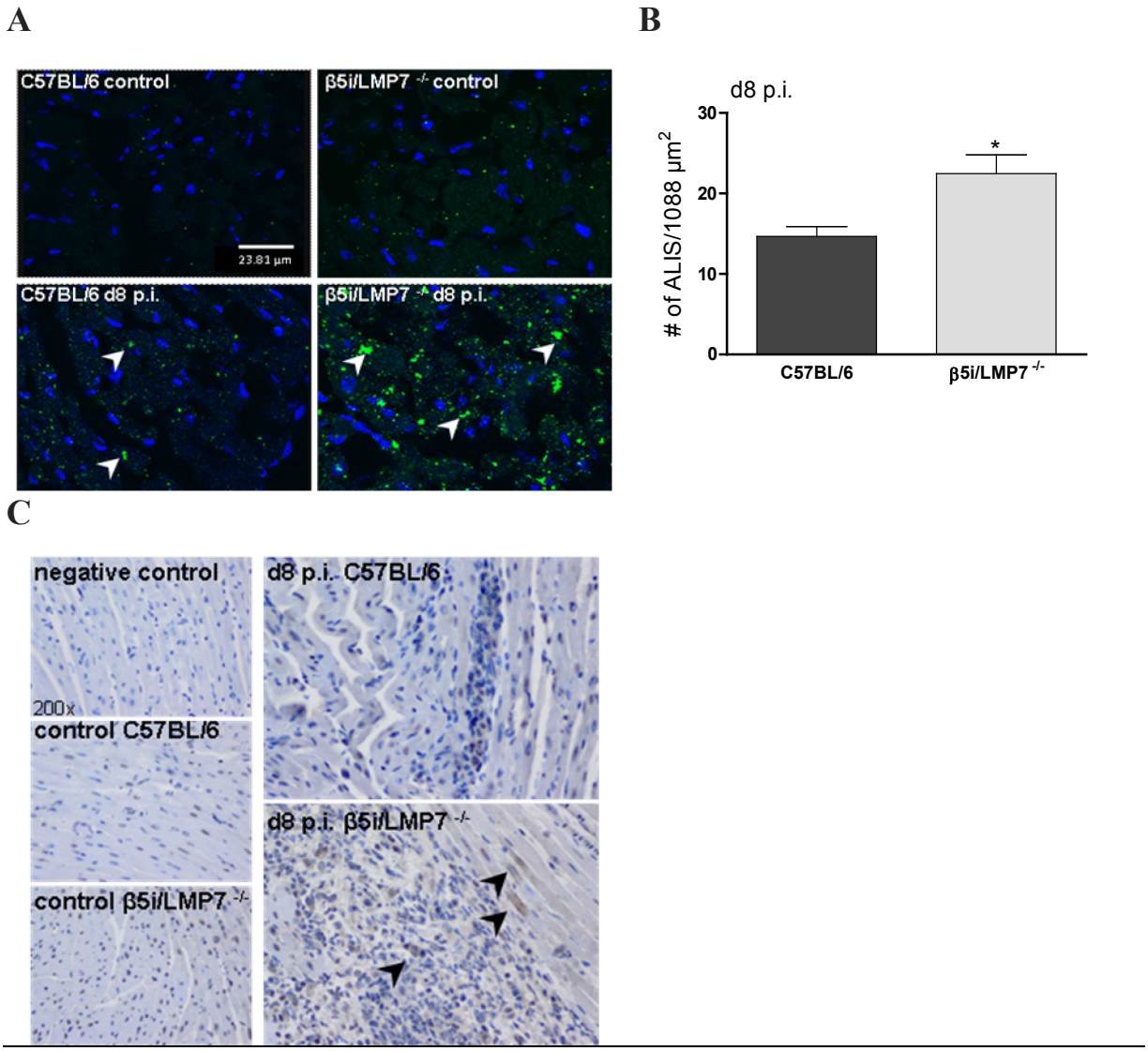

Fig. 26 Formation and localization of poly-ub proteins. A: Immunofluorescence staining of poly-Ub proteins was performed in heart cryosections of naive and infected C57BL/6 and β5i/LMP7$^{-/-}$ mice. White arrowheads mark poly-Ub ALIS (representative for n=6 mice and two independent experiments). **B:** ALIS were quantified in defined areas of cryosections of CVB3-challenged hearts (1088 µm^2 at 200-fold magnification, n=5 areas/section, n=6 mice/group, *p<0.05). **C:** Immunohistochemical staining for ubiquitin was applied in paraffin sections of of naive and infected C57BL/6 and β5i/LMP7$^{-/-}$ mice (n≥7, representative sections are shown).

As a generalized stress response, the formation of aggresome-like structures (ALIS) is induced in several immune and non-immune cell types to store poly-ubiquitylated proteins transiently prior to the degradation by the proteasome (113). To study whether β5i/LMP7-deficiency affects ALIS-formation in CVB3 myocarditis, heart tissue sections were stained for poly-Ub proteins. In both, C57BL/6 and β5i/LMP7$^{-/-}$ heart sections, cytosolic ALIS were detected upon CVB3 infection as compared to sham-treated controls (**Fig. 26**A). However, impairment of IP-formation in β5i/LMP7$^{-/-}$ cells was linked to significantly increased

aggresome-like induced structures. Quantification of ALIS revealed 14.6 ALIS/1088 $\mu m^2 \pm 1.2$ in C57BL/6 mice vs. 22.4 ALIS/1088 $\mu m^2 \pm 2.3$ in β5i/LMP7$^{-/-}$ mice (n=5, *$p<0.05$). As demonstrated by immunohistolochemical staining, these poly-Ub conjugates were primarily detected in invading inflammatory cells and within the cytoplasm of adjacent cardiomyocytes (**Fig. 26**C).

5.4.4 Determination of apoptotic cell death by immunofluorescence

Cardiomyocyte apoptosis is a hallmark of CVB-associated myocardits (141). However, direct cytopathic effects of CVB3 replication cannot explain aggravated myocardial damage as observed in β5i/LMP7$^{-/-}$ mice, because CVB3 titers were found to be within the same range as compared to C57BL/6 mice. To address the question, whether increased aggregation of oxidized and poly-ubiquitylated proteins in β5i/LMP7$^{-/-}$ mice affected the viability of β5i/LMP7$^{-/-}$ cells, genomic DNA fragmentation as an early sign for apoptosis was determined in cardiac tissue sections by *in situ* cell death detection kit/TMR red. No signs of apoptosis were detected in C57BL/6 and β5i/LMP7$^{-/-}$ mice at d4 p.i. (**Fig. 27**A).

At the acute stage of disease (d8 p.i.), TUNEL positive signals were found solely in the myocardium of β5i/LMP7$^{-/-}$ mice. As demonstrated by POD-coupled immunohistochemical analysis, these apoptotic foci exactly corresponded to invading cellular infiltrates and adjacent cardiomyocytes (**Fig. 27**B). By contrast, despite the presence of minor inflammatory lesions in CVB3 challenged C57BL/6 hearts, no significant signs of apoptosis were detectable at d8 p.i. here (**Fig. 27**A).

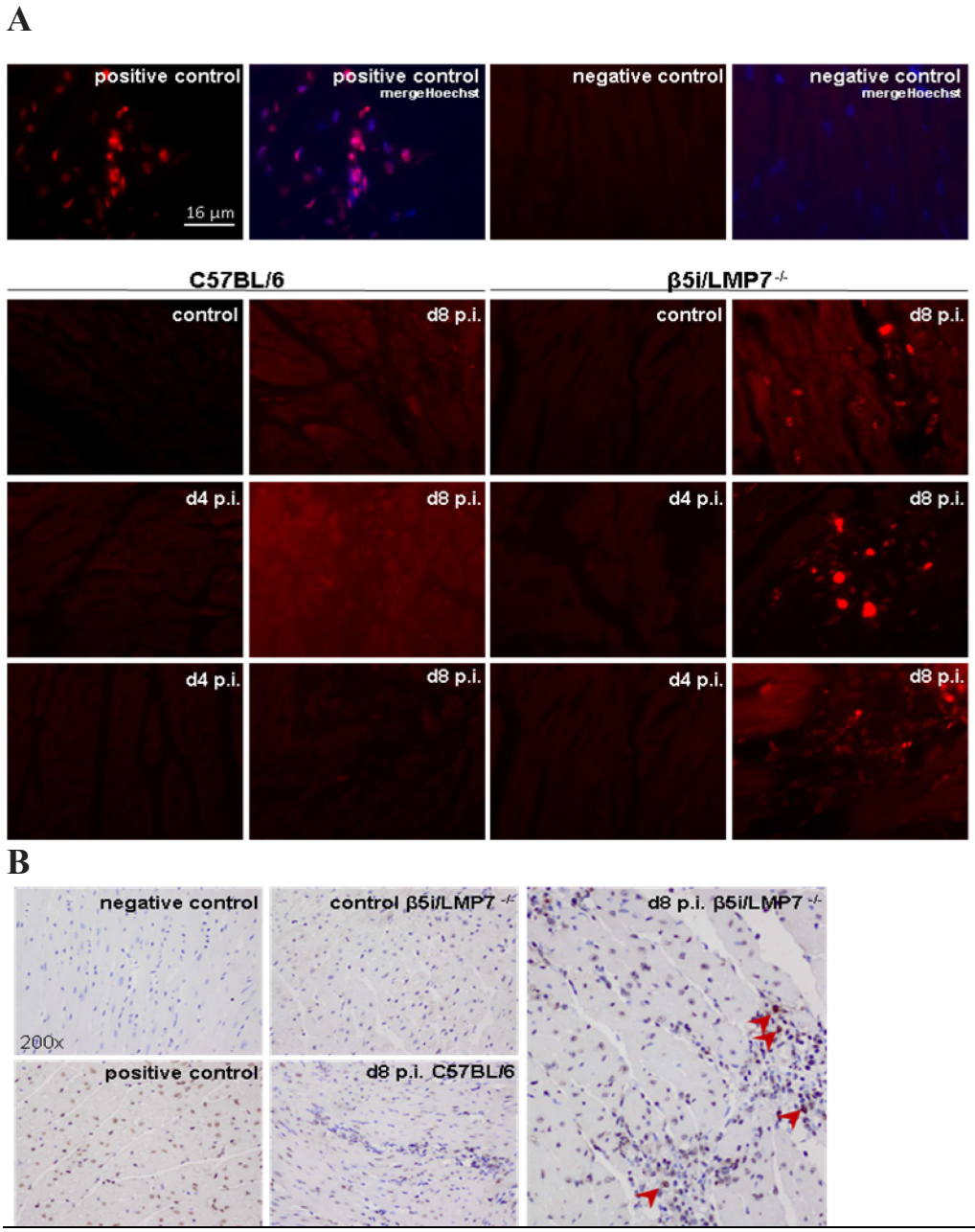

Fig. 27 Analysis of apoptotic cell death. A: Apoptosis was investigated *in vivo* by the application of the *in situ* cell death detection TMR red kit to cardiac tissue sections of naive and CVB3-challenged mice (d8 p.i.). Representative sections from two independent experiments (n=5 mice/experiment) are shown. **B:** Localization of apoptosis was assessed by using the *in situ* cell death detection POD kit.

5.4.5 Gene expression analysis by Affymetrix microarray

To get a comprehensive impression of signaling pathways that were potentially involved in excessive inflammation and apoptosis in β5i/LMP7$^{-/-}$ mice, a cardiac gene expression pattern was generated using RNA from sham-treated and CVB3-infected C57BL/6 and β5i/LMP7$^{-/-}$

mice. As CVB3 infection is associated by the induction of reactive oxygen species (142), the activation of the unfolded protein response, and the increase of apoptosis due to ER-stress (143), it was of interest to focus on these pathways. Affymetrix GeneChip microarray analysis revealed a threefold induction of the redox-sensitive nuclear factor Nrf2 exclusively in C57BL/6 hearts upon CVB3 infection, whereas no changes in the mRNA expression were detected in β5i/LMP7$^{-/-}$ hearts. Equal cardiac mRNA levels of enzymes which mediate the cellular oxidative stress response such as catalase (Cat), glutathione (Gpx), or superoxide dismutase (Sod) were observed. However, the mRNA expression of the Nrf-2-responsive genes Nqo1 (NAD(P)H dehydrogenase) and Gclc (glutamate-cysteine ligase catalytoc subunit) were solely increased in infected C57BL/6 hearts.

	BL6_d4/ Bl6_d0	BL6_d8/ Bl6_d0	LMP7_d4/ LMP7_d0	LMP7_d8/ LMP7_d0	LMP7_d0/ Bl6_d0	LMP7_d4/ Bl6_d4	LMP7_d8/ Bl6_d8	
Nrf2	2.06	3.36	1.22	0.99	0.94	0.56	0.28	nuclear factor, erythroid derived 2, like 2
Sod2	0.77	0.88	0.89	0.83	0.96	1.11	0.91	superoxide dismutase 2, mitochondrial
Sod1	1.38	1.52	1.22	1.21	1.04	0.93	0.83	superoxide dismutase 1, soluble
Cat	1.45	1.11	1.43	0.83	0.96	0.95	0.72	catalase
Gpx6	0.85	0.88	0.81	0.87	1.02	0.97	1.00	glutathione peroxidase 6
Gpx1	1.39	1.21	1.16	1.48	1.07	0.89	1.30	glutathione peroxidase 1
Nqo1	1.66	2.10	1.20	0.86	1.25	0.90	0.51	NAD(P)H dehydrogenase, quinone 1
Gclc	1.81	1.39	1.10	0.92	1.29	0.78	0.85	glutamate-cysteine ligase, catalytic subunit
Sel1l	1.02	1.01	1.05	1.01	1.03	1.06	1.03	sel-1 suppressor of lin-12-like
p97/VCP	0.99	0.95	0.93	0.97	1.00	0.93	1.02	valosin containing protein (p97)/p47 complex interacting protein 1
Hsf1	0.85	0.93	0.87	0.94	0.96	0.98	0.98	heat shock factor 1
Hsp70	0.59	0.68	0.62	0.75	1.02	1.07	1.13	heat shock protein 1A / heat shock protein 1-like
Stip1	0.86	0.86	1.01	1.10	0.91	1.08	1.18	stress-induced phosphoprotein 1
Hspa5	0.81	0.83	0.80	1.16	0.83	0.82	1.15	heat shock protein 5
CHOP	4.53	4.62	4.22	4.22	0.73	0.68	0.66	DNA-damage inducible transcript 3
Atf4	0.95	0.88	1.01	1.17	0.94	1.00	1.25	activating transcription factor 4
PERK	0.98	0.81	0.84	1.02	1.12	0.96	1.41	eukaryotic translation initiation factor 2 alpha kinase 4
Atf6	1.18	1.25	1.07	1.22	0.97	0.89	0.95	activating transcription factor 6
IRE1	0.86	0.93	1.26	1.21	0.74	1.08	0.96	Endoplasmic reticulum (ER) to nucleus signalling 1 (Ern1)
Xbp1	0.79	0.77	1.02	1.35	0.85	1.10	1.49	X-box binding protein 1
SREBP1	1.20	1.03	1.46	2.07	1.01	1.23	2.03	sterol regulatory element binding transcription factor 1
Ptx3	5.14	17.88	2.31	1.65	1.96	0.88	0.18	pentraxin related gene

Fig. 28 Affymetrix microarray expression profile. The affymetrix microarray heatmap illustrates the regulation of genes over the course of CVB3 infection (fold change color as illustrated, n=4 mice/group).

Although pathophysiological stress conditions such as viruses are described to activate the heat shock response, expression of the major transcription regulator Hsf1 or heats shock proteins (Hsp70, Hspa5) was not induced.

Also, no transcriptional induction of the UPR-related genes IRE/Xbp1, PERK, Atf4 or Atf6 was found neither in C57BL/6 nor in β5i/LMP7$^{-/-}$ hearts at the acute stage of disease. By

contrast, a fourfold increase of the proapoptotic transcription factor CHOP (DNA damage-inducible transcript 3 protein) was observed in both hosts at d4 and d8 p.i.

Expression of the sterol regulatory element-binding protein 1 (SREBP1), which is also involved in the apoptotic pathway, was slightly up-regulated in β5i/LMP7$^{-/-}$ mice, but not in C57BL/6 mice at d8 p.i. Further analysis revealed a strong increase of cardiac pentaxin 3 (Ptx3) mRNA expression in C57BL/6 mice at d8 p.i., which was abrogated concomitantly to impaired IP-formation in β5i/LMP7$^{-/-}$ hearts. Notably, baseline expression levels of all indicated genes were found to be in the same range in both hosts. The differential regulation of Nrf2, Ptx3, as well as SREBP2 in IP-deficient hearts upon CVB3 infection thus implicated an involvement of IPs in cell signaling pathways.

6 DISCUSSION

Over the last years, the complexity of the ubiquitin-proteasome system (UPS) and the particular role of immunoproteasomes have become apparent. As part of the adaptive immune response, IPs were initially reported to optimize MHC class I antigen processing. Far from being entirely investigated, the functional spectrum of IPs was extended to various cellular functions in which standard proteasomes are involved, such as the regulation of cell signaling and differentiation, apoptosis, and transcription (63). The present study contributes to the understanding of IP-function, demonstrating the importance of IP-formation for the preservation of proteostasis in inflammatory viral heart disease.

6.1 The proteasome constitution in β1i/LMP2- and β5i/LMP7-deficient hearts upon CVB3 infection

In accordance with a study by Hensley *et al*. (117), an efficient incorporation of β2i/MECL-1 and β5i/LMP7 was detected in β1i/LMP2-deficient hearts upon CVB3 infection (see **Fig. 9**B). This observation is contradictory to previous studies that demonstrated cooperative assembly mechanisms, whereby the presence of β1i/LMP2 was shown to facilitate the incorporation of β2i/MECL-1 (144;145). These differences can be explained by the fact that the present system based on IP- induction by IFN-γ and *in vivo* infection, whereas Griffin and Kingsbury *et al.,* who described cooperative assembly mechanisms, investigated steady state cell lines with fixed expression of standard and immunosubunits (71;144). In contrast to the expression of intermediate proteasomes in β1i/LMP2$^{-/-}$ mice, β5i/LMP7-deficiency led to impaired incorporation of β2i/MECL-1 and β1i/LMP2 (see **Fig. 9**B). A conflicting study by Joeris *et al.* only recently showed that β5 subunits integrate into LMP2/MECL-1 precursor proteasomes in β5i/LMP7-deficient cells upon IFN-γ stimulation. Furthermore, they demonstrated that *Listeria monocytogenes* infection of β5i/LMP7-deficient mice results in the expression of mixed LMP2/MECL-1/β5 proteasomes in the liver (146). Joeris *et al.* suggest that the integration of standard or immunosubunits depends on competition on protein level rather than on cooperative assembly mechanisms (146). However, this cannot explain why the incorporation of β2i/MECL-1 and β1i/LMP2 was impaired in CVB3-infected β5i/LMP7$^{-/-}$ hearts despite the induction of their respective genes on transcriptional level (see **Fig. 9**A).

Instead, the present findings point towards complex proteasome assembly mechanisms in a tissue- and/or disease-dependent manner.

6.2 IP-formation is not necessary for an effective $CD8^+$ T cell response in CVB3 myocarditis

Standard and immunoproteasomes display distinct proteolytic activities (96;147), resulting in the generation of a different CTL epitope repertoire (148). Along with the fact that Henke and Klingel *et al*. demonstrated the involvement of $CD8^+$ CTLs in the limitation of initial CVB3 replication (33;126), it was necessary to clarify the contribution of IPs to CVB3 epitope processing and to the induction of an effective $CD8^+$ T cell response *in vivo*. However, the here studied CVB3-specific MHC class I epitopes only elicit weak $CD8^+$ T cell responses (118;149). In contrast to classical viral mouse models like LCMV or Influenza virus infection, overall epitope-specific $CD8^+$ T cell quantities were found to be rather low in CVB3-infection as shown here for CVB3 VP2 [285-293]-specific $CD8^+$ T cells (see **Fig. 10**B). Therefore, adoptive $CD8^+$ memory T cell transfer experiments were performed, which additionally included potential effects of so far not identified CVB3-specific $CD8^+$ T cell epitopes. The average percentage of β1i/LMP2-deficient donor cells in their respective recipient mice was considerably low (see **Fig. 12**C). These data are in line with the study by Hensley *et al.,* that demonstrated decreased lymphocyte survival in influenza A virus-challenged β1i/LMP2-deficient mice (127). However, the restricted β1i/$LMP2^{-/-}$ lymphocyte survival had no demonstrable consequence. The myocarditis scores of the recipient C57BL/6 or β1i/$LMP2^{-/-}$ mice were found to be within the same range, independent from the origin of donor lymphocytes (see **Fig. 12**E). The observed difference of myocardial inflammation between C57BL/6 and β1i/$LMP2^{-/-}$ recipients was first attributed to a general impact of β1i/LMP2-deficiency (compare **Fig. 5**A). However, the attenuation of acute CVB3 myocarditis in β1i/LMP2-deficient mice was found to be due to background artifacts later on. As demonstrated in detail (see **section 5.3**), the deletion of β1i/LMP2 had actually no effect on the outcome of viral heart disease. Therefore, the reduced lymphocyte survival as observed by $CD8^+$ T cell transfer experiments cannot be properly discussed in the present context.

By contrast, the survival of transferred $CD8^+$ T cells from C57BL/6 or β5i/$LMP7^{-/-}$ donors was found to be within the same range (see **Fig. 12**B). No beneficial effects on CVB3 myocarditis were detected after transfer of $CD8^+$ T cells isolated from IP-competent as compared with transfer of $CD8^+$ T cells from β5i/$LMP7^{-/-}$ mice (see **Fig. 12**D). However, transfer of IP-competent and IP-deficient $CD8^+$ T cells resulted in a slightly milder

myocarditis than in non-transferred animals (compare **Fig. 5**A). In agreement with the fact that both, C57BL/6 and β5i/LMP7$^{-/-}$ mice demonstrated equal viral loads and perforin expression at the acute stage of disease (see **Fig. 7**B/C; **Fig. 6**C), and were both able to effectively eliminate virus and inflammation by d28 p.i. (see **Fig. 7**D), intact cardiac IP-formation was not mandatory for the induction of a sufficient CD8$^+$ T cell response in viral heart disease.

These data are in line with findings by Nussbaum *et al*., which showed that β5i/LMP7-deficiency has no considerable effect on overall CD8$^+$ T cell responses to lymphocytic choriomeningitis virus infection and does not alter the kinetics of virus clearance (150). By contrast, Kincaid *et al*. showed that DCs of triply deficient (LMP2/MECL1/LMP7$^{-/-}$) mice have substantial defects in presenting several MHC class I epitopes. Also, the CD8$^+$ T cell response to LCMV-specific epitopes is lower and the immunodominance hierarchy is markedly altered in these mice (151). They attributed their findings to the fact, that a functional overlap of immunosubunits in mixed proteasomes masks the true importance of IPs for MHC class I presentation (151). These data must not necessarily be contradictory to the present study. First, the impaired incorporation of β1i/LMP2 and β2i/MECL1 in β5i/LMP7-deficient hearts upon CVB3 infection was almost equivalent to a triple knockout as investigated by Kincaid *et al*. However, one cannot directly compare different infection models. LCMV elicits a vigorous CD8$^+$ T cell response that persists at high levels (152), whereas CVB3 infection only results in a weak virus-specific primary CTL response (153). Second, Kincaid *et al*. solely investigated the impact of IP-formation on MHC class I epitope processing by professional antigen presenting cells (APCs), which constitutively express IPs. Therefore, a complete IP-knockout might have more severe functional consequences in APCs than in cardiomyocytes, whose primary function is not antigen presentation. The present study focused on the function of IPs in the heart, once the induction of a CD8$^+$ T cell response was excluded from being a disease-modifying factor.

6.3 Impaired IP formation in β5i/LMP7-deficient mice results in deteriorated acute CVB3 myocarditis

The fact that T lymphocytes and non-infected cells within pathogen-challenged tissues express IPs without having a function as antigen-presenting cells (63;69;154) already indicates that IPs do not exclusively facilitate antigen processing. Indeed, the sufficient CD8$^+$ T cell response in β5i/LMP7$^{-/-}$ mice argued in favor of MHC class I-independent functions of

IPs in the present model. The constitutive knockout of cardiac immunosubunits caused a massive exacerbation of myocardial inflammation upon CVB3 infection (see **Fig. 5**), accompanied by deteriorated systolic and diastolic left ventricular heart function at d8 p.i. (see **Table 1**). Importantly, the ejection fraction as one major determinant of cardiac function was reduced in β5i/LMP7$^{-/-}$ mice, but not in IP-competent C57BL/6 mice upon CVB3 infection. The lack of statistical power has to be discussed in view of the fact that the infection efficiency decisively depends on age and body weight of the mice. Due to these experimental requirements, the dropout rate in the hemodynamically analyzed group of CVB3-infected β5i/LMP7$^{-/-}$ mice was high. As an appropriate sample size is closely related to statistical power, more animals would have been required to detect potential strain-specific differences. Nevertheless, further experiments demonstrated that IP-formation in murine C57BL/6 hearts protected from the accumulation of polyubiquitylated and oxidatively damaged proteins, as well as from enhanced apoptosis of inflammatory cells and cardiomyocytes.

6.3.1 IP-formation protects from aggravated accumulation of poly-Ub and oxidatively damaged proteins

Many cell types that are affected by pathogens produce type I interferons as part of the innate inflammatory response (155). Activated T-lymphocytes, macrophages, and NK cells secrete various proinflammatory cytokines such as IFN-γ and TNF-α (156), which do not only induce the formation of IPs, but also increase protein synthesis via downstream activation of the mTOR pathway (157). As reported by Si *et al*., CVB3 infection generates reactive oxygen species (ROS) (142). Moreover, cytokine-exposed cells, whether they are infected or not, produce ROS and reactive nitrogen (RNS) species e.g. by NADPH-oxidases (NOX) (158). Free radicals do not selectively neutralize pathogenic proteins, but give rise to oxidative damage of cellular proteins, whereby newly synthesized proteins are particularly sensitive to proteotoxic stress (159). Taken together, it becomes evident that exposure to cytokines massively challenges the protein equilibrium. Concomitant with CVB3 infection, oxidative stress and virus-induced alterations of the cellular translation machinery (113;160) may cause the enhanced incurrence of DRIPs. If the degradation capacity of proteasomes is exceeded, DRiPs, long-lived or nascent, poly-ubiquitylated and/or oxidant damaged proteins are temporarily accumulated in aggresome-like induced structures (113). However, excessive protein accumulation upon cellular stress is inherently cytotoxic (117;161). To meet this challenge to proteostasis, the UPS as the key regulator of protein quality control and

physiological protein turnover adapts to pro-inflammatory conditions. UBE2L6 as the major E2-conjugating enzyme as well as the Lys-48 linked polyubiquitylation of proteins is upregulated (162), and IPs are expressed by the *de novo* synthesis (38;162). Thereby, the poly-Ub substrate degradation capacity is enhanced (162). As evidenced by Jakel *et al.,* cardiac IP formation is directly linked to increased peptide-hydolyzing activity in CVB3 myocarditis (118). The present study correlates the induction of cardiac IPs to the enhanced degradation of oxidant-damaged, poly-Ub proteins in viral heart disease.

Here, IFN-γ stimulated IP-deficient primary cardiomyocytes and inflammatory cells were shown to accumulate poly-Ub, oxidant-damaged proteins. Remarkably, IP-competent cells were able to adapt to cytokine-triggered cellular stress, as they prevented prolonged aggregation of potentially toxic proteins *in vitro* (see **Fig. 23**). These findings are in line with a study by Seifert *et al*., which recently reported an association between IP-formation and the ability to clear ALIS in murine embryonal fibroblasts (MEFs). This is attributed to the augmented capactity of IPs to degrade K48-linked poly-Ub substrates (162). The transient increase of polyubiquitylated proteins and the coincident decrease of proteasomal activity after IFN-γ stimulation of non-lymphoid cells can be explained by the dissociation of the standard 26S proteasome until IPs are synthesized after approximately 24 hours. On the basis of their capacity to turn over polyubiquitylated substrates two-fold or three-fold faster than standard proteasomes, IPs represent an adaptation of cells to cope with tremendous physiological stress conditions arising e.g. from infection or cytokine exposure (162).

Furthermore, the present study demonstrates that the induction of cardiac IPs is crucial for the efficient degradation of poly-Ub, oxidant-damaged proteins *in vivo* (see **Fig. 25**). IP-deficient mice failed to efficiently degrade ALIS in the injured myocardium (see **Fig. 26**). These poly-Ub and potentially oxidized proteins were detected within inflammatoy foci and within the cytoplasm and nuclei of adjacent cardiomyocytes (see **Fig. 26**). These results are in agreement with data by Seifert *et al*., that highlight the importance of IPs in experimental autoimmune encephalomyelitis (EAE), the most intensively studied animal model for multiple sclerosis (163). In EAE, IP-formation is accompanied by less severe disease manifestation (162). Beyond that, failures in the elimination of aggregates are associated with the pathogenesis of a wide range of human diseases including cystic fibrosis, Alzheimer's disease, or Parkinson’s disease (164).

6.3.2 IP-deficient hearts are prone to apoptotic cell death

The 26S proteasome can play opposite roles in the regulation of apoptotic cell death, because both, negative and positive mediators undergo proteasomal degradation in a tightly regulated and timely controlled manner (165). A study by Yang *et al*. strongly supports the assumption that IPs contribute to apoptosis regulation. They detected accelerated degradation of the potent pro-survival factor MCL-1 (induced myeloid leukemia cell differentiation protein 1) upon IFN-γ-induced IP-formation, thereby reducing cellular viability (166). On the contrary, Seifert *et al.* demonstrated that β5i/LMP7-deficient fibroblasts are highly susceptible to apoptosis in response to IFN-γ and the apoptosis-inducer etoposide, as reflected by enhanced caspase 3/7 activity (162). Related to viral heart disease, the present work demonstrates that IP-formation prevented apoptotic cell injury of CVB3-challenged inflammatory cells and adjacent cardiomyocytes (see **Fig. 27**). As CVB3 infection was recently reported to activate the unfolded protein response and to trigger ER stress-mediated apoptosis (143), one may argue that deficits in protein degradation as found in IP-deficient β5i/LMP7$^{-/-}$ mice additionally challenge cellular stress-responsive mechanisms. Here, mRNA expression of the central player of the cytosolic heat shock stress response, Hsf1, was not altered upon CVB3 infection, neither in C57BL/6 nor in β5i/LMP7-deficient hearts. Also, no differences in the cardiac mRNA expression of ERAD- or protein folding-associated chaperones such as SEL1L, p97/VCP or Hsp70 were detected (see **Fig. 28**). These findings lead to the conclusion, that increased protein accumulation in β5i/LMP7$^{-/-}$ cells was not attributed to deficits in protein quality control, but rather to the impaired degradation capacity. In line with the study by Zhang *et al*., CVB3 infection caused the fourfold mRNA induction of the proapoptotic transcription factor CHOP, which is involved in the unfolded protein response (143). However, other UPR-related genes, such as ATF6, IRE1, or XBP1 were not regulated during acute myocardits (see **Fig. 28**). Only the sterol regulatory element-binding protein-1 (SREBP1) was slightly induced in β5i/LMP7$^{-/-}$ but not in C57BL/6 mice at d8 p.i. These findings indicate that CVB3 infection activates the UPR, but that increased cytosolic protein aggregation does not induce a differential regulation of ER-associated stress responsive genes in β5i/LMP7$^{-/-}$ hearts.

Macrophages that represent the major fraction of invading inflammatory cells in CVB3 myocarditis (see **Fig. 6**) generate ROS (167) and thus create a highly reactive, pro-apoptotic environment (158) even for IP-competent cells. However, despite the presence of inflammatory lesions, no apoptosis was detectable within cellular infiltrates and

cardiomyocytes of IP-competent C57BL/6 hearts. Therefore, the question was raised whether IP-formation affects protection mechanisms against cytokine- and ROS-induced apoptosis. The complex of the transcription factor Nfr2 (nuclear factor erythroid 2-related factor 2) and its inhibitor Keap1 (kelch-like ECH-associated protein 1) is a cellular sensor of oxidative stress that controls the coordinated expression of antioxidant genes. Furthermore, Nrf2 activity increases the expression of the antiapoptotic protein Bcl-2 (B-cell lymphoma 2) (168) and regulates the sensitivity to Fas-mediated apoptosis in T cells (169). Keap1, which tethers Nrf2 in the cytoplasm, serves as an adaptor for the cullin 3/ring box 1 (Cul3/Rbx1) E3 ubiquitin ligase complex. Under normal cellular conditions, the Keap1/Cul3/Rbx1 complex constantly mediates the degradion of Nrf2 by the proteasome. Oxidative stress induces the stabilization of Nrf2 and its translocation to the nucleus, where it binds to *cis*-acting antioxidant-response elements (ARE) in the promotor region of cytoprotective genes (170). A recent study by Pickering *et al.* highlights the role of the Nrf2 signal transduction pathway in the transient adaptation of the protasome capacity to degrade oxidized proteins. Although concentrating on 20S proteasomes instead of physiological 26S proteasomes, they found an increase of β1, β1i/LMP2 and PA28αβ protein levels in murine embryonal fibroblasts upon H_2O_2 treatment, which was abrogated by Nrf2-siRNA treatment in case of β1 and PA28αβ (171). Interestingly, ARE consensus sequences are present upstream of standard 20S subunits (β1, β2, β6, α1-3) and in the promotor region of β5i/LMP7, whereas they are absent in β1i/LMP2 and β2i/MECL-1 (171). In viral myocarditis, the cardiac expression of Nrf2 was upregulated two- to threefold in IP-competent C57BL/6 mice upon CVB3 infection, whereas the mRNA expression levels did not change in β5i/LMP7$^{-/-}$ hearts (see **Fig. 28**). Notably, baseline expression of Nrf2 did not differ between non-infected C57BL/6 respectively β5i/LMP7$^{-/-}$ hearts. Cardiac mRNA expression levels of important antioxidant enzymes, such as glutathione peroxidase, catalase, or superoxide dismutase were found to be in the same range in both, infected and non-infected C57BL/6 and β5i/LMP7$^{-/-}$ hearts. However, the induction of Gclc (glutamate-cysteine ligase, catalytic subunit) and Nqo1 (NAD(P)H quinone oxidoreductase 1) mRNA expression was increased in C57BL/6 (see **Fig. 28**) but not in β5i/LMP7$^{-/-}$ hearts. Both, Nqo1 and Gclc are Nrf2-driven cytoprotective mediators (172). These findings imply a defective stress-induced apoptosis regulation in β5i/LMP7$^{-/-}$ mice. Nonetheless, the mechanistic link of IP-formation to Nrf2 expression levels remains unclear and could be an aspect of further investigation.

6.3.3 IPs are involved in NF-κB cell signaling in a tissue or disease-specific manner

Given that viral replication and the early induction of inflammatory cytokines were identical in both hosts, it was of considerable interest to examine the increased immune cell recruitment to β5i/LMP7-deficient hearts. One regulator of highest impact is the transcription factor NF-κB, owing to its central role in immunological processes and the vast range of genes that it controls. In resting cells, inactive NF-κB dimers are sequestered in the cytoplasm by the association to I-κB family members (173). Activation of NF-κB requires phosphorylation and K48-linked poly-ubiquitylation of I-κB and subsequent proteasomal degradation. This unmasks a nuclear targeting sequence of NF-κB and promotes the translocation of NF-κB to the nucleus (174) where it regulates gene transcription.

Turnover of I-κB was recently shown to be accelerated in cells expressing IPs compared to cells predominantly expressing standard or mixed proteasomes (127;162;175). This emphasizes the particular role of IPs in cell signaling, demonstrating that the enhanced degradation capacity of IPs is not limited to poly-Ub, oxidatively damaged proteins, but also affects the functionality of cellular substrates such as NF-κB. The present work demonstrates significantly reduced levels of NF-κB p50 subunits in IP-deficient cardiomyocytes and inflammatory cells (see **Fig. 24**). This reflects limited proteasomal degradation of NF-κB p105 precursor proteins upon exposure to cytokines, potentially influencing signal transduction.

Among others, NF-κB acts on the transcription of numerous genes for pro-inflammatory cytokines, chemokines and immune receptors. Besides, NF-κB mediates gene expression of superoxide dismutase and thioredoxin, which provide cellular protection to oxidative stress (176-178). Gene products that are regulated by NF-κB such as interleukin-1β and TNF-α can in turn activate NF-κB in a positive regulatory loop, which boosts inflammatory responses (179). Therefore, constitutive activation of NF-κB pathways is linked to inflammatory diseases like multiple sclerosis, rheumatoid arthritis, inflammatory bowel disease, and asthma (179;180). Targeting the proteasome activity recently led to success in various murine models of autoimmune disorders. Block of NF-κB activity by the proteasome inhibitor bortezomib ameliorates glomerulonephritis and prolongs survival of mice with lupus-like disease (181). Both, partial inhibition of proteasomes by bortezomib and the specific deletion of β5i/LMP7 substantially attenuate inflammation in experimental colitis. This was also ascribed to impaired NF-κB signaling, limiting secretion of pro-inflammatory cyto- and chemokines

(182). In a mouse model of rheumatoid arthritis, inhibition of β5i/LMP7 by the selective epoxyketone inhibitor PR-957 (183) hampers the production of IL-23, IL-2, IL-6, TNF-α and IFN-γ and consequently attenuates disease progression (184). However, in a reporter cell line, PR-957 does not inhibit NF-κB activity, indicating that IPs may regulate cytokine expression also via NF-κB–independent pathways (185). In the present model, cytokine induction in IP-deficient hearts was comparable to that in C57BL/6 mice upon CVB3 infection (see **Fig. 20**). Also serum levels of the selected chemokines RANTES, IP-10, and MCP-1 were observed to be within the same range (see **Fig. 21**).

Given that cytokine stimulation resulted in impaired NF-κB -activation in β5i/LMP7$^{-/-}$ cells *in vitro*, it was of interest to investigate whether IP-deficiency affected NF-kB signaling *in vivo*. One indicator for impaired NF-κB signaling in β5i/LMP7$^{-/-}$ mice is a member of the pentaxin superfamily, Ptx3. The promotor region of pentaxin 3 contains a NF-κB-binding element, which is operative in the response to inflammatory cytokines TNF-α and/or IL-1β (186). Ptx3 belongs to the family of pattern-recognition receptors (PRRs) (187), which are able to detect highly conserved molecular motifs shared by a large group of microorgansims (pathogen-associated molecular patterns=PAMPs) (188). Expressed e.g. by endothelial cells, monocytes/macrophages and fibroblasts, Ptx3 opsonizes various pathogens or pathogen-derived patterns, including human and murine cytomegalovirus (CMV) or H3N2 influenza virus (186). As reviewed by Kunes *et al.*, Ptx3 plays an important role in dampening an inappropriate, exaggerated inflammatory response to acute infections and cardiovascular diseases such myocardial infarction and ischemia/reperfusion injury (186). In murine CVB3 myocarditis, Ptx3 was massively up-regulated in IP-competent C57BL/6, but not in IP-deficient hearts (see **Fig. 28**). One may speculate, that the early cytokine response (e.g. TNF-α, **Fig. 20**) activated Ptx3 via a NF-κB -dependent pathway that was delayed in β5i/LMP7$^{-/-}$ mice, thereby protecting IP-competent mice from excessive inflammation. Therefore, this aspect of PAMP-associated cell signaling upon CVB3-infection could be a worthwhile objective of further investigation.

Besides, apoptotic cell death of invading inflammatory cells and adjacent cardiomyocytes as observed in IP-deficient mice (see **Fig. 27**) may actually cause an increased release of damage-associated molecular patterns (DAMPs). DAMPs mediate tissue repair and signal the threat of infection and cellular injury to the organism (189;190). It is known, that different Toll-like receptors (TLRs) are activated by the recognition of PAMPs and DAMPs (189). In consequence, the downstream induction of transcription factors regulates the expression of

specific genes that modulate the inflammatory response. Notably, DAMPs have been implicated in several pathologies where prolonged inflammation plays a role. This led to the hypothesis, that TLR activation by DAMPs elicits positive feedback loops, resulting in proliferation of pro-inflammatory responses and inflammation (189). Apart from Ptx3 signaling, this can also explain the exacerbation of acute inflammation and killing of non-infected cardiomyocytes in IP-deficient animals.

Together, the present findings emphasize the potential implication of IPs in various signal transduction pathways in a tissue or disease-specific manner.

6.4 Conclusion: IPs exert protective functions in the pathogenesis of CVB3 myocarditis

Expression of IPs as a physiological response to a great variety of stressors modifies the full range of cellular functions in which standard proteasomes are already involved. Based on the underlying disease, IPs may either exert protective effects or they aggravate the consequences of inflammation in a tissue-specific manner. In viral heart disease, intact IP-formation preserves protein homeostasis by the accelerated degradation of oxidatively damaged, poly-Ub proteins and the prevention of apoptotic cell death (see **Fig. 29**).

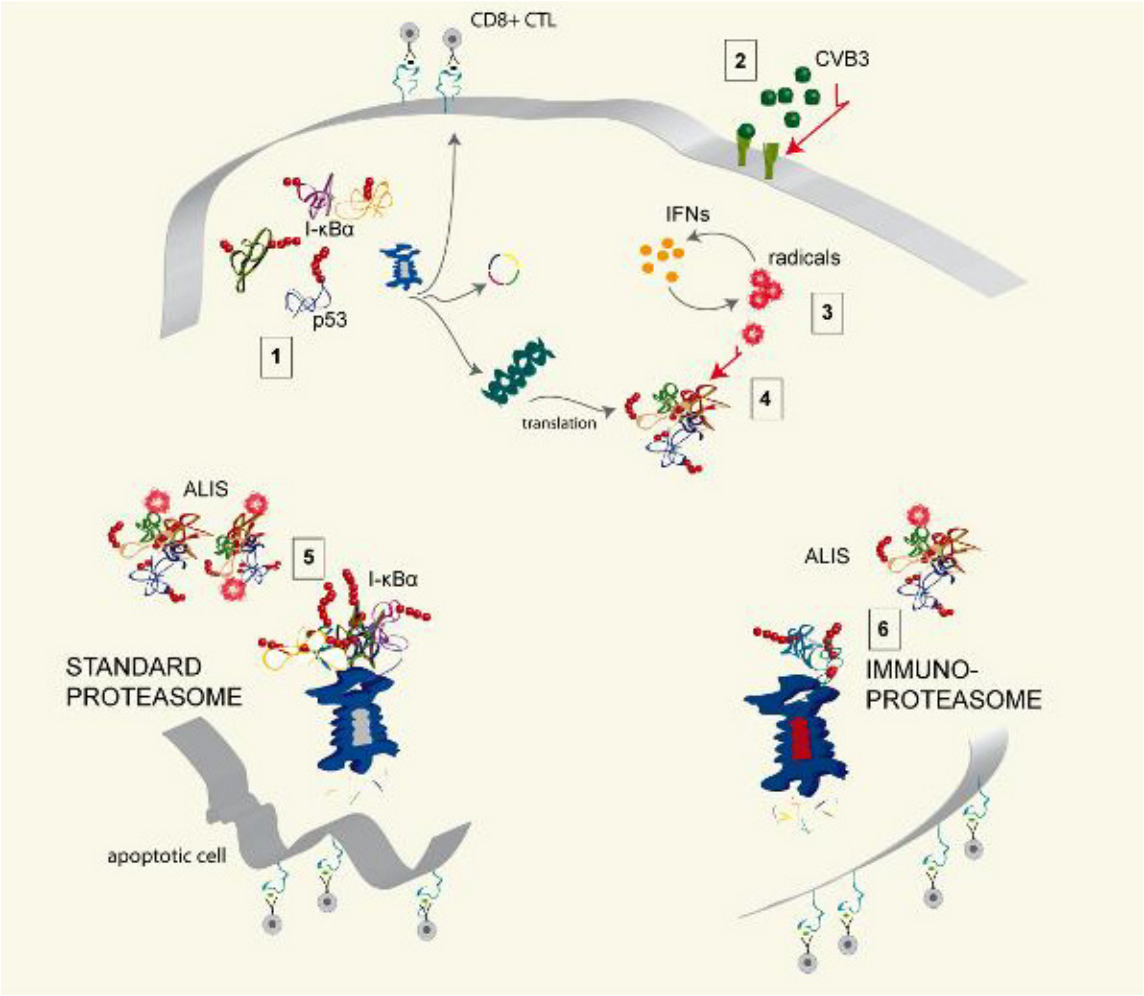

Fig. 29 Working model. Cardiac IP formation protects from apoptotic cell death by the preservation of protein homeostasis. 1: During regular cell metabolims, the proteasome degrades proteins such as I-κB, which are involved e.g. in cell signaling, gene transcription, or differentiation. Antigen presentation from abberant gene products (predominantly DRiPs) contributes to immune surveillance by $CD8^+$ T cells via MHC class I presentation. 2: CVB3 infection represents a massive threat to cellular proteostastis. 3: It triggers an IFN-response and the generation of reactive oxygen species which 4: affect cellular proteins, especially the nascent pool of proteins 5: The standard proteasome is less efficient than the IP in eliminating oxidant-damaged and poly-ubiquitylated proteins resulting in the persistent aggregation of ALIS. Delayed degradation of regulatory proteins such as I-κB impairs NF-κB activation and may contribute to apoptotic cell death in IP-deficient, CVB3 challenged inflammatory cells and cardiomyocytes. 6: The formation of IPs preserves protein homeostasis due to accelerated degradation of transiently accumulated ALIS, which sequester toxic abberant proteins as well as viral proteins.

7 REFERENCES

(1) Aretz HT, Billingham ME, Edwards WD, Factor SM, Fallon JT, Fenoglio JJ, Jr. et al. Myocarditis. A histopathologic definition and classification. Am J Cardiovasc Pathol 1987; 1(1):3-14.

(2) Esfandiarei M, McManus BM. Molecular biology and pathogenesis of viral myocarditis. Annu Rev Pathol 2008; 3:127-155.

(3) Magnani JW, Dec GW. Myocarditis: current trends in diagnosis and treatment. Circulation 2006; 113(6):876-890.

(4) Kindermann I, Barth C, Mahfoud F, Ukena C, Lenski M, Yilmaz A et al. Update on myocarditis. J Am Coll Cardiol 2012; 59(9):779-792.

(5) Kindermann I, Kindermann M, Kandolf R, Klingel K, Bultmann B, Muller T et al. Predictors of outcome in patients with suspected myocarditis. Circulation 2008; 118(6):639-648.

(6) Maisch B, Portig I, Ristic A, Hufnagel G, Pankuweit S. Definition of Inflammatory Cardiomyopathy (Myocarditis): On the Way to Consensus. A status report. Herz 2000; 25(3):200-209.

(7) Lieberman EB, Hutchins GM, Herskowitz A, Rose NR, Baughman KL. A clinicopathologic description of myocarditis. J Am Coll Cardiol 1991; 18(7):1617-1626.

(8) Richardson P, McKenna W, Bristow M, Maisch B, Mautner B, O'Connell J et al. Report of the 1995 World Health Organization/International Society and Federation of Cardiology Task Force on the Definition and Classification of cardiomyopathies. Circulation 1996; 93(5):841-842.

(9) Cooper LT, Jr. Myocarditis. N Engl J Med 2009; 360(15):1526-1538.

(10) D'Ambrosio A, Patti G, Manzoli A, Sinagra G, Di LA, Silvestri F et al. The fate of acute myocarditis between spontaneous improvement and evolution to dilated cardiomyopathy: a review. Heart 2001; 85(5):499-504.

(11) Maron BJ, Towbin JA, Thiene G, Antzelevitch C, Corrado D, Arnett D et al. Contemporary definitions and classification of the cardiomyopathies: an American Heart Association Scientific Statement from the Council on Clinical Cardiology, Heart Failure and Transplantation Committee; Quality of Care and Outcomes Research and Functional Genomics and Translational Biology Interdisciplinary Working Groups; and Council on Epidemiology and Prevention. Circulation 2006; 113(14):1807-1816.

(12) D'Ambrosio A, Patti G, Manzoli A, Sinagra G, Di LA, Silvestri F et al. The fate of acute myocarditis between spontaneous improvement and evolution to dilated cardiomyopathy: a review. Heart 2001; 85(5):499-504.

(13) Grun S, Schumm J, Greulich S, Wagner A, Schneider S, Bruder O et al. Long-term follow-up of biopsy-proven viral myocarditis: predictors of mortality and incomplete recovery. J Am Coll Cardiol 2012; 59(18):1604-1615.

(14) Feldman AM, McNamara D. Myocarditis. N Engl J Med 2000; 343(19):1388-1398.

(15) Melnick J.L. Enteroviruses: Polioviruses, cosackieviruses, echoviruses, and newer enteroviruses. In: Fields B.N., Knipe D.M., Chanock R.M., Melnick J.L., Roizman B., Shope R.E., editors. New York, N.Y.: Raven Press, 1985: 739-794.

(16) Yoon JW, Austin M, Onodera T, Notkins AL. Isolation of a virus from the pancreas of a child with diabetic ketoacidosis. N Engl J Med 1979; 300(21):1173-1179.

(17) Sagar S, Liu PP, Cooper LT, Jr. Myocarditis. Lancet 2012; 379(9817):738-747.

(18) Schultz JC, Hilliard AA, Cooper LT, Jr., Rihal CS. Diagnosis and treatment of viral myocarditis. Mayo Clin Proc 2009; 84(11):1001-1009.

(19) Coyne CB, Bergelson JM. Virus-induced Abl and Fyn kinase signals permit coxsackievirus entry through epithelial tight junctions. Cell 2006; 124(1):119-131.

(20) Cohen CJ, Shieh JT, Pickles RJ, Okegawa T, Hsieh JT, Bergelson JM. The coxsackievirus and adenovirus receptor is a transmembrane component of the tight junction. Proc Natl Acad Sci U S A 2001; 98(26):15191-15196.

(21) Bergelson JM. Receptors for Coxsackieviruses and Echoviruses. In: Semler E.M., Wimmer E., editors. Washington, DC: ASM Press, 2002: 107-113.

(22) Bedard KM, Semler BL. Regulation of picornavirus gene expression. Microbes Infect 2004; 6(7):702-713.

(23) Krausslich HG, Nicklin MJ, Toyoda H, Etchison D, Wimmer E. Poliovirus proteinase 2A induces cleavage of eucaryotic initiation factor 4F polypeptide p220. J Virol 1987; 61(9):2711-2718.

(24) Paul AV, van Boom JH, Filippov D, Wimmer E. Protein-primed RNA synthesis by purified poliovirus RNA polymerase. Nature 1998; 393(6682):280-284.

(25) Yuan J, Cheung PK, Zhang HM, Chau D, Yang D. Inhibition of coxsackievirus B3 replication by small interfering RNAs requires perfect sequence match in the central region of the viral positive strand. J Virol 2005; 79(4):2151-2159.

(26) Rabin ER, Hassan SA, Jenson AB, Melnick JL. Coxsackie virus B3 myocarditis in mice. An electron microscopic, immunofluorescent and virus-assay study. Am J Pathol 1964; 44:775-797.

(27) Marchant DJ, Boyd JH, Lin DC, Granville DJ, Garmaroudi FS, McManus BM. Inflammation in myocardial diseases. Circ Res 2012; 110(1):126-144.

(28) Chow LH, Beisel KW, McManus BM. Enteroviral infection of mice with severe combined immunodeficiency. Evidence for direct viral pathogenesis of myocardial injury. Lab Invest 1992; 66(1):24-31.

(29) Seko Y, Shinkai Y, Kawasaki A, Yagita H, Okumura K, Takaku F et al. Expression of perforin in infiltrating cells in murine hearts with acute myocarditis caused by coxsackievirus B3. Circulation 1991; 84(2):788-795.

(30) Klingel K, Hohenadl C, Canu A, Albrecht M, Seemann M, Mall G et al. Ongoing enterovirus-induced myocarditis is associated with persistent heart muscle infection: quantitative analysis of virus replication, tissue damage, and inflammation. Proc Natl Acad Sci U S A 1992; 89(1):314-318.

(31) Seko Y, Yoshifumi E, Yagita H, Okumura K, Yazaki Y. Restricted usage of T-cell receptor V alpha genes in infiltrating cells in murine hearts with acute myocarditis caused by coxsackie virus B3. J Pathol 1996; 178(3):330-334.

(32) Seko Y, Ishiyama S, Nishikawa T, Kasajima T, Hiroe M, Kagawa N et al. Restricted usage of T cell receptor V alpha-V beta genes in infiltrating cells in the hearts of patients with acute myocarditis and dilated cardiomyopathy. J Clin Invest 1995; 96(2):1035-1041.

(33) Henke A, Huber S, Stelzner A, Whitton JL. The role of CD8+ T lymphocytes in coxsackievirus B3-induced myocarditis. J Virol 1995; 69(11):6720-6728.

(34) Gebhard JR, Perry CM, Harkins S, Lane T, Mena I, Asensio VC et al. Coxsackievirus B3-induced myocarditis: perforin exacerbates disease, but plays no detectable role in virus clearance. Am J Pathol 1998; 153(2):417-428.

(35) Latif N, Zhang H, Archard LC, Yacoub MH, Dunn MJ. Characterization of anti-heart antibodies in mice after infection with coxsackie B3 virus. Clin Immunol 1999; 91(1):90-98.

(36) Esfandiarei M, Boroomand S, Suarez A, Si X, Rahmani M, McManus B. Coxsackievirus B3 activates nuclear factor kappa B transcription factor via a phosphatidylinositol-3 kinase/protein kinase B-dependent pathway to improve host cell viability. Cell Microbiol 2007; 9(10):2358-2371.

(37) Li YF, Wang X. The role of the proteasome in heart disease. Biochim Biophys Acta 2011; 1809(2):141-149.

(38) Kloetzel PM. Antigen processing by the proteasome. Nat Rev Mol Cell Biol 2001; 2(3):179-187.

(39) Weissman AM, Shabek N, Ciechanover A. The predator becomes the prey: regulating the ubiquitin system by ubiquitylation and degradation. Nat Rev Mol Cell Biol 2011; 12(9):605-620.

(40) Goldberg AL. Protein degradation and protection against misfolded or damaged proteins. Nature 2003; 426(6968):895-899.

(41) Wang X, Robbins J. Heart failure and protein quality control. Circ Res 2006; 99(12):1315-1328.

(42) Kuckelkorn U, Ruppert T, Strehl B, Jungblut PR, Zimny-Arndt U, Lamer S et al. Link between organ-specific antigen processing by 20S proteasomes and CD8(+) T cell-mediated autoimmunity. J Exp Med 2002; 195(8):983-990.

(43) Zu L, Bedja D, Fox-Talbot K, Gabrielson KL, Van KL, Becker LC et al. Evidence for a role of immunoproteasomes in regulating cardiac muscle mass in diabetic mice. J Mol Cell Cardiol 2010; 49(1):5-15.

(44) Cai ZP, Shen Z, Van KL, Becker LC. Ischemic preconditioning-induced cardioprotection is lost in mice with immunoproteasome subunit low molecular mass polypeptide-2 deficiency. FASEB J 2008; 22(12):4248-4257.

(45) Szalay G, Meiners S, Voigt A, Lauber J, Spieth C, Speer N et al. Ongoing coxsackievirus myocarditis is associated with increased formation and activity of myocardial immunoproteasomes. Am J Pathol 2006; 168(5):1542-1552.

(46) Pickart CM, Eddins MJ. Ubiquitin: structures, functions, mechanisms. Biochim Biophys Acta 2004; 1695(1-3):55-72.

(47) Kerscher O, Felberbaum R, Hochstrasser M. Modification of proteins by ubiquitin and ubiquitin-like proteins. Annu Rev Cell Dev Biol 2006; 22:159-180.

(48) Liu YC, Penninger J, Karin M. Immunity by ubiquitylation: a reversible process of modification. Nat Rev Immunol 2005; 5(12):941-952.

(49) Lee I, Schindelin H. Structural insights into E1-catalyzed ubiquitin activation and transfer to conjugating enzymes. Cell 2008; 134(2):268-278.

(50) Weissman AM. Themes and variations on ubiquitylation. Nat Rev Mol Cell Biol 2001; 2(3):169-178.

(51) Deng L, Wang C, Spencer E, Yang L, Braun A, You J et al. Activation of the IkappaB kinase complex by TRAF6 requires a dimeric ubiquitin-conjugating enzyme complex and a unique polyubiquitin chain. Cell 2000; 103(2):351-361.

(52) Mukhopadhyay D, Riezman H. Proteasome-independent functions of ubiquitin in endocytosis and signaling. Science 2007; 315(5809):201-205.

(53) Hjerpe R, Rodriguez MS. Efficient approaches for characterizing ubiquitinated proteins. Biochem Soc Trans 2008; 36(Pt 5):823-827.

(54) Hochstrasser M. Origin and function of ubiquitin-like proteins. Nature 2009; 458(7237):422-429.

(55) da Fonseca PC, He J, Morris EP. Molecular model of the human 26S proteasome. Mol Cell 2012; 46(1):54-66.

(56) Saeki Y, Tanaka K. Assembly and function of the proteasome. Methods Mol Biol 2012; 832:315-337.

(57) Groll M, Bochtler M, Brandstetter H, Clausen T, Huber R. Molecular machines for protein degradation. Chembiochem 2005; 6(2):222-256.

(58) Murata S, Yashiroda H, Tanaka K. Molecular mechanisms of proteasome assembly. Nat Rev Mol Cell Biol 2009; 10(2):104-115.

(59) Tanaka K. The proteasome: overview of structure and functions. Proc Jpn Acad Ser B Phys Biol Sci 2009; 85(1):12-36.

(60) Groll M, Bajorek M, Kohler A, Moroder L, Rubin DM, Huber R et al. A gated channel into the proteasome core particle. Nat Struct Biol 2000; 7(11):1062-1067.

(61) Religa TL, Sprangers R, Kay LE. Dynamic regulation of archaeal proteasome gate opening as studied by TROSY NMR. Science 2010; 328(5974):98-102.

(62) Kohler A, Cascio P, Leggett DS, Woo KM, Goldberg AL, Finley D. The axial channel of the proteasome core particle is gated by the Rpt2 ATPase and controls both substrate entry and product release. Mol Cell 2001; 7(6):1143-1152.

(63) Ebstein F, Kloetzel PM, Kruger E, Seifert U. Emerging roles of immunoproteasomes beyond MHC class I antigen processing. Cell Mol Life Sci 2012.

(64) Monaco JJ, McDevitt HO. The LMP antigens: a stable MHC-controlled multisubunit protein complex. Hum Immunol 1986; 15(4):416-426.

(65) Larsen F, Solheim J, Kristensen T, Kolsto AB, Prydz H. A tight cluster of five unrelated human genes on chromosome 16q22.1. Hum Mol Genet 1993; 2(10):1589-1595.

(66) Aki M, Shimbara N, Takashina M, Akiyama K, Kagawa S, Tamura T et al. Interferon-gamma induces different subunit organizations and functional diversity of proteasomes. J Biochem 1994; 115(2):257-269.

(67) Groettrup M, Kraft R, Kostka S, Standera S, Stohwasser R, Kloetzel PM. A third interferon-gamma-induced subunit exchange in the 20S proteasome. Eur J Immunol 1996; 26(4):863-869.

(68) Belich MP, Glynne RJ, Senger G, Sheer D, Trowsdale J. Proteasome components with reciprocal expression to that of the MHC-encoded LMP proteins. Curr Biol 1994; 4(9):769-776.

(69) Griffin TA, Nandi D, Cruz M, Fehling HJ, Kaer LV, Monaco JJ et al. Immunoproteasome assembly: cooperative incorporation of interferon gamma (IFN-gamma)-inducible subunits. J Exp Med 1998; 187(1):97-104.

(70) Heink S, Ludwig D, Kloetzel PM, Kruger E. IFN-gamma-induced immune adaptation of the proteasome system is an accelerated and transient response. Proc Natl Acad Sci U S A 2005; 102(26):9241-9246.

(71) Kingsbury DJ, Griffin TA, Colbert RA. Novel propeptide function in 20 S proteasome assembly influences beta subunit composition. J Biol Chem 2000; 275(31):24156-24162.

(72) Gaczynska M, Goldberg AL, Tanaka K, Hendil KB, Rock KL. Proteasome subunits X and Y alter peptidase activities in opposite ways to the interferon-gamma-induced subunits LMP2 and LMP7. J Biol Chem 1996; 271(29):17275-17280.

(73) Orlowski M, Wilk S. Catalytic activities of the 20 S proteasome, a multicatalytic proteinase complex. Arch Biochem Biophys 2000; 383(1):1-16.

(74) Kloetzel PM, Ossendorp F. Proteasome and peptidase function in MHC-class-I-mediated antigen presentation. Curr Opin Immunol 2004; 16(1):76-81.

(75) Kopp F, Dahlmann B, Kuehn L. Reconstitution of hybrid proteasomes from purified PA700-20 S complexes and PA28alphabeta activator: ultrastructure and peptidase activities. J Mol Biol 2001; 313(3):465-471.

(76) Song X, Mott JD, von KJ, Pramanik B, Tanaka K, Slaughter CA et al. A model for the quaternary structure of the proteasome activator PA28. J Biol Chem 1996; 271(42):26410-26417.

(77) Zhang Z, Krutchinsky A, Endicott S, Realini C, Rechsteiner M, Standing KG. Proteasome activator 11S REG or PA28: recombinant REG alpha/REG beta hetero-oligomers are heptamers. Biochemistry 1999; 38(17):5651-5658.

(78) Hendil KB, Khan S, Tanaka K. Simultaneous binding of PA28 and PA700 activators to 20 S proteasomes. Biochem J 1998; 332 (Pt 3):749-754.

(79) Rechsteiner M, Realini C, Ustrell V. The proteasome activator 11 S REG (PA28) and class I antigen presentation. Biochem J 2000; 345 Pt 1:1-15.

(80) Sijts A, Sun Y, Janek K, Kral S, Paschen A, Schadendorf D et al. The role of the proteasome activator PA28 in MHC class I antigen processing. Mol Immunol 2002; 39(3-4):165-169.

(81) Sijts EJ, Kloetzel PM. The role of the proteasome in the generation of MHC class I ligands and immune responses. Cell Mol Life Sci 2011; 68(9):1491-1502.

(82) Neefjes J, Jongsma ML, Paul P, Bakke O. Towards a systems understanding of MHC class I and MHC class II antigen presentation. Nat Rev Immunol 2011; 11(12):823-836.

(83) Goldberg AL, Cascio P, Saric T, Rock KL. The importance of the proteasome and subsequent proteolytic steps in the generation of antigenic peptides. Mol Immunol 2002; 39(3-4):147-164.

(84) Paulsson KM. Evolutionary and functional perspectives of the major histocompatibility complex class I antigen-processing machinery. Cell Mol Life Sci 2004; 61(19-20):2446-2460.

(85) Hewitt EW. The MHC class I antigen presentation pathway: strategies for viral immune evasion. Immunology 2003; 110(2):163-169.

(86) Hughes EA, Hammond C, Cresswell P. Misfolded major histocompatibility complex class I heavy chains are translocated into the cytoplasm and degraded by the proteasome. Proc Natl Acad Sci U S A 1997; 94(5):1896-1901.

(87) Janeway CA, Travers P. Der Thymus und die Entwicklung der T-Lymphozyten. Immunologie. Heidelberg, Berlin, Oxford: Spektrum Akademischer Verlag GmbH, 1997.

(88) Yewdell JW. DRiPs solidify: progress in understanding endogenous MHC class I antigen processing. Trends Immunol 2011; 32(11):548-558.

(89) Berglund P, Finzi D, Bennink JR, Yewdell JW. Viral alteration of cellular translational machinery increases defective ribosomal products. J Virol 2007; 81(13):7220-7229.

(90) Netzer N, Goodenbour JM, David A, Dittmar KA, Jones RB, Schneider JR et al. Innate immune and chemically triggered oxidative stress modifies translational fidelity. Nature 2009; 462(7272):522-526.

(91) Yewdell JW, Anton LC, Bennink JR. Defective ribosomal products (DRiPs): a major source of antigenic peptides for MHC class I molecules? J Immunol 1996; 157(5):1823-1826.

(92) Dolan BP, Li L, Takeda K, Bennink JR, Yewdell JW. Defective ribosomal products are the major source of antigenic peptides endogenously generated from influenza A virus neuraminidase. J Immunol 2010; 184(3):1419-1424.

(93) Brooks P, Murray RZ, Mason GG, Hendil KB, Rivett AJ. Association of immunoproteasomes with the endoplasmic reticulum. Biochem J 2000; 352 Pt 3:611-615.

(94) Hwang LY, Lieu PT, Peterson PA, Yang Y. Functional regulation of immunoproteasomes and transporter associated with antigen processing. Immunol Res 2001; 24(3):245-272.

(95) Driscoll J, Brown MG, Finley D, Monaco JJ. MHC-linked LMP gene products specifically alter peptidase activities of the proteasome. Nature 1993; 365(6443):262-264.

(96) Gaczynska M, Rock KL, Goldberg AL. Gamma-interferon and expression of MHC genes regulate peptide hydrolysis by proteasomes. Nature 1993; 365(6443):264-267.

(97) Kloetzel PM. The proteasome and MHC class I antigen processing. Biochim Biophys Acta 2004; 1695(1-3):225-233.

(98) Sijts AJ, Ruppert T, Rehermann B, Schmidt M, Koszinowski U, Kloetzel PM. Efficient generation of a hepatitis B virus cytotoxic T lymphocyte epitope requires the structural features of immunoproteasomes. J Exp Med 2000; 191(3):503-514.

(99) Strehl B, Seifert U, Kruger E, Heink S, Kuckelkorn U, Kloetzel PM. Interferon-gamma, the functional plasticity of the ubiquitin-proteasome system, and MHC class I antigen processing. Immunol Rev 2005; 207:19-30.

(100) Nussbaum AK, Rodriguez-Carreno MP, Benning N, Botten J, Whitton JL. Immunoproteasome-deficient mice mount largely normal CD8+ T cell responses to lymphocytic choriomeningitis virus infection and DNA vaccination. J Immunol 2005; 175(2):1153-1160.

(101) Chen W, Norbury CC, Cho Y, Yewdell JW, Bennink JR. Immunoproteasomes shape immunodominance hierarchies of antiviral CD8(+) T cells at the levels of T cell repertoire and presentation of viral antigens. J Exp Med 2001; 193(11):1319-1326.

(102) Balch WE, Morimoto RI, Dillin A, Kelly JW. Adapting proteostasis for disease intervention. Science 2008; 319(5865):916-919.

(103) Anckar J, Sistonen L. Regulation of HSF1 function in the heat stress response: implications in aging and disease. Annu Rev Biochem 2011; 80:1089-1115.

(104) Bukau B, Craig EA, Morimoto RI, Horwich AL. Stress-Induced Expression of Heat Shock Proteins and Action of the Heat Shock Protein Effectors. Encyclopedia of Molecular Cell Biology and Molecular Medicine. Wiley-VCH Verlag GmbH & Co. KGaA, 2006: 463-515.

(105) Liu Y, Chang A. Heat shock response relieves ER stress. EMBO J 2008; 27(7):1049-1059.

(106) Guerriero CJ, Brodsky JL. The delicate balance between secreted protein folding and endoplasmic reticulum-associated degradation in human physiology. Physiol Rev 2012; 92(2):537-576.

(107) Schroder M, Kaufman RJ. ER stress and the unfolded protein response. Mutat Res 2005; 569(1-2):29-63.

(108) Hong M, Li M, Mao C, Lee AS. Endoplasmic reticulum stress triggers an acute proteasome-dependent degradation of ATF6. J Cell Biochem 2004; 92(4):723-732.

(109) Smith MH, Ploegh HL, Weissman JS. Road to ruin: targeting proteins for degradation in the endoplasmic reticulum. Science 2011; 334(6059):1086-1090.

(110) Christianson JC, Shaler TA, Tyler RE, Kopito RR. OS-9 and GRP94 deliver mutant alpha1-antitrypsin to the Hrd1-SEL1L ubiquitin ligase complex for ERAD. Nat Cell Biol 2008; 10(3):272-282.

(111) Vecchi L, Petris G, Bestagno M, Burrone OR. Selective Targeting of Proteins within Secretory Pathway for Endoplasmic Reticulum-associated Degradation. J Biol Chem 2012; 287(24):20007-20015.

(112) Greenblatt EJ, Olzmann JA, Kopito RR. Derlin-1 is a rhomboid pseudoprotease required for the dislocation of mutant alpha-1 antitrypsin from the endoplasmic reticulum. Nat Struct Mol Biol 2011; 18(10):1147-1152.

(113) Szeto J, Kaniuk NA, Canadien V, Nisman R, Mizushima N, Yoshimori T et al. ALIS are stress-induced protein storage compartments for substrates of the proteasome and autophagy. Autophagy 2006; 2(3):189-199.

(114) Lelouard H, Ferrand V, Marguet D, Bania J, Camosseto V, David A et al. Dendritic cell aggresome-like induced structures are dedicated areas for ubiquitination and storage of newly synthesized defective proteins. J Cell Biol 2004; 164(5):667-675.

(115) Liu XD, Ko S, Xu Y, Fattah EA, Xiang Q, Jagannath C et al. Transient aggregation of ubiquitinated proteins is a cytosolic unfolded protein response to inflammation and endoplasmic reticulum stress. J Biol Chem 2012; 287(23):19687-19698.

(116) Lelouard H, Gatti E, Cappello F, Gresser O, Camosseto V, Pierre P. Transient aggregation of ubiquitinated proteins during dendritic cell maturation. Nature 2002; 417(6885):177-182.

(117) Dantuma NP, Lindsten K. Stressing the ubiquitin-proteasome system. Cardiovasc Res 2010; 85(2):263-271.

(118) Jakel S, Kuckelkorn U, Szalay G, Plotz M, Textoris-Taube K, Opitz E et al. Differential interferon responses enhance viral epitope generation by myocardial immunoproteasomes in murine enterovirus myocarditis. Am J Pathol 2009; 175(2):510-518.

(119) Kandolf R, Hofschneider PH. Molecular cloning of the genome of a cardiotropic Coxsackie B3 virus: full-length reverse-transcribed recombinant cDNA generates infectious virus in mammalian cells. Proc Natl Acad Sci U S A 1985; 82(14):4818-4822.

(120) Westermann D, Walther T, Savvatis K, Escher F, Sobirey M, Riad A et al. Gene deletion of the kinin receptor B1 attenuates cardiac inflammation and fibrosis during the development of experimental diabetic cardiomyopathy. Diabetes 2009; 58(6):1373-1381.

(121) Szalay G, Sauter M, Hald J, Weinzierl A, Kandolf R, Klingel K. Sustained nitric oxide synthesis contributes to immunopathology in ongoing myocarditis attributable to interleukin-10 disorders. Am J Pathol 2006; 169(6):2085-2093.

(122) Seizer P, Klingel K, Sauter M, Westermann D, Ochmann C, Schonberger T et al. Cyclophilin A affects inflammation, virus elimination and myocardial fibrosis in coxsackievirus B3-induced myocarditis. J Mol Cell Cardiol 2012; 53(1):6-14.

(123) Opitz E, Koch A, Klingel K, Schmidt F, Prokop S, Rahnefeld A et al. Impairment of immunoproteasome function by beta5i/LMP7 subunit deficiency results in severe enterovirus myocarditis. PLoS Pathog 2011; 7(9):e1002233.

(124) Heukeshoven J, Dernick R. Improved silver staining procedure for fast staining in PhastSystem Development Unit. I. Staining of sodium dodecyl sulfate gels. Electrophoresis 1988; 9(1):28-32.

(125) Trapani JA, Smyth MJ. Functional significance of the perforin/granzyme cell death pathway. Nat Rev Immunol 2002; 2(10):735-747.

(126) Klingel K, Schnorr JJ, Sauter M, Szalay G, Kandolf R. beta2-microglobulin-associated regulation of interferon-gamma and virus-specific immunoglobulin G confer resistance against the development of chronic coxsackievirus myocarditis. Am J Pathol 2003; 162(5):1709-1720.

(127) Hensley SE, Zanker D, Dolan BP, David A, Hickman HD, Embry AC et al. Unexpected role for the immunoproteasome subunit LMP2 in antiviral humoral and innate immune responses. J Immunol 2010; 184(8):4115-4122.

(128) Leipner C, Grun K, Schneider I, Gluck B, Sigusch HH, Stelzner A. Coxsackievirus B3-induced myocarditis: differences in the immune response of C57BL/6 and Balb/c mice. Med Microbiol Immunol 2004; 193(2-3):141-147.

(129) Tanaka K. Role of proteasomes modified by interferon-gamma in antigen processing. J Leukoc Biol 1994; 56(5):571-575.

(130) Tanaka K, Kasahara M. The MHC class I ligand-generating system: roles of immunoproteasomes and the interferon-gamma-inducible proteasome activator PA28. Immunol Rev 1998; 163:161-176.

(131) Van Kaer L., Ashton-Rickardt PG, Eichelberger M, Gaczynska M, Nagashima K, Rock KL et al. Altered peptidase and viral-specific T cell response in LMP2 mutant mice. Immunity 1994; 1(7):533-541.

(132) Sadler AJ, Williams BR. Interferon-inducible antiviral effectors. Nat Rev Immunol 2008; 8(7):559-568.

(133) Seong E, Saunders TL, Stewart CL, Burmeister M. To knockout in 129 or in C57BL/6: that is the question. Trends Genet 2004; 20(2):59-62.

(134) Chow LH, Gauntt CJ, McManus BM. Differential effects of myocarditic variants of Coxsackievirus B3 in inbred mice. A pathologic characterization of heart tissue damage. Lab Invest 1991; 64(1):55-64.

(135) Wang JP, Cerny A, Asher DR, Kurt-Jones EA, Bronson RT, Finberg RW. MDA5 and MAVS mediate type I interferon responses to coxsackie B virus. J Virol 2010; 84(1):254-260.

(136) Wessely R, Klingel K, Knowlton KU, Kandolf R. Cardioselective infection with coxsackievirus B3 requires intact type I interferon signaling: implications for mortality and early viral replication. Circulation 2001; 103(5):756-761.

(137) Hospital F. Size of donor chromosome segments around introgressed loci and reduction of linkage drag in marker-assisted backcross programs. Genetics 2001; 158(3):1363-1379.

(138) Forman HJ, Torres M. Redox signaling in macrophages. Mol Aspects Med 2001; 22(4-5):189-216.

(139) Nathan CF. Secretory products of macrophages. J Clin Invest 1987; 79(2):319-326.

(140) Morgan MJ, Liu ZG. Reactive oxygen species in TNFalpha-induced signaling and cell death. Mol Cells 2010; 30(1):1-12.

(141) Saraste A, Arola A, Vuorinen T, Kyto V, Kallajoki M, Pulkki K et al. Cardiomyocyte apoptosis in experimental coxsackievirus B3 myocarditis. Cardiovasc Pathol 2003; 12(5):255-262.

(142) Si X, McManus BM, Zhang J, Yuan J, Cheung C, Esfandiarei M et al. Pyrrolidine dithiocarbamate reduces coxsackievirus B3 replication through inhibition of the ubiquitin-proteasome pathway. J Virol 2005; 79(13):8014-8023.

(143) Zhang HM, Ye X, Su Y, Yuan J, Liu Z, Stein DA et al. Coxsackievirus B3 infection activates the unfolded protein response and induces apoptosis through downregulation of p58IPK and activation of CHOP and SREBP1. J Virol 2010; 84(17):8446-8459.

(144) Griffin TA, Nandi D, Cruz M, Fehling HJ, Kaer LV, Monaco JJ et al. Immunoproteasome assembly: cooperative incorporation of interferon gamma (IFN-gamma)-inducible subunits. J Exp Med 1998; 187(1):97-104.

(145) Groettrup M, Standera S, Stohwasser R, Kloetzel PM. The subunits MECL-1 and LMP2 are mutually required for incorporation into the 20S proteasome. Proc Natl Acad Sci U S A 1997; 94(17):8970-8975.

(146) Joeris T, Schmidt N, Ermert D, Krienke P, Visekruna A, Kuckelkorn U et al. The Proteasome System in Infection: Impact of beta5 and LMP7 on Composition, Maturation and Quantity of Active Proteasome Complexes. PLoS One 2012; 7(6):e39827.

(147) Boes B, Hengel H, Ruppert T, Multhaup G, Koszinowski UH, Kloetzel PM. Interferon gamma stimulation modulates the proteolytic activity and cleavage site preference of 20S mouse proteasomes. J Exp Med 1994; 179(3):901-909.

(148) Toes RE, Nussbaum AK, Degermann S, Schirle M, Emmerich NP, Kraft M et al. Discrete cleavage motifs of constitutive and immunoproteasomes revealed by quantitative analysis of cleavage products. J Exp Med 2001; 194(1):1-12.

(149) Voigt A, Jakel S, Textoris-Taube K, Keller C, Drung I, Szalay G et al. Generation of in silico predicted coxsackievirus B3-derived MHC class I epitopes by proteasomes. Amino Acids 2010; 39(1):243-255.

(150) Nussbaum AK, Rodriguez-Carreno MP, Benning N, Botten J, Whitton JL. Immunoproteasome-deficient mice mount largely normal CD8+ T cell responses to lymphocytic choriomeningitis virus infection and DNA vaccination. J Immunol 2005; 175(2):1153-1160.

(151) Kincaid EZ, Che JW, York I, Escobar H, Reyes-Vargas E, Delgado JC et al. Mice completely lacking immunoproteasomes show major changes in antigen presentation. Nat Immunol 2011; 13(2):129-135.

(152) Karrer U, Oxenius A, Phillips R, Klenerman P. Memory T cells: total recall or just a sense of deja vu? Nat Immunol 2001; 2(11):991-993.

(153) Kemball CC, Harkins S, Whitmire JK, Flynn CT, Feuer R, Whitton JL. Coxsackievirus B3 inhibits antigen presentation in vivo, exerting a profound and selective effect on the MHC class I pathway. PLoS Pathog 2009; 5(10):e1000618.

(154) Yewdell JW. The seven dirty little secrets of major histocompatibility complex class I antigen processing. Immunol Rev 2005; 207:8-18.

(155) Nagarajan U. Induction and function of IFNbeta during viral and bacterial infection. Crit Rev Immunol 2011; 31(6):459-474.

(156) Feldmann M, Saklatvala J. Proinflammatory cytokines. In: Oppenheim JJ, Feldmann M, editors. Cytokine Reference. A Compendium of Cytokines and Other Mediators of Host Defense. San Diego: Elsevier Science Publishing Co Inc, 2000: 291.

(157) Kroczynska B, Kaur S, Platanias LC. Growth suppressive cytokines and the AKT/mTOR pathway. Cytokine 2009; 48(1-2):138-143.

(158) Droge W. Free radicals in the physiological control of cell function. Physiol Rev 2002; 82(1):47-95.

(159) Medicherla B, Goldberg AL. Heat shock and oxygen radicals stimulate ubiquitin-dependent degradation mainly of newly synthesized proteins. J Cell Biol 2008; 182(4):663-673.

(160) Rassmann A, Henke A, Zobawa M, Carlsohn M, Saluz HP, Grabley S et al. Proteome alterations in human host cells infected with coxsackievirus B3. J Gen Virol 2006; 87(Pt 9):2631-2638.

(161) Bucciantini M, Giannoni E, Chiti F, Baroni F, Formigli L, Zurdo J et al. Inherent toxicity of aggregates implies a common mechanism for protein misfolding diseases. Nature 2002; 416(6880):507-511.

(162) Seifert U, Bialy LP, Ebstein F, Bech-Otschir D, Voigt A, Schroter F et al. Immunoproteasomes preserve protein homeostasis upon interferon-induced oxidative stress. Cell 2010; 142(4):613-624.

(163) Batoulis H, Recks MS, Addicks K, Kuerten S. Experimental autoimmune encephalomyelitis-achievements and prospective advances. APMIS 2011; 119(12):819-830.

(164) Sherman MY, Goldberg AL. Cellular defenses against unfolded proteins: a cell biologist thinks about neurodegenerative diseases. Neuron 2001; 29(1):15-32.

(165) Naujokat C, Hoffmann S. Role and function of the 26S proteasome in proliferation and apoptosis. Lab Invest 2002; 82(8):965-980.

(166) Yang Z, Gagarin D, St LG, III, Hammell N, Toma I, Hu CA et al. Cardiovascular inflammation and lesion cell apoptosis: a novel connection via the interferon-

inducible immunoproteasome. Arterioscler Thromb Vasc Biol 2009; 29(8):1213-1219.

(167) Swindle EJ, Hunt JA, Coleman JW. A comparison of reactive oxygen species generation by rat peritoneal macrophages and mast cells using the highly sensitive real-time chemiluminescent probe pholasin: inhibition of antigen-induced mast cell degranulation by macrophage-derived hydrogen peroxide. J Immunol 2002; 169(10):5866-5873.

(168) Niture SK, Jaiswal AK. Nrf2 protein up-regulates antiapoptotic protein Bcl-2 and prevents cellular apoptosis. J Biol Chem 2012; 287(13):9873-9886.

(169) Morito N, Yoh K, Itoh K, Hirayama A, Koyama A, Yamamoto M et al. Nrf2 regulates the sensitivity of death receptor signals by affecting intracellular glutathione levels. Oncogene 2003; 22(58):9275-9281.

(170) Kaspar JW, Niture SK, Jaiswal AK. Nrf2:INrf2 (Keap1) signaling in oxidative stress. Free Radic Biol Med 2009; 47(9):1304-1309.

(171) Pickering AM, Linder RA, Zhang H, Forman HJ, Davies KJ. Nrf2-dependent induction of proteasome and Pa28alphabeta regulator are required for adaptation to oxidative stress. J Biol Chem 2012; 287(13):10021-10031.

(172) Mathers J, Fraser JA, McMahon M, Saunders RD, Hayes JD, McLellan LI. Antioxidant and cytoprotective responses to redox stress. Biochem Soc Symp 2004;(71):157-176.

(173) Baldwin AS, Jr. The NF-kappa B and I kappa B proteins: new discoveries and insights. Annu Rev Immunol 1996; 14:649-683.

(174) Karin M, Ben-Neriah Y. Phosphorylation meets ubiquitination: the control of NF-[kappa]B activity. Annu Rev Immunol 2000; 18:621-663.

(175) Visekruna A, Joeris T, Seidel D, Kroesen A, Loddenkemper C, Zeitz M et al. Proteasome-mediated degradation of IkappaBalpha and processing of p105 in Crohn disease and ulcerative colitis. J Clin Invest 2006; 116(12):3195-3203.

(176) Hollander J, Fiebig R, Gore M, Ookawara T, Ohno H, Ji LL. Superoxide dismutase gene expression is activated by a single bout of exercise in rat skeletal muscle. Pflugers Arch 2001; 442(3):426-434.

(177) Mercken EM, Hageman GJ, Langen RC, Wouters EF, Schols AM. Decreased exercise-induced expression of nuclear factor-kappaB-regulated genes in muscle of patients with COPD. Chest 2011; 139(2):337-346.

(178) Zhang J, Velsor LW, Patel JM, Postlethwait EM, Block ER. Nitric oxide-induced reduction of lung cell and whole lung thioredoxin expression is regulated by NF-kappaB. Am J Physiol 1999; 277(4 Pt 1):L787-L793.

(179) Barnes PJ, Karin M. Nuclear factor-kappaB: a pivotal transcription factor in chronic inflammatory diseases. N Engl J Med 1997; 336(15):1066-1071.

(180) Verma IM. Nuclear factor (NF)-kappaB proteins: therapeutic targets. Ann Rheum Dis 2004; 63 Suppl 2:ii57-ii61.

(181) Neubert K, Meister S, Moser K, Weisel F, Maseda D, Amann K et al. The proteasome inhibitor bortezomib depletes plasma cells and protects mice with lupus-like disease from nephritis. Nat Med 2008; 14(7):748-755.

(182) Schmidt N, Gonzalez E, Visekruna A, Kuhl AA, Loddenkemper C, Mollenkopf H et al. Targeting the proteasome: partial inhibition of the proteasome by bortezomib or deletion of the immunosubunit LMP7 attenuates experimental colitis. Gut 2010; 59(7):896-906.

(183) Huber EM, Basler M, Schwab R, Heinemeyer W, Kirk CJ, Groettrup M et al. Immuno- and constitutive proteasome crystal structures reveal differences in substrate and inhibitor specificity. Cell 2012; 148(4):727-738.

(184) Muchamuel T, Basler M, Aujay MA, Suzuki E, Kalim KW, Lauer C et al. A selective inhibitor of the immunoproteasome subunit LMP7 blocks cytokine production and attenuates progression of experimental arthritis. Nat Med 2009; 15(7):781-787.

(185) Basler M, Youhnovski N, van den Broek M, Przybylski M, Groettrup M. Immunoproteasomes down-regulate presentation of a subdominant T cell epitope from lymphocytic choriomeningitis virus. J Immunol 2004; 173(6):3925-3934.

(186) Kunes P, Holubcova Z, Kolackova M, Krejsek J. Pentraxin 3(PTX 3): an endogenous modulator of the inflammatory response. Mediators Inflamm 2012; 2012:920517.

(187) Presta M, Camozzi M, Salvatori G, Rusnati M. Role of the soluble pattern recognition receptor PTX3 in vascular biology. J Cell Mol Med 2007; 11(4):723-738.

(188) Iwasaki A, Medzhitov R. Regulation of adaptive immunity by the innate immune system. Science 2010; 327(5963):291-295.

(189) Piccinini AM, Midwood KS. DAMPening inflammation by modulating TLR signalling. Mediators Inflamm 2010; 2010.

(190) Pisetsky D. Cell death in the pathogenesis of immune-mediated diseases: the role of HMGB1 and DAMP-PAMP complexes. Swiss Med Wkly 2011; 141:w13256.

8 ABBREVIATIONS

ALIS	aggresome-like induced structures
Å	ångström
ATP	adenosine-5'-triphosphate
AMC	amino-4-methylcoumarin
AMP	adenosine monophosphate
Akt	protein Kinase B
ARE	*cis*-acting antioxidant-response element
ATF6	activating transcription factor 6
BCA	bicinchoninic acid assay
bp	base pair
BSA	bovine serum albumin
CD	cluster of differentiation
CAR	coxsackievirus and adenovirus receptor
Cat	catalase
CTL	cytotoxic T lymphocyte
CHOP	DNA damage-inducible transcript 3 protein
C-	carboxy-
CVB3	coxsackie virus B3
DTT	dithiothreitol
dNTP	desoxy nucleoside trophosphate
DEPC	diethylpyrocarbonate
DNA/DNAse	deoxyribonucleic acid/deoxyribonuclease
DAF	decay-acceletating factor
DRIPs	defective ribosomal products
DAPI	4',6-diamidino-2-phenylindole
DCM	dilative cardiomyopathy
DUB	deubiquitinating enzyme
DAMPs	damage associated molecular pattern molecules
DC	dendritic cell

EAE	experimental autoimmune encephalomyelitis
ECL	electrogenerated chemiluminescence
et al.	et alia
ex.	extinction
em.	emission
e.g.	for example
eIF4G	eukaryotic translation initiation factor 4 gamma
ER	endoplasmic reticulum
E13	embryonic day 13
ELISA	enzyme linked immuno-absorbent assay
ERAD	endoplasmic-reticulum-associated degradation
FITC	fluoreszeinisothiozyanat
FPLC	fast protein liquid chromatography
FACS	fluorescence activated cell sorting
F	**F**ilial or inbreeding (sister x brother) generations. **Examples:** F1, first filial generation; F2, second filial generation
Fig.	figure
GTP	guanosine-5'-triphosphate
GBP1	guanylate-binding protein 1
Gclc	glutamate-cysteine ligase catalytoc subunit
Gpx	glutathione
GO	gene ontology
g	relative centrifugal force
HPRT	hypoxanthineguanine phosphoribosyltransferase
HE	hematoxylin - eosin
HSR	heat shock response
HRD	3-hydroxy 3-methylgutaryl coenzyme A reductase degradation protein
Hsf1	heat shock factor 1
h	hour(s)
HRP	horseradish peroxidase
IP	immunoproteasome
IP-10	interferon-γ-induced protein 10

i.p.	intraperitoneal injection
i.v.	intravenous injection
ISG15	interferon-stimulated gene 15
IL	interleukine
IgG	immunoglobulin G
I-κB	inhibitor of nuclear factor κB
IRE1	serine/threonine-protein kinase/endoribonuclease
iNOS	inducible nitric oxide synthase
IRES	internal ribosome entry site
JAK/STAT	Janus kinase/signal transducer and activator of transcription
Keap1	kelch-like ECH-associated protein 1
LMP	low molecular weight protein
Lys	lysine
LCMV	lymphocytic choriomeningitis virus
MAPK	mitogen-activated protein kinase
MOI	multiplicity of infection
MACS	magnetic Activated Cell Sorting
mg	milligram
ml	milliliter
min	minute
µm/µg	micrometer/microgram
M	molar
MHC	major histocompatibility complex
MCP-1	monocyte chemotactic protein-1
Mx	myxovirus resistance protein
mTOR	mammalian target of rapamycin
MCL-1	myeloid leukemia cell differentiation protein
MS	mass spectrometry
MW	molecular weight
N	**N**umber of backcross generations. **Examples:** N1, first backcross generation; N2, second backcross generation
nm	nanometer

NEM	N-ethylmaleimide
NK cells	natural killer cells
NF-κB	nuclear factor kappa-light-chain-enhancer
NOX	nitrogen oxide
NADPH	nicotinamide adenine dinucleotide phosphate
Nqo1	NAD(P)H dehydrogenase (quinone 1)
Nrf2	nuclear factor (erythroid-derived 2)-like 2
p-	pico
PA28	proteasome activator
PAMPs	pathogen-associated molecular patterns
PFU	plaque forming unit
POD	peroxidase
PVDF	polyvinylidene fluoride
PI3K	phosphoinositide 3-kinase
PKR	protein kinase R
PCR	polymerase chain reaction
p	p-value
p.i.	post infectionem
PB	pacific Blue
PE	phycoerythrin
PFA	paraformaldehyde
PBS	phosphate buffered saline
PERK	protein kinase-like ER kinase
Ptx3	pentraxin-related protein
r	radius
RANTES	regulated upon activation
Rpn	regulatory particle
RP	regulatory protein
ROS	reactive oxygen species
RNS	reactive nitrogen species
RNA	ribonucleic acid
rpm	rounds per minute
SOD	superoxide dismutase

SDS-PAGE	sodium dodecyl sulfate polyacrylamide gel electrophoresis
SEM	standard error of the mean
SD	standard deviation
SEL1L	protein sel-1 homolog 1
ss	single strand
SREBP1	sterol regulatory element-binding protein 1
TEAD	triethylammonium acetate
TNF-α	tumor necrosis factor α
TAP	Transporter associated with antigen processing
TUNEL	terminal deoxynucleotidyl transferase dUTP nick end labeling
TLR	Toll-like receptor
TEMED	tetramethylethylenediamine
U	units
Ub	ubiquitin
UBE2L6	ubiquitin/ISG15-conjugating enzyme E2 L6
UTR	untranslated region
UPS	ubiquitin-proteasome system
UPR	unfolded protein response
XBP1	X-box binding protein 1

9 PUBLICATIONS

MANUSCRIPTS

- Opitz E, Koch A, Klingel K, Schmidt F, Prokop S, Rahnefeld A, Sauter M, Heppner FL, Völker U, Kandolf R, Kuckelkorn U, Stangl K, Krüger E, Kloetzel PM, Voigt A. *Impairment of immunoproteasome function by beta5i/LMP7 subunit deficiency results in severe enterovirus myocarditis*. **PLoS Pathog 2011**; 7(9):e1002233.
- Rahnefeld A, Ebstein F, Albrecht N, Opitz E, Kuckelkorn U, Stangl K, Rehm A, Kloetzel PM, Voigt A. *Antigen-presentation capacity of dendritic cells is impaired in ongoing enterovirus myocarditis*. **Eur J Immunol 2011**; 41(9):2774-2781.
- Jakel S, Kuckelkorn U, Szalay G, Plotz M, Textoris-Taube K, Opitz E, Klingel K, Stevanovic S, Kandolf R, Kotsch K, Stangl K, Kloetzel PM, Voigt A. *Differential interferon responses enhance viral epitope generation by myocardial immunoproteasomes in murine enterovirus myocarditis*. **Am J Pathol 2009**; 175(2):510-518.

POSTERS

- *Immunoproteasomal subunit iβ5 is crucial for an efficient immune response in acute enterovirus myocarditis in mice.* Voigt A, Savvatis K, Opitz E, Klingel K, Westermann D, Kuckelkorn U, Baumann G, Stangl K, Kloetzel PM. **Congress of German Society of Cardiology, Mannheim, Germany 04/2009**
- § *Deletion of the catalytic subunit iβ1 of immunoproteasomes is linked to less severe enterovirus myocarditis in mice.* Opitz E, Savvatis K, Klingel K, Westermann D, Baumann G, Kuckelkorn U, Stangl K, Kloetzel PM, Voigt A. **Congress of German Society of Cardiology, Mannheim, Germany 04/2009**
- *The Role of the Catalytic Subunit LMP2 of Stress-Induced Immunoproteasomes in Enterovirus Myocarditis.* Voigt A, Opitz E, Savvatis K, Klingel K, Stangl K, Kloetzel PM. **11th International Congress on Amino Acids, Peptides and Proteins Vienna, Austria 08/09**
- *Catalytic Subunit LMP2 of Stress-Induced Immunoproteasomes is Crucial in the Pathogenesis of Enterovirus Myocarditis.* Voigt A, Opitz E, Savvatis K, Klingel K, Stangl K, Stangl K. Baumann G, Kloetzel PM. **European Society of Cardiology, Congress; Barcelona, Spain 09/2009**
- *The Role of the Catalytic Subunit LMP2 of Stress-Induced Immunoproteasomes in Enterovirus Myocarditis.* Voigt A, Opitz E, Savvatis K, Klingel K, Stangl K, Stangl K. Baumann G, Kloetzel PM. **European Congress on Immunity; Berlin, Germany 09/2009**
- *Failure of the Catalytic Subunit LMP2 of Cytokine-Induced Immunoproteasomes Protects Mice from Enterovirus Myocarditis.* Opitz E, Klingel K, Savvatis K, Tschöpe C, Stangl K, Kuckelkorn U, Kloetzel PM, Voigt A. **International Symposium Inflammatory Cardiomyopathy Berlin, 01/10**
- *ISG-15 is Crucial in the Pathogenesis of Enterovirus Myocarditis.* Diny N*, Opitz E*, Klingel K, Riad A, Tschöpe C, Stangl K, Kuckelkorn U, Kloetzel PM, Voigt A. **International Symposium Inflammatory Cardiomyopathy Berlin, 01/10**
- *Impairment of the Ubiquitin-Proteasome-System is crucially involved in Dendritic Cell Function in the Murine Model of Enterovirus Myocarditis.* Rahnefeld A, Ebstein F, Opitz

E, Kuckelkorn U, Baumann G, Kloetzel PM, Stangl K, Voigt A. **Congress of German Society of Cardiology, Mannheim, Germany 04/2010**

- *Deletion of the catalytic subunit LMP2 of cytokine-induced immunoproteasomes protects mice from enterovirus myocarditis.* Opitz E, Klingel K, Savvatis K, Baumann G, Stangl K, Kloetzel PM, Voigt A. **Congress of German Society of Cardiology, Mannheim, Germany 04/2010**
- *Functional Impairment of Cardiac Inducible Proteasome Subunit LMP2 Protects Mice from Acute and Chronic Myocarditis.* Voigt A, Opitz E, Klingel K, Savvatis K, Tschöpe C, Stangl K, Kloetzel PM. **Heart Failure Congress of European Society of Cardiology, Berlin, Germany 05/2010**
- *Functional Impairment of Cardiac Inducible Proteasome Subunit LMP2 Protects Mice from Acute and Chronic Myocarditis.* Voigt A, Opitz E, Klingel K, Savvatis K, Tschöpe C, Stangl K, Kloetzel PM. **European Congress of Cardiology, ESC Stockholm, Sweden 08/2010**
- *ISG-15 is Crucial in the Pathogenesis of Enterovirus Myocarditis.* Diny N*, Opitz E*, Klingel K, Riad A, Tschöpe C, Stangl K, Kuckelkorn U, Knobeloch KP, Kloetzel PM, Voigt A. **European Congress of Cardiology, ESC Stockholm, Sweden 08/2010**

*equal contribution

§ AWARDS

Rudolf-Thauer-Poster Award, **75th Annual meeting of the German Cardiac Society, Mannheim (Germany), 2009**

10 EIDESSTATTLICHE ERKLÄRUNG

Hiermit erkläre ich, die vorliegende Arbeit selbständig ohne fremde Hilfe verfasst und nur die angegebene Literatur verwendet zu haben. Ein Teil der beschriebenen Ergebnisse wurde in Zusammenarbeit mit den Arbeitsgruppen von Prof. Karin Klingel, Prof. Elke Krüger, Prof. Carsten Tschöpe, Prof. Frank Heppner, sowie Prof. Uwe Völker erzielt. Diese sind entsprechend gekennzeichnet.
Ich besitze keinen entsprechenden Doktorgrad und habe mich anderwärts nicht um einen Doktorgrad beworben.
Die dem Promotionsverfahren zugrunde liegende Promotionsordnung vom 1.9.2005 ist mir bekannt.

Elisa Opitz

11 ACKNOWLEDGEMENTS

First I would like to express special thanks to Prof. Dr. Peter-Michael Kloetzel for giving me the opportunity to work on this project, and also for his guiding supervision and many productive discussions.

I am very thankful to Prof. Dr. Karl Stangl for giving me the possibility to work in the research lab for cardiology and angiology.

Particularly, I am very grateful to my supervisor PD Dr. Antje Voigt. I appreciate her enduring impulses to reconsider ideas, her analytical support and continuous guidance. Her great effort and knowledge was the basis for the present thesis.

Moreover, I would like to thank Prof. Dr. Karin Klingel, Prof. Dr. Elke Krüger, Dr. Frank Schmidt, Dr. Stefan Prokop, Dr. Ulrike Kuckelkorn, Prof. Dr. Carsten Tschöpe, PD Dr. Alexander Riad and PD Dr. Dirk Westermann for kindly providing technical, analytical, and contentual support.

I am very thankful to Dr. Konstantinos Savvatis and Dr. Annett Koch for their practical help and patience.

Huge thanks to Angela Zepp, Kornelia Buttke, Andrea Weller, Dr. Antje Ludwig and all other members of this research lab for their permanent help. Also Ilse Drung, Daniela Ludwig and Andrea Lehmann need to be named.

I am especially indebted to all my lab mates for being friends rather than just colleagues. Nadine, I can hardly express my gratitude for your patient and humorous technical as well as personal support. Warmest thanks Anna, for lending your ear at any time and many lifesaving Fridays. Thousand thanks Fritz, Netti, Philipp, and not least Grit for your encouragement and all the fun that we had.

Finally, I gratefully acknowledge funding by the German Research Foundation (DFG SFB TR19).